ISTANBUL TECHNICAL UNIVERSITY ★ INFORMATICS INSTITUTE

DESIGN OF THE FOUR ARM-DUAL POLARIZED SINUOUS ANTENNA WITH A NEW FEEDING APPROACH

M.Sc. THESIS

Sulayman JOOF

Department of Communication Systems

Satellite Communication and Remote Sensing Programme

DECEMBER, 2019

ISTANBUL TECHNICAL UNIVERSITY ★ INFORMATICS INSTITUTE

DESIGN OF THE FOUR ARM-DUAL POLARIZED SINUOUS ANTENNA WITH A NEW FEEDING APPROACH

M.Sc. THESIS

Sulayman JOOF
(705171036)

Department of Communication Systems

Satellite Communication and Remote Sensing Programme

Thesis Advisor: Assoc. Prof. Dr. Mehmet ÇAYÖREN

DECEMBER, 2019

İSTANBUL TEKNİK ÜNİVERSİTESİ ★ BİLİŞİM ENSTİTÜSÜ

YENİ BİR BESLEME YAKLAŞIMI İLE DÖRT KOLLU DUAL POLARİZE SİNUOUS ANTEN TASARIMI

YÜKSEK LİSANS TEZİ

Sulayman JOOF
(705171036)

İletişim Sistemleri Anabilim Dalı

Uydu Haberleşmesi ve Uzaktan Algılama Programı

Tez Danışmanı: Doç. Dr. Mehmet ÇAYÖREN

ARALIK, 2019

Sulayman JOOf , a **M.Sc.** student of ITU Informatics Institute student ID **705171036** successfully defended the **thesis** entitled "**DESIGN OF THE FOUR-ARM DUAL POLARIZED SINUOUS ANTENNA WITH A NEW FEEDING APPROACH**", which he prepared after fulfilling the requirements specified in the associated legislations, before the jury whose signatures are below.

Thesis Advisor :	**Assoc. Prof. Mehmet ÇAYÖREN** İstanbul Technical University	.....
Jury Members :	**Assoc. Prof. Serkan ŞİMŞEK** İstanbul Technical University	.....
	Asst. Prof. Evrim TETIK İstanbul Arel University	.....

Date of Submission : 15 November 2019
Date of Defense : 12 December 2019

To my family and friends,

FOREWORD

Under the teaching supervision of Prof. Mehmet Çayören, this thesis was successfully written in the 2019 Autumn semester at Istanbul technical University. I am eternally grateful to all the people that have put an effort to see the success of this thesis.

I would first like to thank my thesis advisor Prof. Mehmet Çayören for his continued support and advice throughout my masters studies. Working with him have been a huge learning curve in both academics and in the practical field of Electromagnetics which I will forever be thankful. I would also like to thank Assist. Prof. Tuba Yılmaz Abdolsaheb who motivated me to pursue my graduate studies. Prof. Yilmaz supported my education in every way possible. I was able to publish academic papers and participate in two different conference through her research. Thank you Prof. Yılmaz for your unconditional support and guidance throughout the past few years.

This work was supported in part by Istanbul Technical University (ITU) Vodafone Future Lab under Project No. ITUVF20180901P10. I was lucky to be granted a scholarship for the past year from İTÜ Vodafone Future Lab which has been a huge financial assistant during my studies and for the duration of this thesis.

A huge thanks to my fellow lab friends and teaching assistants that have shared their vast knowledge during my studies. A special thank you to Prof. Ibrahim Akduman for taking me in as a member of his team and for allowing me use all necessary instruments during the course of my studies and this thesis.

Finally, I would like to thank my family and close friends for all the support and patience.

December 2019

Sulayman JOOF
B.Sc. Electronics and
Telecommunication Engineering

TABLE OF CONTENTS

Page

FOREWORD ..... **ix**
TABLE OF CONTENTS ..... **xi**
ABBREVIATIONS ..... **xiii**
SYMBOLS ..... **xv**
LIST OF TABLES ..... **xvii**
LIST OF FIGURES ..... **xix**
SUMMARY ..... **xxiii**
ÖZET ..... **xxv**
1. INTRODUCTION **1**
1.1 Purpose of Thesis 2
1.2 Literature Review 2
1.2.1 Frequency independent antennas 2
1.2.1.1 The biconical antenna 4
1.2.1.2 Equiangular spiral antenna 5
1.2.1.3 Log-periodic antennas 7
1.2.1.4 Dipole array 11
1.2.2 Antenna radiation pattern 13
1.3 The Sinuous Antenna 14
2. SINUOUS ANTENNA DESIGN **17**
2.1 Antenna Geometry and Design Specifications 17
2.2 The Standard Four-Arm Sinuous Antenna Simulation 18
2.3 Performance of the Standard Four Arm Sinuous Antenna 18
2.4 The Standard Four-Arm Sinuous Antenna with Substrate 23
2.5 Modification of the Sharp Ends of the Four-Arm Sinuous Antenna 26
2.6 Feeding point Modification 28
2.7 Radiation Patterns of the Modified Four-Arm Sinuous Antenna 32
3. FEEDING NETWORK DESIGN **35**
3.1 Balun Design 36
3.2 Performance of the Baluns 40
4. INTEGRATION OF THE BALUNS WITH THE FOUR-ARM FEED POINT MODIFIED ANTENNAS **41**
4.1 Performance of The Integrated Antennas 42
4.2 The Modified Feed Four-Arm Sinuous Antenna with Cavity-backed Configuration 46
4.3 Performance of The Modified Feed Cavity-Backed Four-Arm Sinuous Antenna 48
4.4 Fabrication and Measurement of the Cavity-Backed Modified Feed1 Four-Arm Sinuous Antenna 53

5. CONCLUSION **61**
REFERENCES **63**
CURRICULUM VITAE **65**

ABBREVIATIONS

AR **:** Axial Ratio
FASA **:** Four Arm Sinuous Antenna
MFASA **:** Modified Four Arm Sinuous Antenna
UWB **:** Ultra-Wideband

SYMBOLS

a	: Equiangular spiral constant
Di	: Inner diameter of the sinuous antenna
Do	: Outer diameter of the sinuous antenna
d_n	: Distance between the nth and n+1 element of the log-periodic array
f	: Frequency
g	: Microstrip balun width
L	: Total length of spiral antenna
L_f	: Length of feed line
l_n	: Total length of the nth element for log-periodic array
N	: Number of arms of the sinuous antenna
R_b	: Radial distance of the biconical antenna
R_n	: Distance from the tip to the nth element of the log-periodic array
R_p	: The outer radius of the pth cell
P	: Number of cells of the sinuous antenna
$\underline{P}$	: Conducting arm of the spiral antenna
$\underline{Q}$	: Conducting arm of the spiral antenna
s	: Radial distance to a point on the equiangular spiral antenna
s_n	: Gap between elements of the log-periodic array
Z_o	: Characteristic impedance
α_p	: Angular width of the pth cell
β	: Angle between the teeth of the log-periodic antenna
Γ	: Scaling constant for log-periodic antenna
γ	: Geometric ratio of the log-periodic antenna
$\underline{\delta}$	: Dirac delta function
δ	: Rotation angle of the sinuous antenna
ε_r	: Relative permittivity
θ	: Elevation plane angle
κ	: Log-periodic antenna function
Λ	: Sinuous curve equation
λ	: Wavelength
μ	: Angle of planar log periodic
η	: Equiangular spiral angle with respect to x axis
ρ	: Radial distance of the equiangular spiral antenna
σ	: Spacing factor of log-periodic array
τ	: Growth rate
τ_p	: Ratio of the inner to the outer radius of the pth cell for the sinuous
ϕ	: Azimuth plane angle
φ	: Angle between the equiangular spiral and radial line from origin
χ	: Slot width of the log periodic antenna
ψ	: Angle between radial distance and the tangent to the spiral antenna

LIST OF TABLES

Page

Table 3.1 : Feed network dimensions 40
Table 4.1 : Final dimensions of the modified Feed1 and Feed2 antennas 49

LIST OF FIGURES

Page

Figure 1.1 : Biconical antenna. 4
Figure 1.2 : Spiral wire antennas: (a) Single spiral. (b) Two spiral ($\varphi_0 = 0, \pi$). (c) Multi spiral ($\varphi_0 = 0, \pi/2, \pi, 3\pi/2$). (d) Multi spiral ($\varphi_0 = 0, \pi/2, \pi, 3\pi/2$) 6
Figure 1.3 : Spiral plate and spiral slot antennas: (a) Single plate. (b) Two slot 7
Figure 1.4 : Typical metal strip log-periodic configuration and antenna structure: (a) Metal strip log-periodic configuration: (b) Log-periodic metal strip antenna 9
Figure 1.5 : Planar and wire logarithmically periodic antennas: (a) Planar. (b) Wire 9
Figure 1.6 : Planar and wire trapezoidal toothed log-periodic antennas: (a) Planar. (b) Wire. 10
Figure 1.7 : Log-periodic dipole array and associated connections: (a) Dipole array. (b) Straight connection. (c) Crisscross connection. (d) Coaxial connection. 12
Figure 1.8 : Coordinate system for antenna analysis. 13
Figure 1.9 : The sinuous geometry: (a) Sinuous curve. (b) Sinuous arm. 15
Figure 2.1 : Sinuous antenna design parameters. 17
Figure 2.2 : The standard four arm sinuous antenna: (a) Antenna orientation. (b) Discreet port feeding. 18
Figure 2.3 : The s-parameters of the standard four-arm sinuous antenna. 19
Figure 2.4 : Radiation patterns of the standard four-arm sinuous antenna: (a) f_0 = 2GHz, $\phi = 0°$. (b) f_0 = 2GHz, $\phi = 90°$. (c) f_0 = 3.05GHz, $\phi = 0°$. (d) f_0 = 3.05GHz, $\phi = 90°$. (e) f_0 = 4.1GHz, $\phi = 0°$. (f) f_0 = 4.1GHz, $\phi = 90°$. (g) f_0 = 5GHz, $\phi = 0°$ (h) f_0 = 5GHz, $\phi = 90°$. 20
Figure 2.5 : Radiation patterns of the standard four-arm sinuous antenna: (a) f_0 = 2GHz, $\phi = 0°$. (b) f_0 = 2GHz, $\phi = 90°$ (c) f_0 = 4.1GHz, $\phi = 0°$ (d) f_0 = 4.1GHz, $\phi = 90°$. (e) f_0 = 5GHz, $\phi = 0°$. (f) f_0 = 5GHz, $\phi = 90°$. 21
Figure 2.6 : The axial ratio of the standard four arm sinuous antenna at (a) $\phi = 0°$. (b) $\phi = 90^{\circ}$ 22
Figure 2.7 : The maximum gain at broadside of the SFASA $\phi = 0°$. 23
Figure 2.8 : Input impedance analysis of the SFASA with substrate: (a) Antenna with substrate. (b) S-parameters. 24
Figure 2.9 : Radiation patterns of the SFASA with substrate: (a) $\phi = 0°$. (b) $\phi = 90°$. 25
Figure 2.10 : Gain at broadside of the SFASA with substrate. 25
Figure 2.11 : Axial ratios of the SFASA with substrate: (a) $\phi = 0°$. (b) $\phi = 90°$. 26
Figure 2.12 : Sharp end modification of the SFASA with substrate: (a) Modification in [12]. (b) New modification 27
Figure 2.13 : Effect of Sharp end modification on the return loss of the antenna. 28
Figure 2.14 : Feeding modification of the FASA: (a) Modification in [18]. (b) Modification in [14]. (c) Modification in [15] 29

Figure 2.15 : Feed1 modification of the FASA: (a) Feed1 geometry. (b) Feed1 dimensions.....30
Figure 2.16 : Feed2 modification of the FASA: (a) Feed2 geometry. (b) Feed2 dimensions.....30
Figure 2.17 : S-parameters of the modified with average input impedance of 185Ω: (a) Feed1. (b) Feed2 31
Figure 2.18 : Comparison of the radiation patterns of the modified feeds with the SFASA: (a) 2GHz, $\phi = 0°$. (b) 3.05 GHz, $\phi = 0°$. (c) 4.1GHz, $\phi = 0°$. (d) 5GHz $\phi = 0°$.....33
Figure 2.19 : Comparison of the maximum gain at broadside of the modified feeds with the SFASA. 33
Figure 2.20 : Comparison of the axial ratios of the modified feeds with the SFASA: (a) 2GHz, $\phi = 0°$. (b) 3.05 GHz, $\phi = 0°$. (c) 4.1GHz, $\phi = 0°$. (d) 5GHz $\phi = 0°$ 34
Figure 3.1 : FASA feed network: (a) linear polarization. (b) Circular polarization. 35
Figure 3.2 : Microstrip baluns: (a) linearly tapered. (b) Exponentially tapered. 37
Figure 3.3 : The image theory: microstrip to paired strip 37
Figure 3.4 : The design exponentially tapered microstrip baluns: (a) Front and back view of the Feed1 balun. (b) Front and back view of the Feed2 balun. 38
Figure 3.5 : Feed network impedance matching with 185Ω resistor 39
Figure 3.6 : The S-parameters of the matched feed network with 185Ω resistor: (a) Feed1 s-parameters. (b) Feed2 s-parameters. 40
Figure 4.1 : The modified antennas integrated with the baluns: (a) Feed1 geometry and connections. (b) Feed2 geometry and connections. 41
Figure 4.2 : The s-parameters of the integrated antennas: (a) Feed1. (b) Feed2.....43
Figure 4.3 : Radiation patterns of the modified integrated four-arm sinuous antenna of Feed1 and Feed2: (a) f_0 = 2GHz, $\phi = 0°$. (b) f_0 = 2GHz, $\phi = 90°$. (c) f_0 = 3.05GHz, $\phi = 0°$. (d) f_0 = 3.05GHz, $\phi = 90°$. (e) f_0 = 4.1GHz, $\phi = 0°$. (f) f_0 = 4.1GHz, $\phi = 90°$. (g) f_0 = 5GHz, $\phi = 0°$. (h) f_0 = 5GHz, $\phi = 90°$.....44
Figure 4.4 : AR of the modified integrated antennas at $\phi = 90°$. (a) Feed1. (b)Feed2. 45
Figure 4.5 : Maximum Gain of the modified integrated antennas at broadside.....46
Figure 4.6 : Configurations of the antennas with cavity-backed: (a) Feed1 configuration. (b) Feed2 configuration. (c) Feed1 with absorber 47
Figure 4.7 : S-parameters comparıson of the cavity-backed Feed1 antenna with and without absorber: (a) Port1 return loss. (b) Port2 return loss. (c) Isolation 49
Figure 4.8 : S-parameters comparıson of the cavity-backed Feed2 antenna with and without absorber: (a) Port1 return loss. (b) Port2 return loss. (c) Isolation 50
Figure 4.9 : Radiation patterns of the modified cavity-backed four-arm sinuous antenna of Feed1 and Feed2 with absorbing material: (a) 2GHz, $\phi = 0°$. (b) 2GHz, $\phi = 90°$. (c) 3.05GHz, $\phi = 0°$. (d) 3.05GHz, $\phi = 90°$. (e) 4.1GHz, $\phi = 0°$ (f) 4.1GHz, $\phi = 90°$. (g) 5GHz, $\phi = 0°$. (h) 5GHz, $\phi = 90°$. 51
Figure 4.10 : AR of the modified cavity-backed antennas at $\phi = 90°$: (a) Feed1. (b)Feed2. 52
Figure 4.11 : Comparıson of the maximum Gain of the modified cavity-backed antennas at broadside with and without absorbing material: (a) Feed1. (b) Feed2 53
Figure 4.12 : Fabricated Feed1 FASA without cavity-backed measurement set-up. 54
Figure 4.13 : S-parameters of fabricated Feed1 FASA without cavity-backed: (a) Port1 return loss and isolation. (b) Port2 return loss and isolation 55

Figure 4.14 : Fabricated Feed1 FASA with absorber filled cavity-backed measurement set-up..... 56
Figure 4.15 : S-parameters of fabricated Feed1 FASA with absorber filled cavity-backed: (a) Port1 return loss and isolation. (b) Port2 return loss and isolation . 57
Figure 4.16 : Polarization measurement setup. 58
Figure 4.17 : S_{21} plots (a) Port1 sinuous antenna co and x-polarized. (b) Port1 sinuous antenna co and x-polarized. 59
Figure 4.18 : Maximum gain at broadside: (a) Port1 simulated and measured gain. (b) Port2 simulated and measured. 60

DESIGN OF THE FOUR-ARM DUAL POLARIZED SINUOUS ANTENNA WITH A NEW FEEDING APPROACH

SUMMARY

The several application of electromagnetics to the progression of technology have demanded the investigation and exploitation of a wider frequency spectrum. Moreover, emergence of broadband systems has necessitated the design of broadband antennas. Therefore, it is most desirable to design an antenna which is lightweight, simple and cost-effective operating over a wide frequency bandwidth. One candidate of antennas that meets most of the desired properties from the range of wideband antennas is the Sinuous Antenna. The sinuous antenna is an ultra-wideband, planar or conical shaped, self-complimentary geometry, frequency independent input impedance and can produce broadside radiation patterns with dual circular or linear polarization across broad beamwidths with a good gain across the entire frequency band. Because of its superior broadband characteristics and simultaneous polarization capability, the sinuous antenna has several applications in both the civil and military systems such as electronic warfare systems, direction finding systems, reflector-based searching systems, radio astronomy, radar and imaging systems. The key factor that limits the popularity of the sinuous antenna is the complexity of its feeding network. Virtually, the sinuous antenna has an unlimited bandwidth and the only limiting factor is its feeding network. In this thesis the four-arm sinuous antenna is design using two new feeding approaches. The proposed feeding approaches are done by modification of the standard fed sinuous antenna design by DuHamel (1987). The standard feed-point geometry of the four-arm sinuous antenna is practically impossible to be fed using a microstrip balun. Therefore, modifications must be made on the feed-points to practically fit in a microstrip feed line. The work on this thesis begins by free space simulation and analysis of the standard fed four-arm sinuous antenna . Then a substrate is added to the radiating four arms and the antenna properties such as the s-parameters, radiation patterns, gain, input impedance and axial ratio of the antenna with the substrate is analyzed. After the analysis of the standard antenna with substrate, two different modifications are implemented on the feeding point of the standard antenna. The modifications are made in such a way that a microstrip balun can be incorporated with the modified feed-points without causing much damage to the characteristics of the antenna. With the new modified feed points, the input impedance is determined so that the output of the balun can be calculated. Furthermore, the characteristics of the modified antennas are analyzed and compared. After the determination of the input impedance of the modified antennas, an exponential microstrip balun consisting of two feed lines to feed the two ports of the sinuous antenna are design. The baluns are then integrated with the modified antennas and both antennas are analyzed and compared. The sinuous antenna without a cavity-backed reflector has a bidirectional radiation pattern which is not desirable in most application. Therefore, the antennas are integrated with a metallic cavity and analyzed. The

analysis of the cavity-backed is based on the cavity filled with an absorbing material or without an absorbing material. Although in most cases, the cavity of the sinuous antenna is loaded with an absorbing material. Performance of the antennas with and without cavity backed show a good return loss, good gain, desired radiation patterns and low axial ratio compared to the modified feed antennas in literature. Additionally, a prototype of one of the proposed feeding structure is fabricated and measured in an anechoic chamber from 2-5GHz which is the intended working frequency bandwidth. A good agreement is observed between the simulated and measured results.

YENİ BİR BESLEME YAKLAŞIMI İLE DÖRT KOLLU DUAL POLARİZE SİNUOUS ANTEN TASARIMI

ÖZET

Son dönemde elektromanyetik teori ve ilgili alanlarda sağlanan teknolojik gelişmeler ve bunlarla bağlantılı uygulamalar giderek daha geniş bir frekans spektrumunun incelenmesini ve bu geniş bant aralığında çalışacak sistemler tasarlanmasını zorunlu kılmaktadır. Dahası, bu geniş bantlı sistemlerin hızla yayılması ve kullanıma girmesi geniş bantlı anten tasarımını öncelikli araştırma ve geliştirme konuları arasında üst sıralara taşımaktadır. Dolayısıyla, hafif, tasarımı ve üretimi kolay, düşük maliyetli, çok geniş bir frekans bandında kullanılabilecek anten tasarımlarının değeri ve önemi giderek artmaktadır. Bu sıralanan özellikleri haiz geniş bantlı anten tipleri arasında en kayda değer olanlardan biri spiral anten olarak adlandırılır. Bu tip antenler istenen geniş bantlı uygulamalar için en uygun adaylardan biridir. Spiral anten, ultra geniş bantlı, düzlemsel veya konik şekilli olabilen, frekanstan bağımsız giriş empedansına sahip bir anten tipidir. Bu antenlerin enine ışımalı bir radyasyon paterni vardır. En önemli özelliği olarak tüm frekans bandında geniş bir demet genişliğiyle ve yüksek kazançla ışıma yapar. Gene bu geniş bant aralığında ikili dairesel veya düzlemsel polarizasyon kullanımına uygun bir yapısı vardır. İşte bu geniş bant karakteristik özellikleri ve simültane polarizasyon kabiliyeti sayesinde spiral antenler hem sivil hem de askeri çeşitli uygulamalarda yaygın olarak kullanılmaktadır. Bunların arasında elektronik harp uygulamaları, yön bulma sistemleri, yansıtıcı bazlı arama sistemleri, radyo astronomisi, radar ve görüntüleme sistemleri sayılabilir. Spiral antenlerin daha yaygın olarak kullanılmasının önündeki en büyük engel besleme devresinin karmaşıklığıdır. Spiral antenin kolları arasında faz uyumunun sağlanması oldukça karmaşık ve pahalı besleme sistemlerinin kullanılmasını zorunlu kılmaktadır. Teorik olarak spiral antenlerin bant genişliği sınırsız olmasına ragmen pratikte besleme devresi bant genişliğini sınırlamaktadır.

Bu kısıtlama göz önünde bulundurularak bu çalışmada dört kollu spiral antenin beslenmesi için iki yeni yaklaşım geliştirilmiş ve anten tasarımında uygulanmıştır. Bu yeni geliştirilen besleme sitemleri DuHamel (1987) tarafından ortaya konulmuş mevcut standart spiral anten beslemesinin modifiye edilmesi ile elde edilmiştir. Geliştirilen besleme sistemi simetrik olmamakla beraber yine de spiral antenlerde istenilen ikili polarizasyon karakteristiğini koruyacak şekilde optimize edilmiştir. Standart besleme noktası geometrisi kullanıldığı durumda dört kollu spiral antenin mikroşerit balun kullanılarak beslenmesi mümkün değildir. Dolayısıyla pratik uygulamalarda mikroşerit bir hatla antenin beslenmesi için besleme noktalarında değişiklik yapılması gerekmektedir. Bu tezdeki çalışmlarda başlangıç olarak standart dört kollu spiral antenin boş uzaydaki davranışı incelenmiştir. Bu amaçla antenin boşluktaki ışıması simüle edilmiş ve sonuçlar analiz edilmiştir. Daha sonra aşamada ise ışıyan dört kollu anten yapısına bir substrat eklenmiş ve anten karakteristik

özellikleri analiz edilmiştir. S-parametreleri, ışıma paterni, anten kazancı, demet genişliği, giriş empedansı gibi karakteristik özellikler üzerinden substuratın dört kollu spiral antenin davranışına etkisi incelenmiştir. Standart anten ve substratın davranışı analiz edildikten sonra antenin besleme noktasında bu çalışmanın temelini oluşturan iki farklı değişiklik yapılmıştır. Bu değişiklikler yapılırken göz önünde bulundurulan temel husus mikroşerit balunun dört kollu spiral antenin boş uzay simülasyonlarında gözlenmiş olan karakteristik özelliklerinde fazla değişiklik yapmadan sisteme entegre edilmesidir. Standart anten tasarımında mikroşerit balunun besleme noktasından yapıya entegrasyonu anten karakteristiklerine ciddi zarar vermektedir. Burada arzulanan besleme noktasında yapılan modifikasyonlarla bu zararın asgariye indirgenmesidir. Bu amaç tez çalışmasının temel motivasyonunu oluşturmaktadır. Bu aşamada antenin giriş empedansı gerekli değişiklikler yapılmış yeni besleme noktaları göz önüne alınarak belirlenir. Bu giriş empedansının doğru şekilde belirlenmesi sistem tasarımı açısından hayati öneme sahiptir çünkü besleme devresinin çıkışı bu giriş empedansı değerine göre tasarlanmaktadır. Dolayısıyla sonraki aşamada bu değer göz önüne alınarak balunun çıkışında gözlenecek karakteristik özellikler hesaplanabilir. Bu aşamada antenin keskin uçlarının modifiye edilmesiyle düşük frekanslarda anten kaybını azaltacak bir değişiklik daha yapılmıştır. Bu işlemlerle beraber değiştirilmiş yeni dört kollu spiral anten tasarımının karakteristik özellikleri de analiz edilip eski standart anten tasarımıyla karşılaştırılmıştır. Üzerinde değişikler yapılmış antenlerin giriş empedansları hesaplandıktan sonra spiral antenin iki portunu besleyecek iki besleme hattından oluşan eksponansiyel mikro şerit balun tasarlanmıştır. Balun uyumsuz ve uyumlu uçları uygun sonlandırılarak test edilmiş ve kayıp değerleri ölçülerek empedans uyumu için bu balunun kullanılabileceği gösterilmiştir. Bu balunun tasarımı ve modifiye edilmiş spiral anten yapısına entegrasyonu tamamlandıktan sonra ortaya çıkan yapının bütünü analiz edilmiş ve bir kez daha mevcut standart dört kollu spiral anten yapısıyla sonuçlar karşılaştırılmıştır. Burada yapılan simülasyonlar ve analizler tasarlanan yapının yüksek kazanç ve düşük yansıma kaybına sahip olduğunu ortaya koymaktadır. Bu simülasyonlarda gözlenen diğer bir durum da antenin çift yönlü (bidirectional) ışıma paternine sahip olduğudur. Bu gözlem tez çalışmasının ikinci kısmına kaynaklık oluşturmaktadır.

Bu tez çalışmasının ikinci kısmında boşlukla desteklenmiş yansıtıcıların (cavity-backed reflector) anten davranışı üzerindeki etkisi analiz edilmiş ve bu yapıların spiral anten yapısına entegrasyonu sağlanmıştır. Bu işlemin arkasındaki temel motivasyon metalik boşlukla desteklenmiş yansıtıcıların anten karakteristikleri üzerindeki olumlu etkisidir. Bu etki özellikle spiral antenlerin verimliliğine önemli katkı sağlamaktadır. Boşlukla desteklenmiş yansıtıcı kullanılmayan spiral anten yapılarında çift yönlü (bidirectional) ışıma paterni gözlenmektedir. Bu durum pek çok pratik uygulamada istenmeyen etkiler oluşturmaktadır. Bunu göz önünde bulundurarak bu çalışmada dört kollu spiral anten tasarımına boşlukla desteklenmiş yansıtıcı entegre edilmiştir. Bu entegre yapı analiz edilirken boşluğun emici bir malzeme ile doldurulduğu ve doldurulmadan sadece hava içerdiği iki farklı durum incelenmiş ve anten karakteristikleri karşılaştırılmıştır. Yapılan karşılaştırmalar sonucu emici maddenin kullanıldığı durumda anten karakteristiklerinin istenilen özelliklere daha çok yaklaştığı gözlenmiş, ve bunun sonucunda incelenen durumların çoğunda spiral anten emici bir maddeyle doldurulmuş boşluk destekli yansıtıcıyla entegre edilmiş halde kullanılmıştır. Emici madde geriye doğru yönelen radyasyonu absorbe ederek istenilen ışıma paterninin oluşumuna katkı vermektedir. Bu maddeyi eklemenin bir diğer etkisi de düşük frekanslarda uyumluluğu arttırmasıdır. Genel olarak bu çalışma kapsamında geliştirilen dört kollu spiral anten tasarımlarının yansıtıcılı veya yansıtıcısız her iki

durumda da literatürde mevcut modifiye anten beslemelerine kıyasla daha yüksek kazanç ve daha düşük yansıma kaybına sahip oldukları analiz sonuçlarından anlaşılmaktadır. Işıma paterni de yine yansıtıcılı ve yansıtıcısız her iki durum için de pek çok uygulamada istenilen karakteristiklere sahiptir. Bu çalışmada tasarlanan antenin testleri sadece simülasyon ortamında yapılmamış aynı zamanda pratik olarak da ölçümler yapılmıştır. Bu amaçla tez kapsamında geliştirilen besleme tiplerinden birine sahip bir spiral anten prototipi üretilmiş ve test edilmiştir. Ölçümler istenilen çalışma bandı olan 2-5 GHz aralığında yapılmıştır. Bu ölçüm sonuçları simülasyon verileriyle deneysel ölçümler arasında yüksek seviyede bir uyuşma olduğunu ortaya koymuştur.

1. INTRODUCTION

The term sinuous can be defined as “moving in a twisting, curving, or turning, or having many curves”. Thus the sinuous antenna can be described as an antenna with zigzagging curves created in an alternating way. The dual polarized sinuous antenna was first invented and patented by DuHamel in 1987 [1]. The purpose of this invention was to design a wide bandwidth antenna which has two orthogonal senses of polarization. To be more precise, the sinuous antenna invented by DuHamel was designed to have a dual circularly polarized pattern and bandwidth characteristics identical to the singly circularly polarized log-spiral and Archimedes antennas. Before the invention of the dual polarized sinuous antenna, the Archimedes spiral and log-spiral antennas were implemented for many years to basically offer frequency independent performance over highly wide bandwidths. The most valuable type of spiral antennas used in applications such as direction finding and surveillance systems were mainly characterized by the following characteristics: two-arm cavity backed planar configuration with unidirectional rotationally symmetric patterns, a very small axial ratio and a unique sense of circular polarization over a hemisphere. Although the Archimedes and log-spiral antennas have important properties such as frequency independence, achieving both sense of circular polarization lead to problems such as feeding complexity and antenna dimensions. DuHam’s main aim was to achieve an antenna having practically unlimited bandwidth, frequency independent characteristics, dual senses of circular polarization and having radiation pattern comparable to the spiral antennas. The log-periodic antennas which is also a frequency independent antenna defined by angles was a good candidate in achieving the properties mentioned above. With a bit of modification in the parameters of the periodic antenna, DuHam invented a quasi-log-periodic sinuous antenna consisting of N conducting arms, where N is larger than two, emerging from a focal point and placed on a conical surface or a plane. The arms of the antenna swing up and down with growing radius over a sector of the surface and are specified by sinuous curves which are quasi-log-periodic or log-periodic in nature. Furthermore, the arms are placed at

equal distance and are identical such that the antenna structure is unmodified when rotated 360/N about its central axis.. Because of its planar configuration capability, the sinuous antenna has become familiar in many wideband applications in both the civil and military fields. There are several commercially available sinuous antennas for different frequency ranges found in market today.

1.1 Purpose of Thesis

The sinuous antenna is an ultra-wideband (UWB) antenna and can offer a variety of applications for UWB systems. Compared to the spiral antennas, the sinuous antenna has superior characteristics which are very useful for many UWB applications. It's an antenna that can be implemented as a planar antenna, it has a frequency independent property, and has a dual linear/circular polarized radiation pattern with a single aperture. With all its superiority, the sinuous antenna also has its drawbacks and one of its main contributors for the unpopularity of the sinuous antenna is its feeding network. In this thesis two new type of feeding approach is proposed for the four arm sinuous antenna. Additionally, a cavity backed reflector is integrated with the antenna in order to improve the gain of the antenna and an overall better performance across its working frequency.

1.2 Literature Review

Before the 1950s, the available broadband antennas with broadband impedance characteristics and broadband pattern possess bandwidths not higher than about 2:1. An evolutionary discovery which expanded the antenna bandwidth significantly to 40:1 or further was accomplished in the 1950s. The antennas developed by this discovery were named frequency independent and their configurations where defined by angles. These antennas where mainly utilized in the 10-1000MHz region in multiple applications such as TV, point-to-point communication, feeds for reflectors and lenses etc.

1.2.1 Frequency independent antennas

The theoretical breakthrough of frequency independent antennas were first introduced by Rumsey [2] and theoretical simplification for three dimensional structures was made by Elliott [3]. In antenna theory basics, the impedance and the pattern

characteristics of any radiating element can be defined by its unique shape and size with respect to the wavelength at a specified operating frequency. A frequency independent antenna is defined as an antenna that does not change its properties when scaled arbitrarily to a larger or smaller size and this theory is valid given that if the scaled version of the structure stays the same as the original or its rotated form. The antenna scale modeling theory states that, properties like pattern, polarization, impedance etc. are invariant to a change of physical size if the same change is likewise carried out in the wavelength or operating frequency. For instance, suppose all the physical dimensions of the antenna are decreased by a factor of three, then by increasing the operating frequency by a factor of three will hinder the performance of the antenna to remain same. In short, the performance of the antenna is unvarying if the electrical dimensions stay unchanged. Hence, by the theory developed by Rumsey, the pattern and impedance properties would have to be independent of frequency if the configuration of the antenna where totally defined by angles [1].

Research and design of wideband antennas have been focus for antenna engineers since the 1940s. The biconical antenna was designed and its performance was described using Maxwell's equations by Schelcunoff in 1943 [4]. Furthermore, he introduced analytical equations for antenna impedance characteristic for numerous antenna configurations of identical shape to the biconical. The biconical is still a widely used antenna and its discovery has inspired the development of several types of antennas such as the planar bow-tie antenna created by Brown and Woodward in 1952 [5]. Instigated by the work of Rumsey, a new class of frequency independent antennas was introduced in the 1950s. The Equiangular and Archimedean spiral antennas were introduced first and spiral antennas are known to realized up to 10:1 bandwidth while offering circular polarization in a small low profile structure [5][6]. As advancement it's been done on spiral antennas, DuHamel and Isbell developed the first ever successful log-periodic antenna integrated with a self-complimentary geometry comprised of two angular strips supporting curved teeth [6]. Since there were some limitations with the spiral antennas in achieving dual polarization over a wide bandwidth, inspired by the log-periodic antenna, DuHamel invented and patented the sinuous antenna. For many years, a broadband antenna that can simultaneously allow orthogonal senses of polarization has been of interest to researchers and different methods have been utilized to achieve such requirements using spiral antennas and

cross-log periodic antennas with little success. The main encountered problems where due impractical size, complex feeding network, mismatch E and H plane radiation pattern, or not frequency independent [1][6]. DuHamel figured out that a circumferential current distribution is the solution in aligning the E and H plane radiation pattern beamwidths and for the purpose of minimizing the antenna size, he designed a zigzagged geometry. Finally, the sinuous antenna maintained the characteristics of spiral antenna including low profile, small size, gain and beam widths while offering dual linear or dual circular polarization.

1.2.1.1 The biconical antenna

As shown in Figure 1.1, the biconical antenna is an uncomplicated configuration that can be utilized to realize broadband characteristics constructed by placing two cones of infinite length together. The working principle of the biconical antenna is based on the fact that the thicker the radiator or wire, the wider the impedance bandwidth and supposed the conductors were flared there will be a further increment in the bandwidth [7]. Although the biconical antenna geometry can be entirely defined by angles, the current on its geometry does not weaken with distance away the input terminals and lack of limiting pattern form with frequency. It is evident that there is phase but no amplitude changes with the radial distance R_b. Thus the biconical configuration cannot be shortened to create a frequency independent antenna [8]. Additionally, the biconical is not planar and does not have UWB capabilities but it initiated the research towards increasing the bandwidth of antennas.

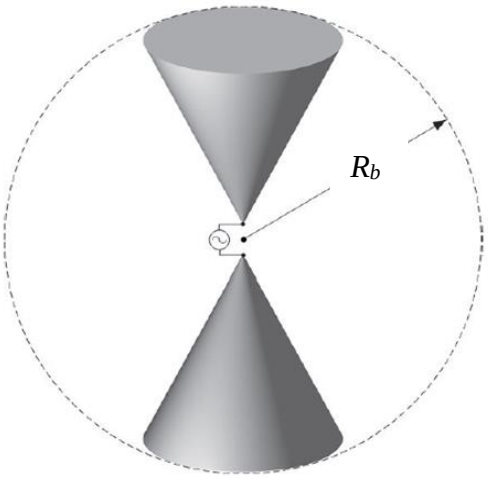

Figure 1.1 : Biconical antenna.

1.2.1.2 Equiangular spiral antenna

One of the existing geometrical structures whose surface can be entirely described by angles is the equiangular spiral antennas. Consequently, it meets all the requisite for frequency independent antennas geometries. The curve along the surface of the equiangular antennas extend to infinity, therefore, in order to define finite size of the antenna it is essential to assign the length of the arm. The minimum frequency of operation take place when the total arm length is analogous to the wavelength [9]. The pattern and impedance characteristics are frequency independent for all frequencies above this. The surface of the equiangular planar spiral curve can generated by the equation**:**

$$s = e^{a\varphi} f(\eta) \tag{1.1}$$

where *s* represents the distance along the surface or edge and $f(\eta)$ is given by

$$f(\eta) = \left(A\underline{\delta}\left(\frac{\pi}{2} - \eta\right)\right) \tag{1.2}$$

Here, A is a constant and $\underline{\delta}$ represents the Dirac delta function. Using (1.1) reduces (1.2) to

$$s|_{\eta=\frac{\pi}{2}} = \rho = \begin{cases} Ae^{a\varphi} = \rho_0 e^{a(\varphi-\varphi_0)} & \eta = \pi/2 \\ 0 & \text{elsewhere} \end{cases} \tag{1.3}$$

Where,

$$A = \rho_0 e^{a(\varphi-\varphi_0)} \tag{1.4}$$

In wavelengths (1.4) can be given as:

$$\rho_\lambda = \frac{\rho}{\lambda} = \frac{Ae^{a\varphi}}{\lambda} = Ae^{a[\varphi - ln(\lambda)/a]} = Ae^{a(\varphi-\varphi_1)} \tag{1.5}$$

Where,

$$\varphi_1 = \frac{1}{a} ln(\lambda) \tag{1.6}$$

An alternative form is given as:

$$\varphi = \frac{1}{a} ln\left(\frac{\rho}{A}\right) = \tan\psi \ln\left(\frac{\rho}{A}\right) = \tan\psi \ (\ln\rho - \ln A\ ) \tag{1.7}$$

where $1/a$ is the rate of growth of the spiral and ψ is the angle between the radial distance ρ and the tangent to the spiral, as depicted in Figure 1.2 (a). The total length L of the spiral can be found by

$$L = \ (\rho_1 - \ \rho_0)\sqrt{1 + \frac{1}{a^2}} \tag{1.8}$$

Where ρ_0 and ρ_1 correspond to the inner and outer radii of the spiral. Several kinds of structure can be used to generate different forms of the spiral antenna system. Figure 1.2(b) is generated when φ_0 in (1.3) is chosen as 0 and π while the geometries in Figure 1.2(c) and Figure 1.2(d) are generated when φ_0 = 0, π/2, π and 3π/2.

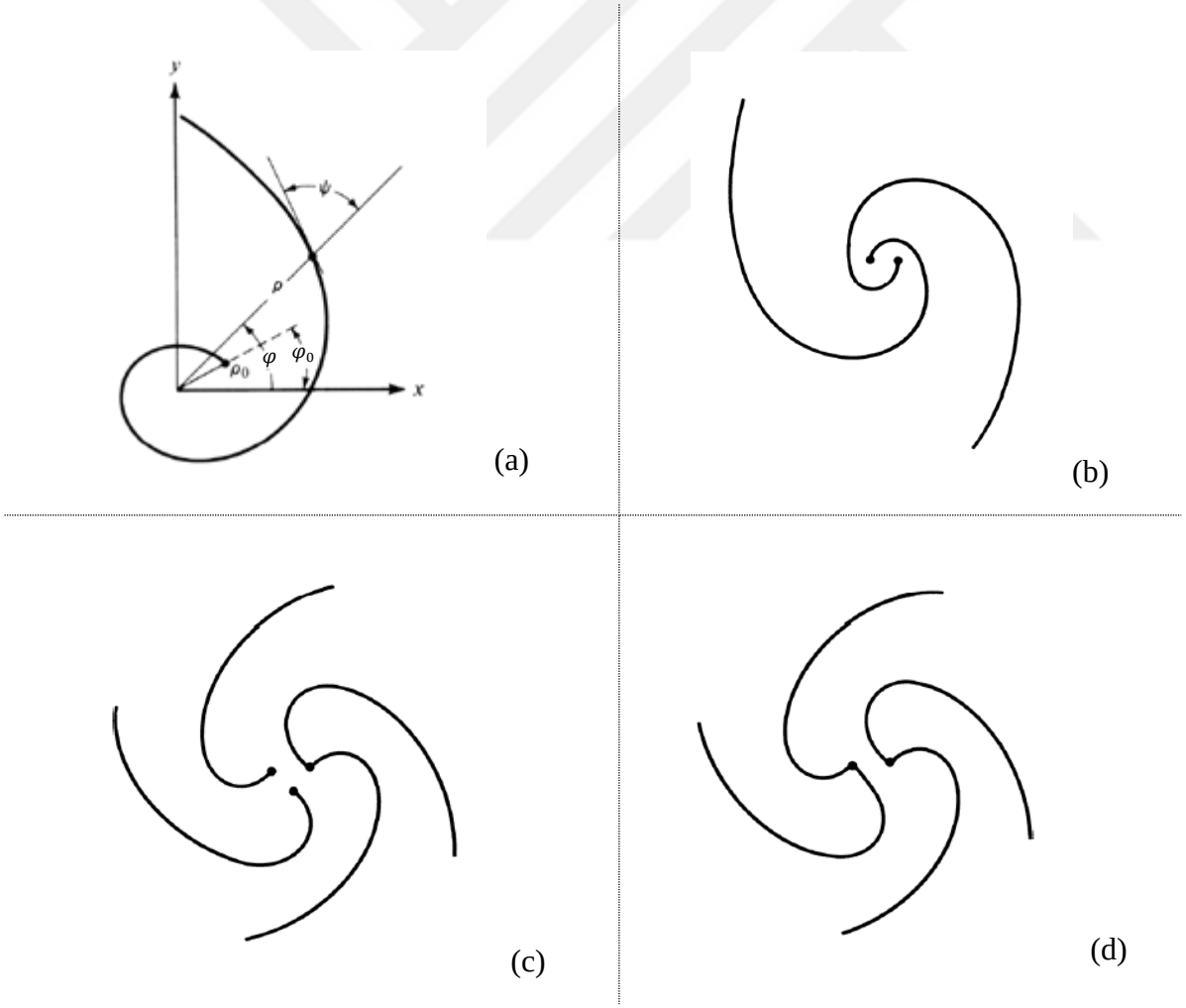

Figure 1.2 : Spiral wire antennas: (a) Single spiral. (b) Two spiral (φ_0 = 0, π). (c) Multi spiral (φ_0 = 0, π/2, π, 3π/2). (d) Multi spiral (φ_0= 0, π/2, π, 3π/2).

Additionally, an equiangular metallic solid surface, designated as $\underline{P}$ and Q, can be generated by determining the curves of its edges, using (1.3). As shown in Figure 1.3, the system is consisting of the two conducting arms, $\underline{P}$ and Q represents a symmetrical system. The definite length L_0 spiraling along the center line of the arm specifies the finite length of the structure. The whole structure can be entirely specified by the rotation angle $\underline{\delta}$, the arm length L_0, the rate of spiral $1/a$, and the terminal size ρ. Furthermore, each arm is generally tapered at its end, shown by dashed lines in Figure 1.3 (a), to offer a better matching termination. With $\underline{\delta} = \pi/2$ the antenna is self-complementary, as defined by Babinet's principle [9], and its input impedance for an infinite structure should be $188.5 \simeq 60\pi\ \Omega$s. Similarly, same analytical procedure can be used to create another type of spiral antenna called spiral slot which is formed on a large conducting plane as shown is Figure 1.3 (b). To keep the overall balance of the antenna, the slot antenna can be easily feed by a balanced coaxial arrangement which makes it the most practical [10].

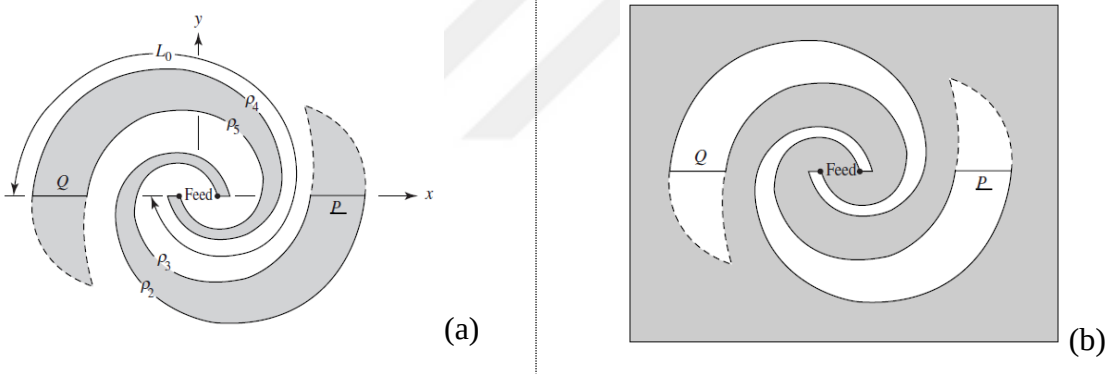

Figure 1.3 : Spiral plate and spiral slot antennas: (a) Single plate. (b) Two slot.

1.2.1.3 Log-periodic antennas

In 1957, DuHamel and Isbell invented another antenna structure which closely analogue the frequency independent notion [6]. The concept of log periodic antennas is based on the fact if an antenna is transformed or its rotated form when scaled by a specific constant Γ it would become a periodic function with similar characteristics at frequencies f and Γf. Considering that the period of the periodic function is of the logarithmic form ($|\log \Gamma|$), they are referred to as log periodic antennas [11]. Generally, log periodic antennas are specified by angles and a scale factor γ. It is possible to limit

the deviation of performance by within the required band by setting γ approximately to zero. Additionally, quasi-log-periodic antenna are formed if γ and or the angles depended on a particular parameter of the dimensions of the antenna.

A planar log periodic is comprises of a metal strip whose edges are defined by the angle $\mu/2$ as shown in Figure 1.4(a). Nonetheless, for the purpose of specifying a length from the origin to any point on the configuration, a distance attribute have to be incorporated. Therefore, using spherical coordinates, the shape of the structure can be given as:

$$\kappa = \text{ periodic function of } [b\ ln\ (r)] \tag{1.9}$$

an instance of a structure is given as:

$$\kappa = \kappa_0\ sin\left[b\ ln\left(\frac{r}{r_0}\right)\right] \tag{1.10}$$

from (1.10), it is apparent that the values of κ are recurrent every time that the logarithm of the radial frequency ln(ω) = ln(2π*f*) varies by 2π/b. A periodic system performance as a function of the logarithm of the frequency is obtained. Hence, the name log-periodic or logarithmic-periodic.. A linearly polarized log-periodic antenna is given in Figure 1.4(b). It comprises of two coplanar arms configuration and the pattern created is unidirectional toward the tip of the cone created by the two arms. Even though the patterns of the presented log-periodic and similar configurations are not entirely frequency independent, there is a small variation in amplitude of certain designs. Therefore, basically, they are frequency independent.

While examining the current distribution on surface of the geometry depicted in Figure 1.5(a), DuHamel realized a sharp attenuation with the field on the radiators with distance. This implies that maybe there is a substantial current intensity at or almost the edges of the radiators. Consequently, the decision to remove the inner surface to create a wire antenna as shown in Figure 1.5(b), shouldn't critically affect the antenna performance. This discovery lead to a much simpler, lighter in weight, cheaper, and less wind resistant antenna.

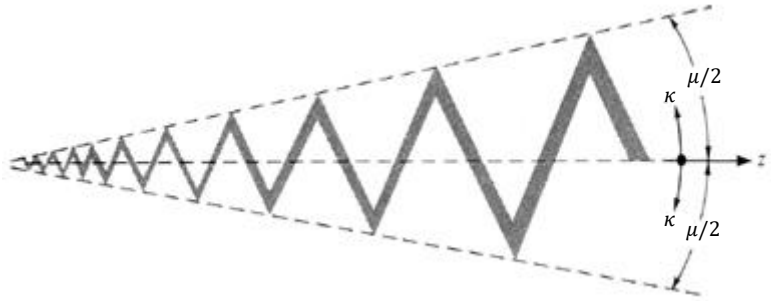

(a)

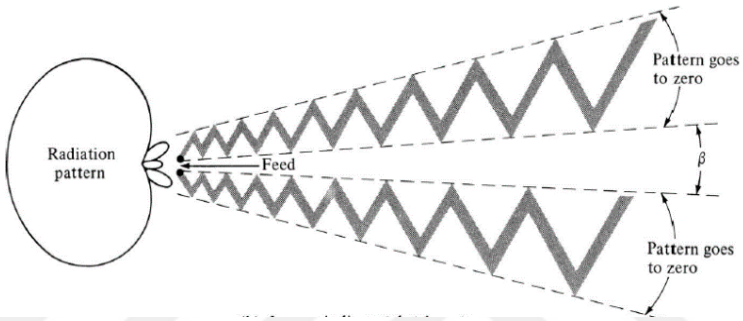

(b)

Figure 1.4 : Typical metal strip log-periodic configuration and antenna structure: (a) Metal strip log-periodic configuration. (b) Log-periodic metal strip antenna.

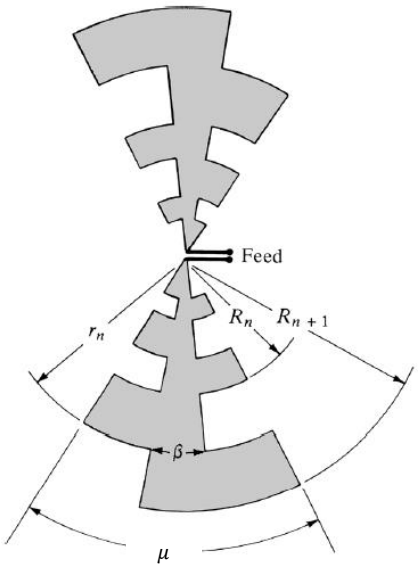

(a)

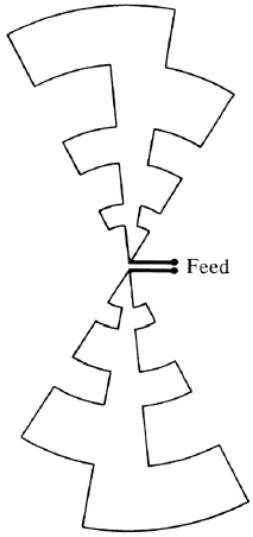

(b)

Figure 1.5 : Planar and wire logarithmically periodic antennas: (a) Planar. (b) Wire.

Given that the configurations of Figure 1.5 utilize uniform periodic teeth, the geometric ratio of the log-periodic structure is defined by

$$\gamma = \frac{R_n}{R_{n+1}} \tag{1.11}$$

the width of the antenna slot is also defined as:

$$\chi = \frac{r_n}{R_{n+1}} \tag{1.12}$$

The period of operation is defined by the geometric ratio τ in equation (1.11). for instance the geometric ratio γ is related to two frequencies f_1 and f_2 which are separated by one period as

$$\gamma = \frac{f_1}{f_2}, \qquad f_2 > f_1 \tag{1.13}$$

Suppose that the edges or the wires of the plates of the structures shown in Figure 1.5 are linear instead of curved, then the structures are reduced to the trapezoidal tooth log-periodic as shown in Figure 1.6. Such streamlining lead to more suitable fabrication geometries with practically no loss in performance.

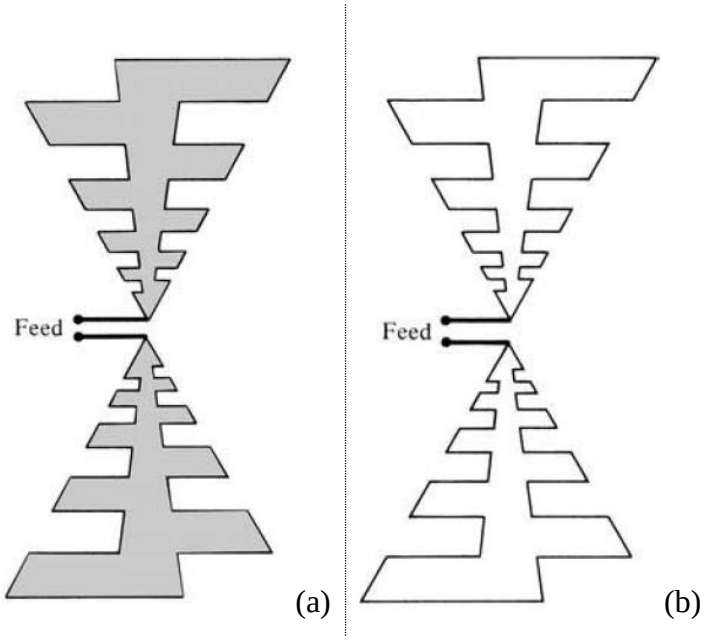

Figure 1.6 : Planar and wire trapezoidal toothed log-periodic antennas: (a) Planar. (b) Wire.

Typically, these geometries have similar performance like the planar spiral structures. The major key difference is the log-periodic configurations are linearly polarized instead of circular.

1.2.1.4 Dipole array

To the armature person, the log-periodic antenna shown in Figure 1.7(a) is the most familiar antenna structure developed by Isbell [8]. The configuration is comprising of series of side-by-side parallel linear dipoles generating a coplanar array. Compared to the Yagi-Uda antennas, dipole antennas have somewhat lesser directivities but they are realizable and sustained over much wider bandwidths. Although their significant differences between them. For instance, while a single element of the Yagi–Uda array is directly excited by the feed line, while the rest act like parasitic elements, all the elements of the log-periodic array are connected.

The lengths $(l_n's)$, spacings $(R_n's)$, diameters $(d_n's)$ and gap spacing at the diapole centers $(s_n's)$ of the log-periodic array expand logarithmically as defined by the inverse of the geometric ratio γ given by

$$\frac{1}{\Gamma} = \frac{l_2}{l_1} = \frac{l_{n+1}}{l_1} = \frac{R_2}{R_1} = \frac{R_{n+1}}{R_n} = \frac{d_2}{d_1} = \frac{d_{n+1}}{d_n} = \frac{s_2}{s_1} = \frac{s_{n+1}}{s_n} \tag{1.14}$$

The spacing factor σ is another parameter that is commonly related to the log-periodic antenna given by

$$\sigma = \frac{R_{n+1} - R_n}{2R_{n+1}} \tag{1.15}$$

As seen in Figure 1.7(a), the log-periodic antenna possess the frequency independent characteristics when an angle 2μ is created by the straight lines that meet through the dipole ends. Figure 1.7(b) and 1.7(c) shows the two fundamental methods of feeding the log-periodic antenna. While Figure 1.7(d) shows a more practical method using a coaxial cable as a feed line to achieve the 180° phase reversal between adjacent elements. Feeding is done at the small end of the configuration in all cases.

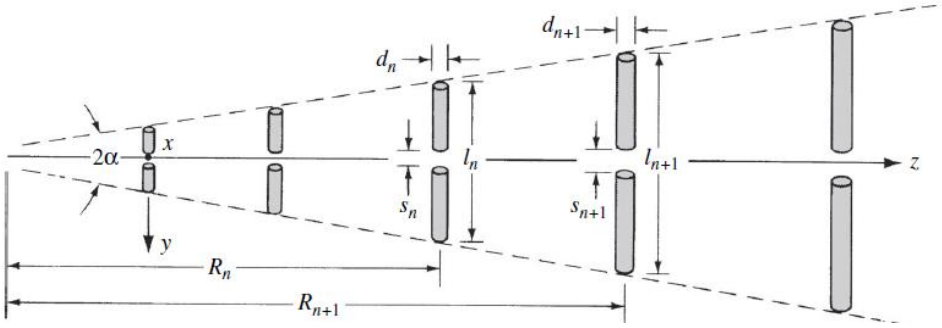

(a)

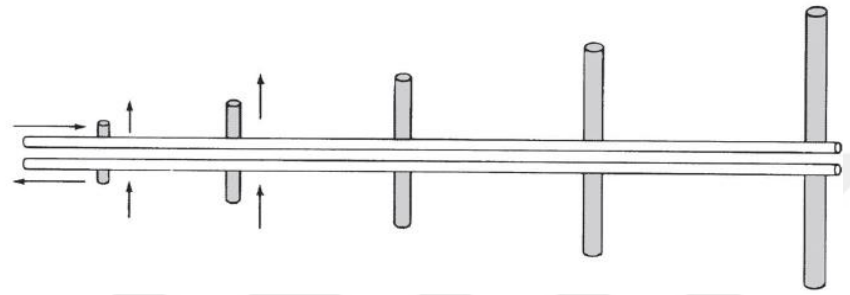

(b)

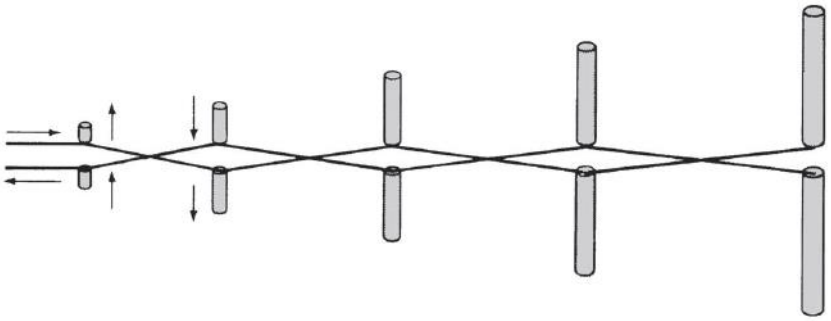

(c)

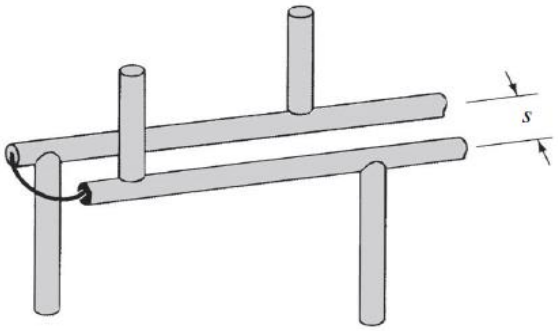

(d)

Figure 1.7 : Log-periodic dipole array and associated connections: (a) Dipole array. (b) Straight connection. (c) Crisscross connection. (d) Coaxial connection.

1.2.2 Antenna radiation pattern

An antenna radiation pattern or antenna pattern is defined as "a mathematical function or a graphical representation of the radiation properties of the antenna as a function of space coordinates. Usually, the patterns are defined using spherical coordinates implemented in the Fairfield region of the antenna where the magnitudes of electric and magnetic fields have inversely proportional dependence on constant radius r. A suitable set of corordinates used to describe the dependence of the patterns on the angles is shown in Figure 1.8. This set of coordinates will also be used as a reference for the placement of the sinuous antenna in this thesis. In this thesis, all the antennas are positioned at the origin and placed flat in the xy plane. Without a reflector, the sinuous antenna is bidirectional broadside antenna. Therefore $\theta = 0^{\circ}$ and $\theta = 180^{\circ}$ can represent two oppositely directed radiation lobes directed in the positive and negative z-direction respectively. For analysis purpose, two-dimensional radiation patterns will be presented. The set of standard cuts will be taken at $\phi = 0^{\circ}$ and $\phi = 90$. Analyzing the antenna at these angles should give a complete narrative of the general three dimentional performance of the antenna.

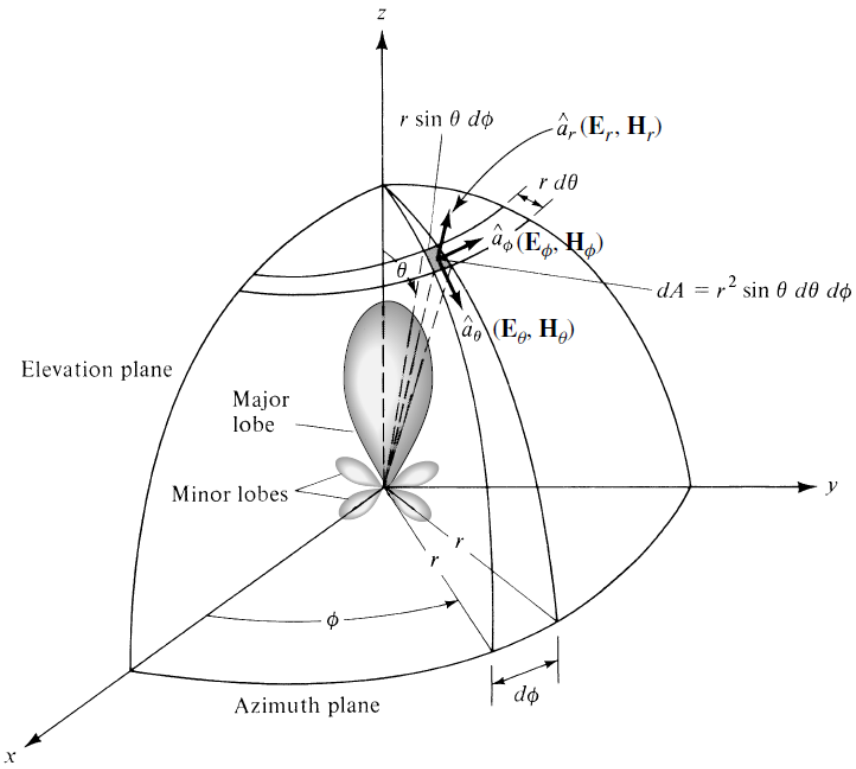

Figure 1.8 : Coordinate system for antenna analysis.

1.3 The Sinuous Antenna

From the previous information discussed, the sinuous antenna is considered as frequency independent log-periodic or quasi-log antenna meaning that it is specified by angles and design ratio τ. The sinuous antenna is created with N "arms" consisting of P "cells" that are scaled in dimensions with respect to each other. The P^{th} cell can vary from the biggest, first and outermost cell to the smallest and innermost cell P where R_p represents the outer radius of the P^{th} cell. As mentioned in [1], the sinuous curve is generated for the P^{th} is defined by the equation:

$$\Lambda = (-1)^p \alpha_p \sin\left[\frac{180 ln\left(m/R_p\right)}{ln(\tau_p)}\right] \qquad R_{p+1} \leq m \leq R_p \tag{1.16}$$

Where α_p is a positive number determining the angular width and the ratio $\tau_p = \frac{R_p}{R_{p-1}}$ is the ratio of the inner and outer radius of cell P as shown in Figure 1.9(a). The sinuous curve follows the log-periodic principle if τ and α are constants and is considered as quasi-log periodic if τ_p and α_p are dependent on the cell number.

Generating the sinuous arm from the sinuous curve requires the addition of a new parameter delta δ. The parameter $\alpha_p + \delta$ is responsible for shifting two curves and creating an arm while doing so as shown in Figure 1.9(b). Therefore, the sinuous arm equation can be written as:

$$\Lambda = (-1)^p \alpha_p \sin\left[\frac{180 ln\left(m/R_p\right)}{ln(\tau_p)}\right] \pm \delta \quad R_{p+1} \leq m \leq R_p \tag{1.17}$$

The designed parameters of the sinuous antenna mention above are design friendly in the sense that it is up to the designer to choose the appropriate dimensions but there are some know constrains that needs to be considered. For instance, the sum of τ_p and δ are known to affect the gain, efficiency, and frequency response of the antenna and therefore should be carefully chosen. In [1] and [6] good gain efficiency is maintain when $\tau_p + \delta < 70^{\circ}$. For an N arm sinuous antenna δ is the parameter that is used to satisfy the self-complimentary property. Therefore, The frequency independence of

the sinuous antenna heavily depends of the delta parameter δ. The self-complimentary condition of the sinuous antenna is given as:

$$\delta = \frac{180}{2N} \tag{1.18}$$

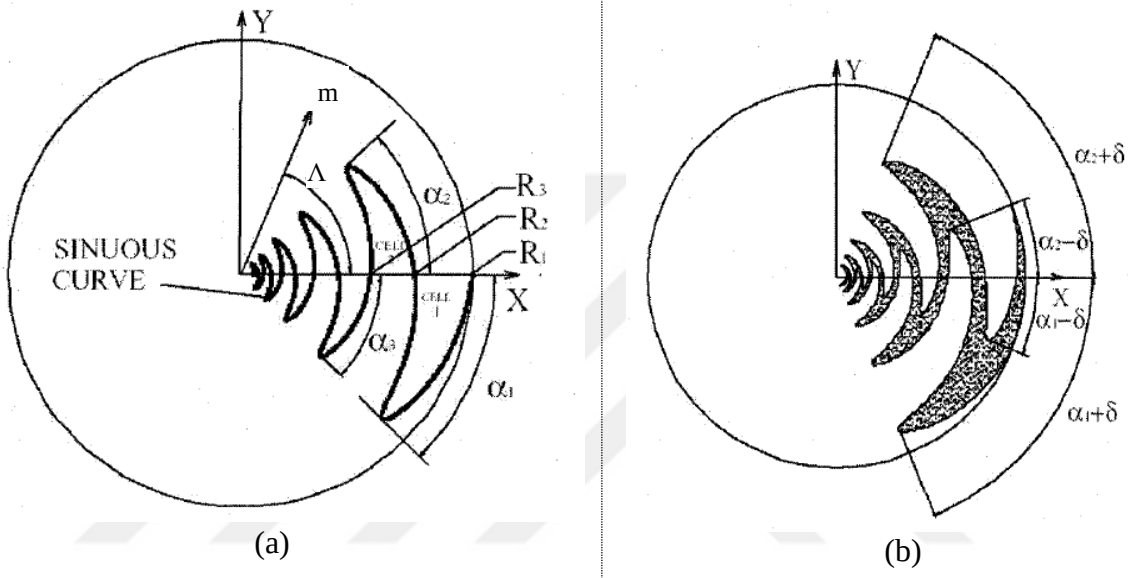

Figure 1.9 : The sinuous geometry: (a) Sinuous curve. (b) Sinuous arm.

For a self-complimentary configuration, the input impedance of each antenna arm-pair is given as:

$$Z = \frac{60\pi}{\sin\left(\frac{180}{N}\right)} \ [\Omega] \tag{1.19}$$

Practically, for a sinuous antenna design on a substrate, the input impedance is expected to be less than the value given in (1.19) due to the effects of the dielectric substrate. There is a direct relationship between the bandwidth and the physical dimension of the radius of the sinuous curve. The R_1 and R_p parameters define the lower and upper frequency limits and can be achieve due to the approximate relation given as :

$$2m(\alpha_p + \delta) \approx \frac{\lambda}{2} \tag{1.20}$$

Therefore,

$$R_1 = \frac{\frac{\lambda_L}{4}}{(\alpha_p + \delta)}, \qquad R_p = \frac{\frac{\lambda_H}{4}}{(\alpha_p + \delta)} \tag{1.21}$$

Where λ_L and λ_L are the lower and upper frequencies for the required bandwidth. To implement a balance feeding network for the opposite arms of the antenna, it is advantageous to decrease the radius R_p by half. Furthermore, when the design parameter τ which is defined as the ratio of the inside to the outside radius of each cell approaches unity, there is an increment in the number of cells and therefore generates a lower progressive change between each radiating region. Based on this property, higher resolution in frequency radiating parts are created.

When designing a sinuous antenna, it is paramount as a designer to be able to make a good trade-off between the totality of coupling between the neighboring arms, between the size of the arms, the amount of loss, the number of cells and the amount of frequency radiating resolution.

2. SINUOUS ANTENNA DESIGN

2.1 Antenna Geometry and Design Specifications

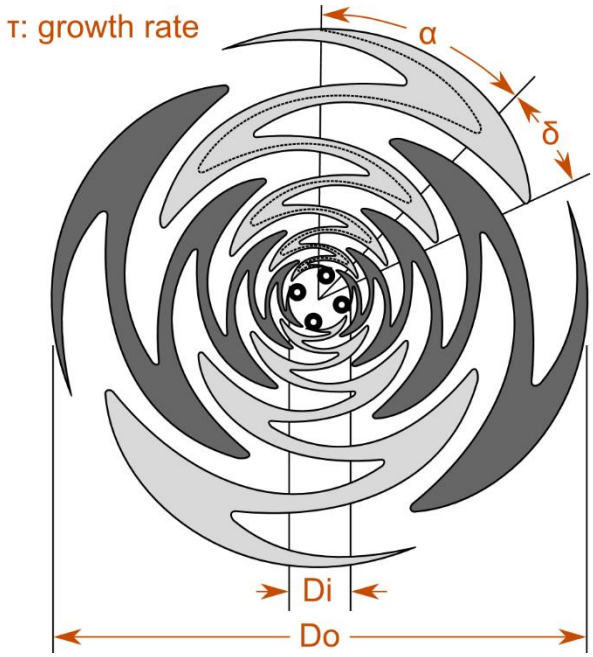

Figure 2.1 : Sinuous antenna design parameters.

Figure 2.1 shows the design parameters required to generate a single arm of the sinuous antenna where τ is the growth rate**,** α is the angular width**,** δ is the rotation angle**,** Di is the inner diameter and Do is the outer diameter**.** Additionally, P is the number of cells per arm. After the single arm is generated the other 3 arms can be created by a rotating the single arm $90°, 180°$ and $270°$ respectively. The lower frequency of the antenna may be decreased by increasing the outer diameter of the antenna and vice versa. Similarly, the upper frequency may be increased by decreasing the inner diameter of the antenna and vice versa. The default design for a self-complementary antenna with rotation angle δ = 22.5 degrees which gives average input resistance over the band close to 267Ωs, i.e. the Deschamps value for an infinite four-arm self-complementary antenna with appropriate excitation [1].

2.2 The Standard Four-Arm Sinuous Antenna Simulation

Initially, the standard self-complimentary antenna with an input impedance of 267Ωs is designed. The design parameters for the intended frequency band are taken as $\delta = 22.5$, $\alpha = 45°$ and $\tau = 0.8$. For these parameters the inner and outer diameters are given as Di = 12.72 and Do = 76.34. Figure 2.2(a) shows the orientation of the generated four arm sinuous antenna with 9 cell arm (P = 9). This antenna is first simulated in free space without a substrate. Two opposite arms where used to form a single port and each is feed using a discreet port with reference input impedance at both ports as 267Ωs as shown in Figure 2.2(b). All the simulations are performed using CST microwave studio.

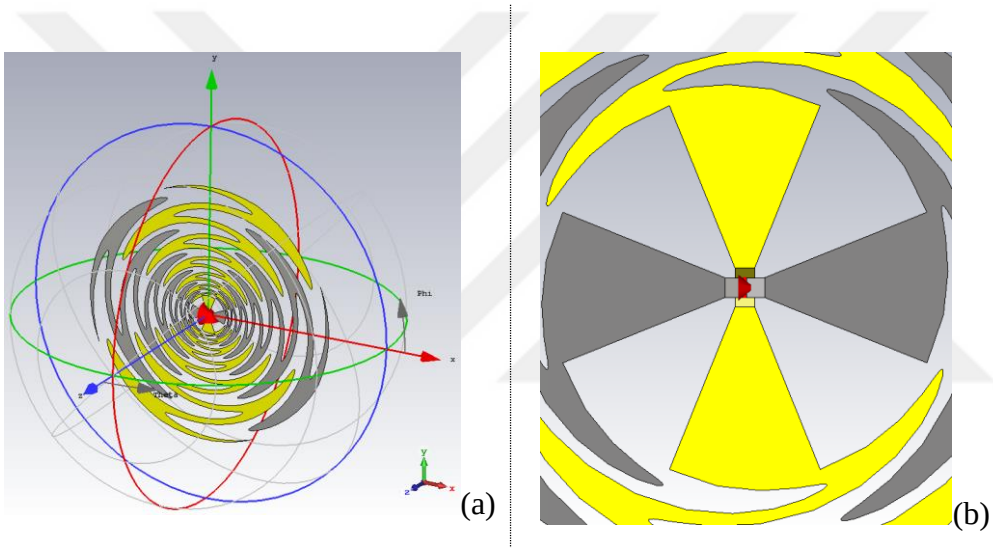

(a) (b)

Figure 2.2 : The standard four arm sinuous antenna: (a) Antenna orientation. (b) Discreet port feeding.

2.3 Performance of the Standard Four Arm Sinuous Antenna

First, S-Parameters of the antenna is analyzed. Figure 2.3 shows the s_{11}, s_{22}, s_{21} and s_{12} parameters of the antenna. It can be seen that the antenna has less than -15dB for both the s_{11} (return loss of port 1) and s_{22} (return loss of port 2) parameters over the 2-5GHz frequency range. The s_{21} and s_{12} parameters also indicates a good isolation between the two ports.

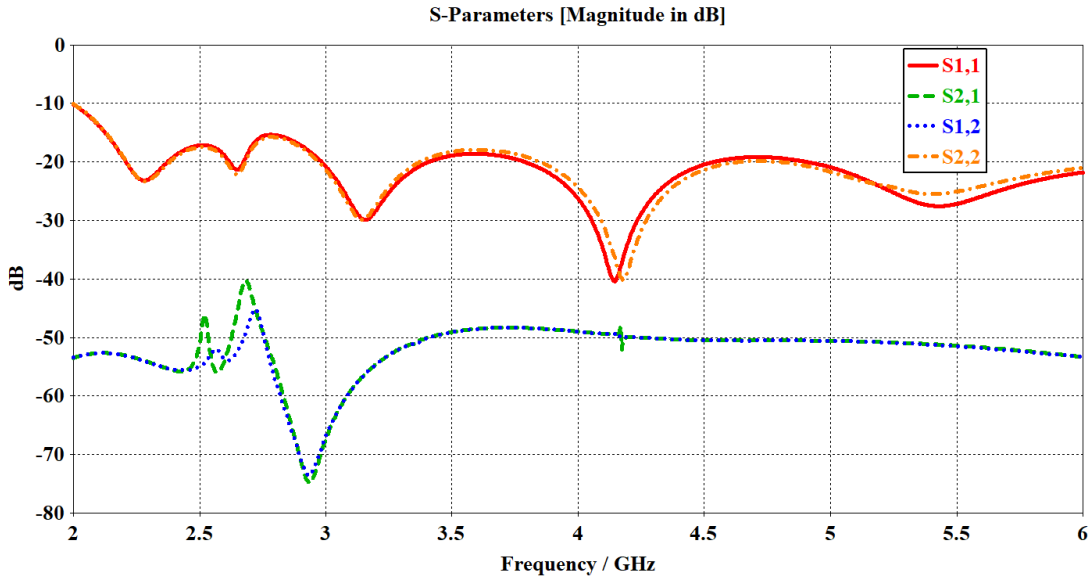

Figure 2.3 : The s-parameters of the standard four-arm sinuous antenna.

Furthermore, the far-field monitors were added in the simulation in order to monitor the performance of the antenna over the desired frequency band. As mentioned earlier, the antenna is positioned at the origin and placed flat in the xy plane as shown in Figure 2.2(a). Therefore , the set of standard cuts will be taken at $\phi = 0^{\circ}$ and $\phi = 90°$ in order to analyze the radiation pattern of the antenna. Since the antenna is symmetric as seen from Figure 2.3, in this case only one port is analyzed. Figure 2.4 shows the radiation patterns for $\phi = 0^{\circ}$ and $\phi = 90°$ at different frequency points. Without a cavity backed, the four-arm sinuous antenna possesses a bidirectional radiation pattern for all frequencies as depicted in Figure 2.4. In addition, the 3D radiation patterns are also shown for some selected frequencies in Figure 2.5. The frequency independence property of the antenna can be evidently seen since the patterns are all identical to each other.

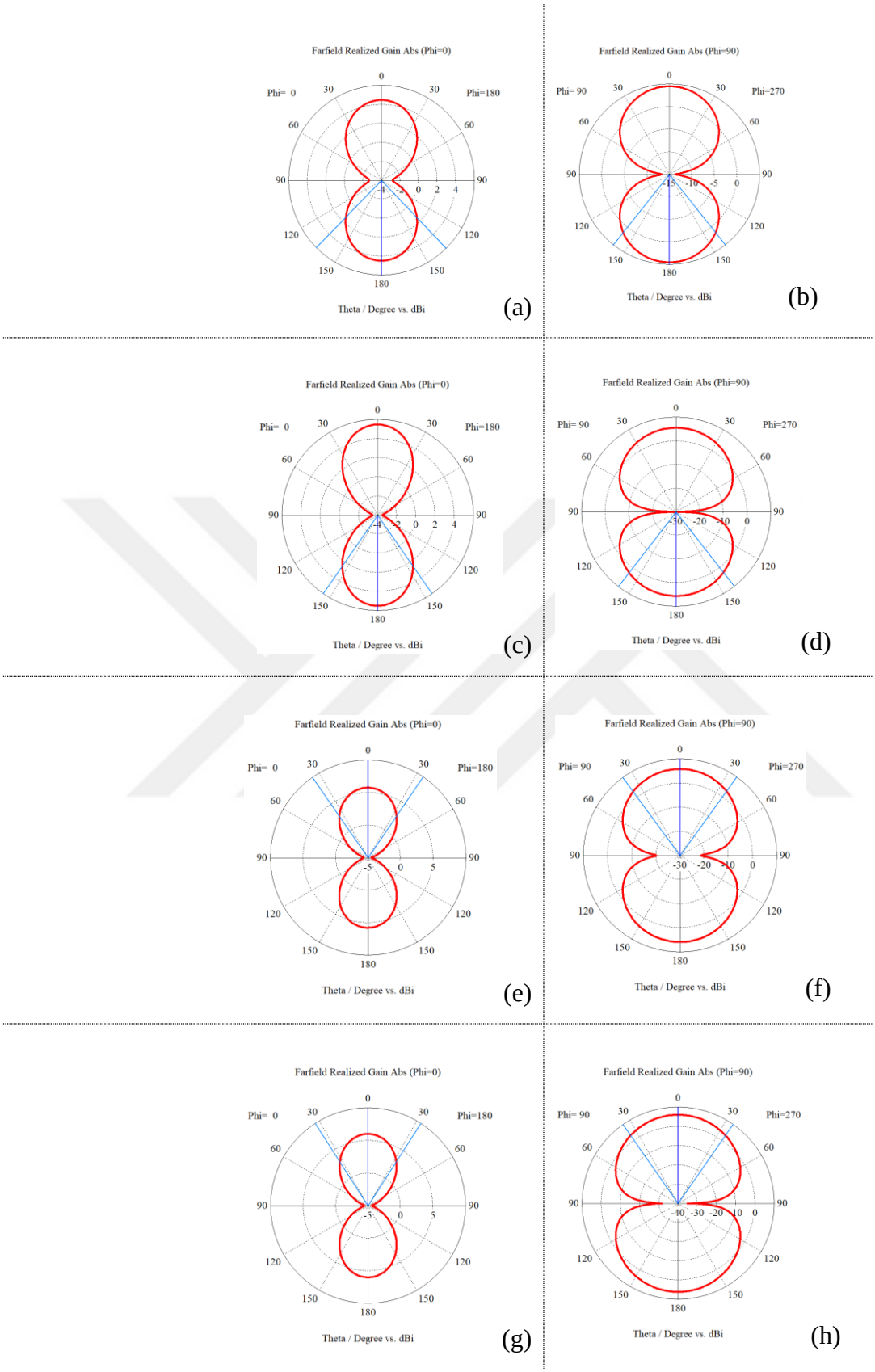

Figure 2.4 : Radiation patterns of the standard four-arm sinuous antenna: (a) f_0 = 2GHz, $\phi = 0^{\circ}$. (b) f_0 = 2GHz, $\phi = 90^{\circ}$. (c) f_0 = 3.05GHz, $\phi = 0^{\circ}$. (d) f_0 = 3.05GHz, $\phi = 90^{\circ}$. (e) f_0 = 4.1GHz, $\phi = 0^{\circ}$. (f) f_0 = 4.1GHz, $\phi = 90^{\circ}$. (g) f_0 = 5GHz, $\phi = 0^{\circ}$. (h) f_0 = 5GHz, $\phi = 90^{\circ}$.

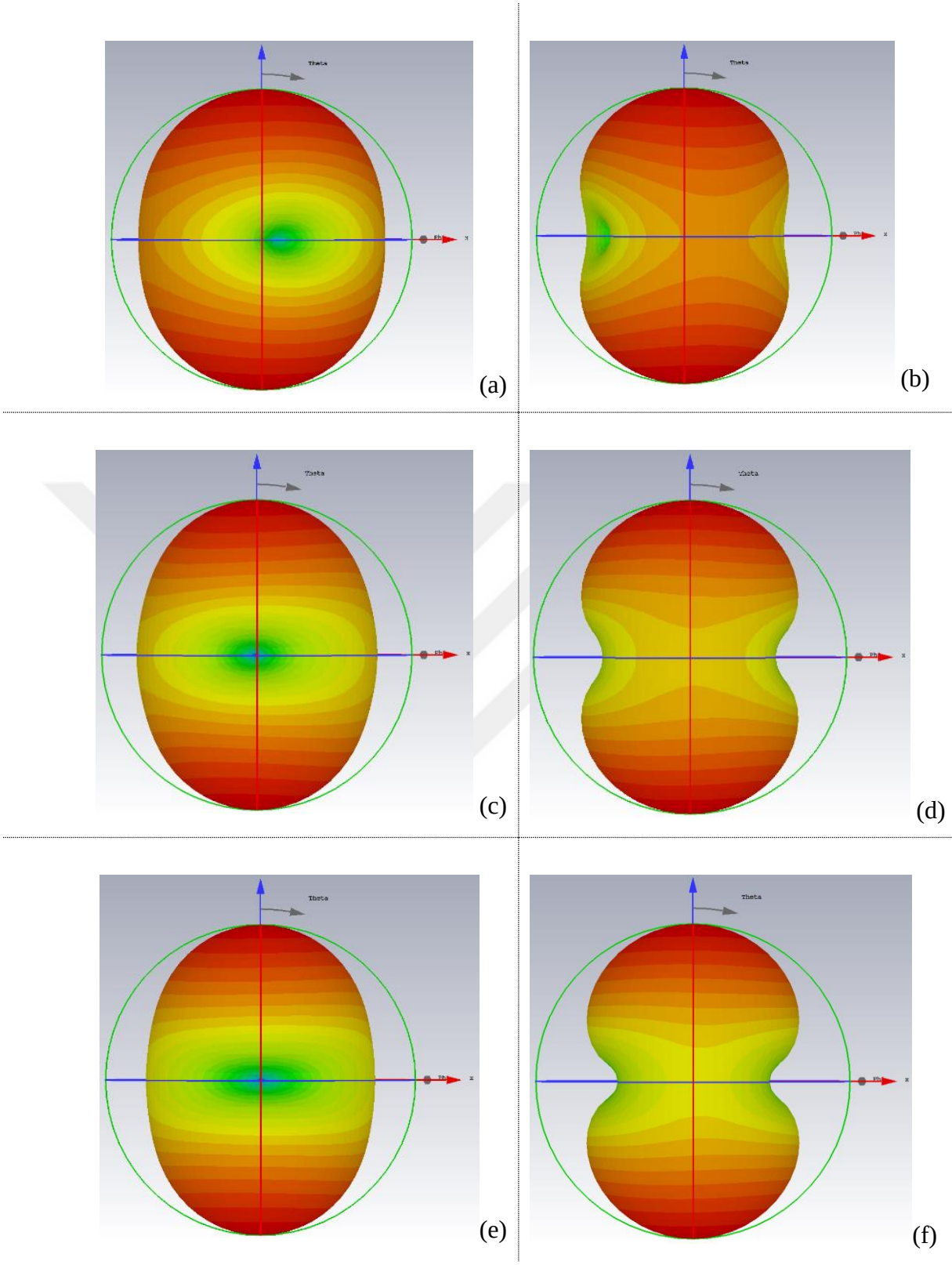

Figure 2.5 : Radiation patterns of the standard four-arm sinuous antenna: (a) f_0 = 2GHz, $\phi = 0^{\circ}$. (b) f_0 = 2GHz, $\phi = 90^{\circ}$. (c) f_0 = 4.1GHz, $\phi = 0^{\circ}$. (d) f_0 = 4.1GHz, $\phi = 90^{\circ}$. (e) f_0 = 5GHz, $\phi = 0^{\circ}$. (f) f_0 = 5GHz, $\phi = 90^{\circ}$.

To analyzed the dual circular property of the four arm sinuous antenna, the orthogonal arm pairs are exited ±90° out of phase with respect to each other and the axial ratio of the antanna is ploted across the frequency band. Figure 2.6 shows the axial ratio for the selected frequency points for $\phi = 0^{\circ}$ and $\phi = 90°$ cuts**.** Minimum AR below 1dB is displayed for both cuts across the bandwidth.

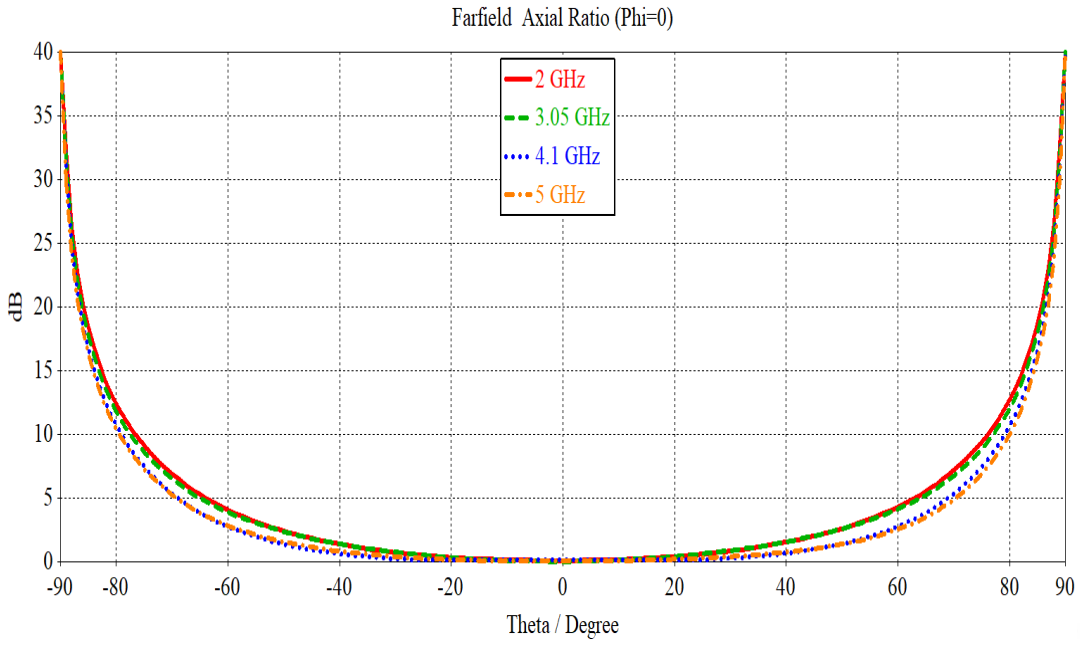

(a)

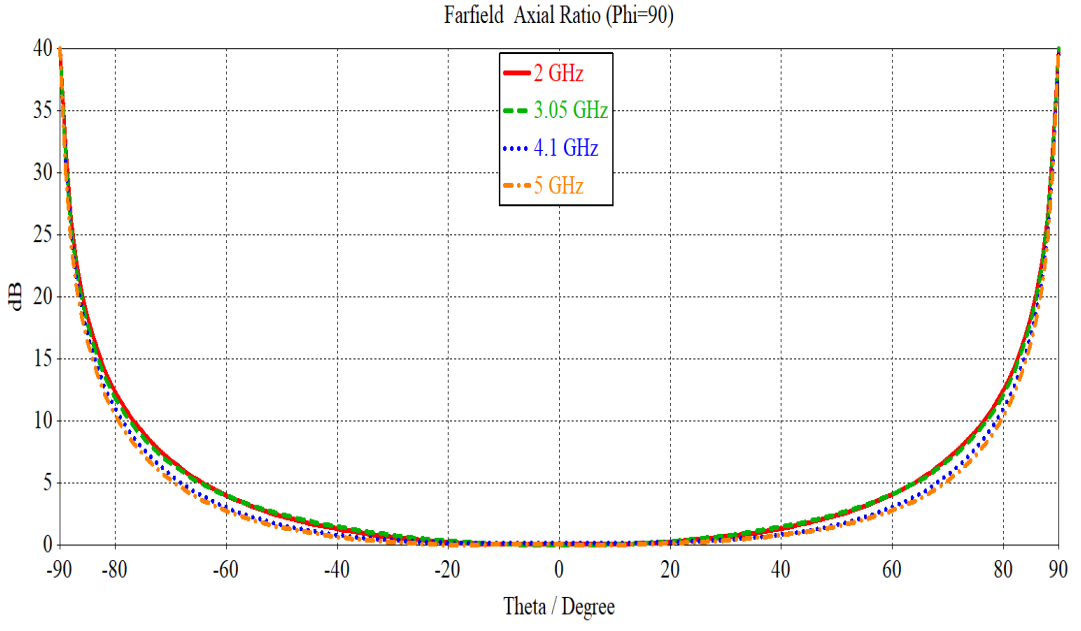

(b)

Figure 2.6 : The axial ratio of the standard four arm sinuous antenna at: (a) $\phi = 0^{\circ}$. (b) $\phi = 90^{\circ}$.

And finally, Figure 2.7 shows the maximum gain taken at broadside of the antenna that is at $\theta = 0^{\circ}$ and $\phi = 0^{\circ}$ across 2-5 GHz frequency bandwidth . It can be seen that there is a downward notch around 2.6 GHz and this can be due to the sharp edges of the antenna as mention in [12]. Otherwise the is a steady increase in gain across the frequency bandwidth.

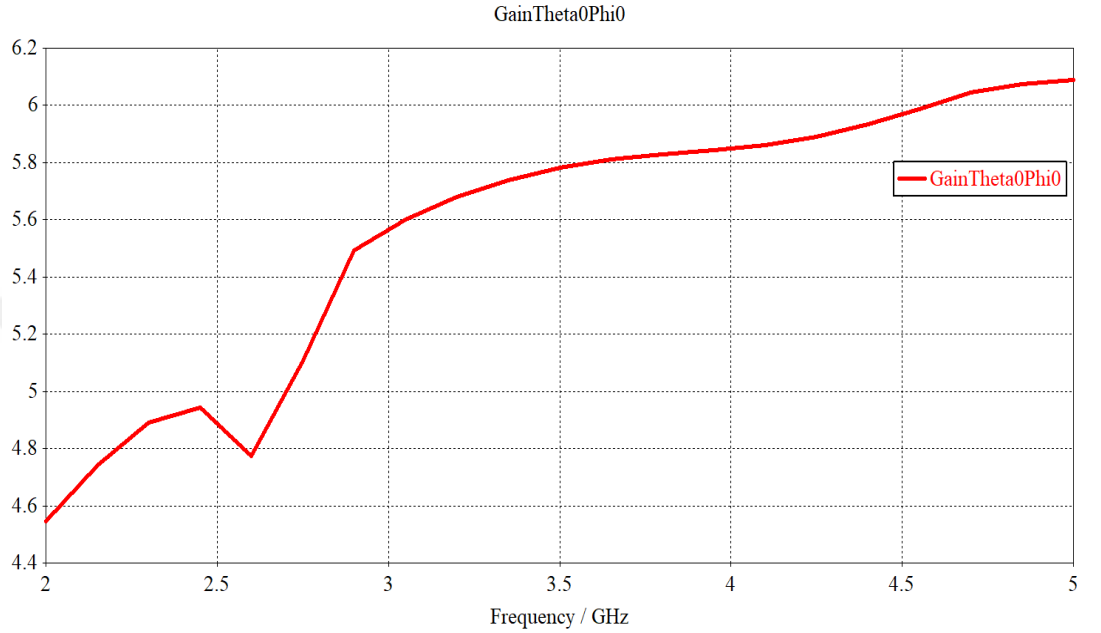

Figure 2.7 : The maximum gain at broadside of the SFASA $\phi = 0^{\circ}$.

2.4 The Standard Four-Arm Sinuous Antenna with Substrate

Although the sinuous antenna without substrate exhibits excellent performance in terms of its gain, radiation pattern and beamwidth, the antenna needs to be fabricated and therefore requires to be placed on a substrate. In [13], different types of substrates with different dielectric properties and thickness were investigated. The results suggest that the addition of a substrate with different thickness decreases AR beamwith in most cases. It was further stated that the 0.254 mm Duriod substrate resulted in the smallest level of deterioration in performance. For this thesis ,the Rogers 0.81mm-R04003C with relative permittivity of $\varepsilon_r = 3.38$ is used as a substrate due to its aviability within the thesis duration and it's also used as a substrate in [14][15]. In addition, it was mentioned before that the addition of a substrate will reduce the input impedance form 267Ω to lower input impedance [13].

To analyze the new input impedance with the addition of a substrate, the Rogers 0.81mm-R04003C substrate is integrated with the four arms as shown in Figure 2.8(a). The input impedance of the two ports is varied to find the optimum input impedance. Figure 2.8(b) shows the return loss of a single port when the input impedance of the ports is varied from 276Ω to lower input impedances. According to the Figure 2.8(b), the average input impedance at the balance port that can be fed with a realizable balun is around 185 Ω. Therefore, the baluns should be designed according to this input impedance.

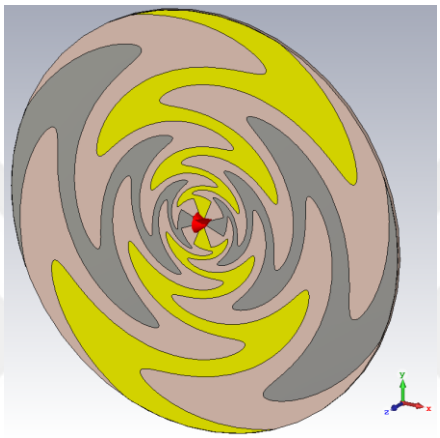

(a)

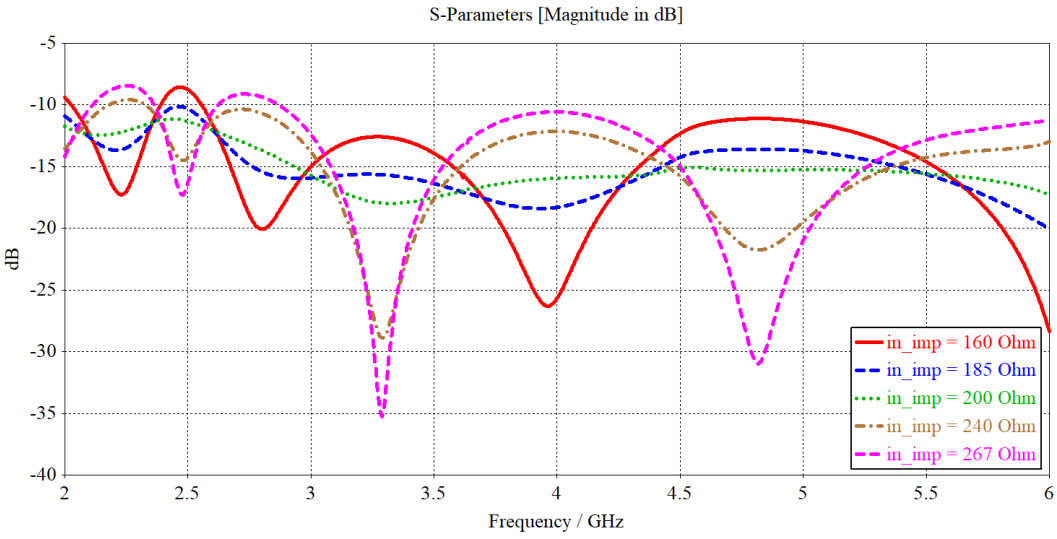

(b)

Figure 2.8 : Input impedance analysis of the SFASA with substrate: (a) Antenna with substrate. (b) S-parameters.

Furthermore, the radiation patterns of the integrated four arms antenna with the substrate is also analyzed. The patterns depicted in Figure 2.9 show similar bidirectional performance as the antenna without substrate. Figure 2.10 shows the maximum gain of the antenna which is also similar to the maximum gain obtained with the antenna without substrate. Finally, the axial ratio of the standard antenna with substrate is also analyzed for $\phi = 0^{\circ}$ and $\phi = 90^{\circ}$ standard cuts shown in Figure 2.11 the axial ratio is below 1dB similar with the axial ratio without substrate across the intended bandwidth.

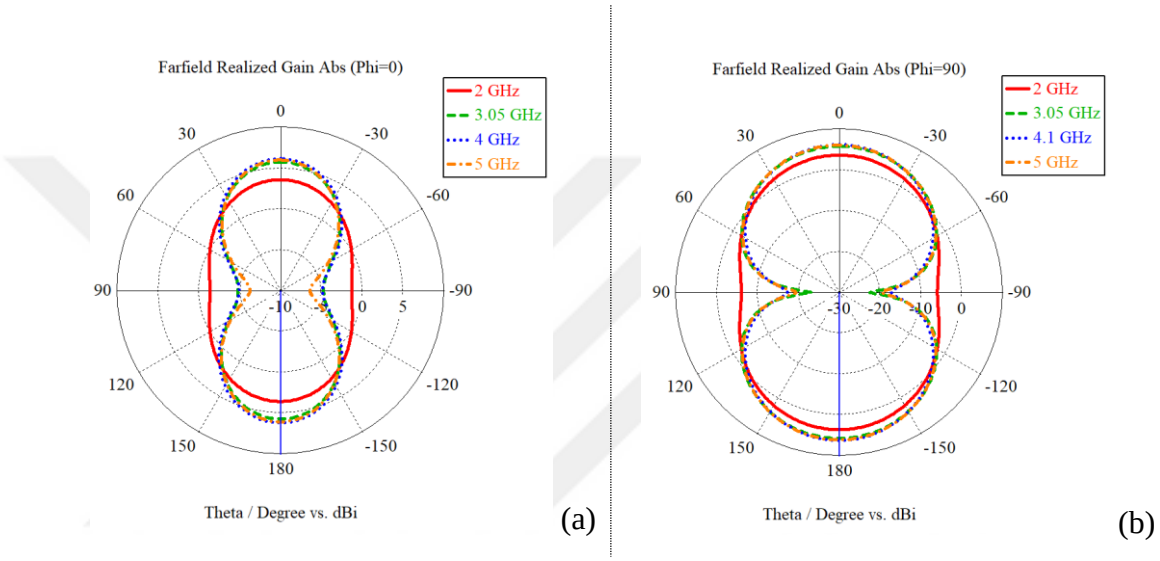

Figure 2.9 : Radiation patterns of the SFASA with substrate: (a) $\phi = 0^{\circ}$. (b) $\phi = 90^{\circ}$.

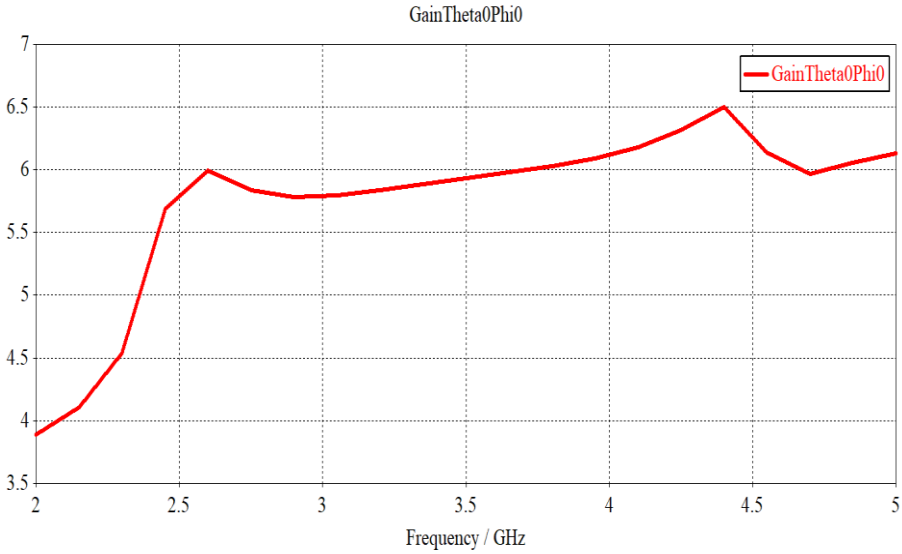

Figure 2.10 : Gain at broadside of the SFASA with substrate.

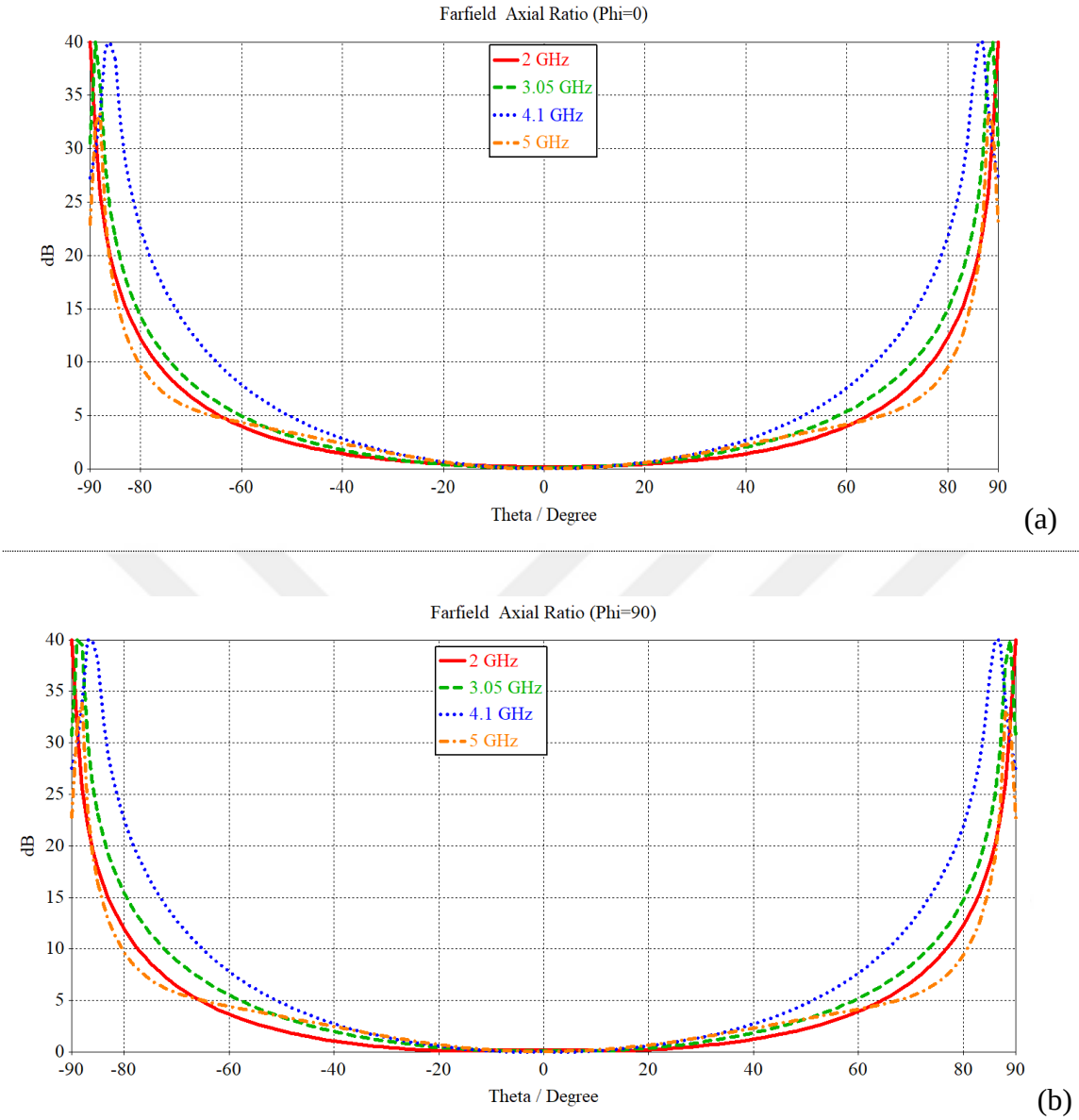

Figure 2.11 : Axial ratios of the SFASA with substrate: (a) $\phi = 0^{\circ}$. (b) $\phi = 90^{\circ}$.

2.5 Modification of the Sharp Ends of the Four-Arm Sinuous Antenna

The sinuous antenna is known to resonate in two forms: a log-periodic resonance on the arms, and a resonance due to the sharp ends left by the outer truncation. The resonance due to the sharp ends is known to degrade the performance of the antenna especially in lower frequencies and such resonances produce late time ringing, which is particularly troubling for pulsed close-in sensing applications [16, 17]. Figure 2.12(a) shows the modification method proposed in [12] to remove the sharp end

resonances of the sinuous antenna. The proposed method improved the gain to have a smooth resonance in the frequency bandwidth. In this thesis, the outer edges of the antenna are removed by blending the edges to have a circular shape instead of pointy edge as shown in Figure 2.12(b). Figure 2.14 shows the effect of new proposed modification on the return loss of the antenna and an improvement in return loss of the antenna at lower frequencies is observed.

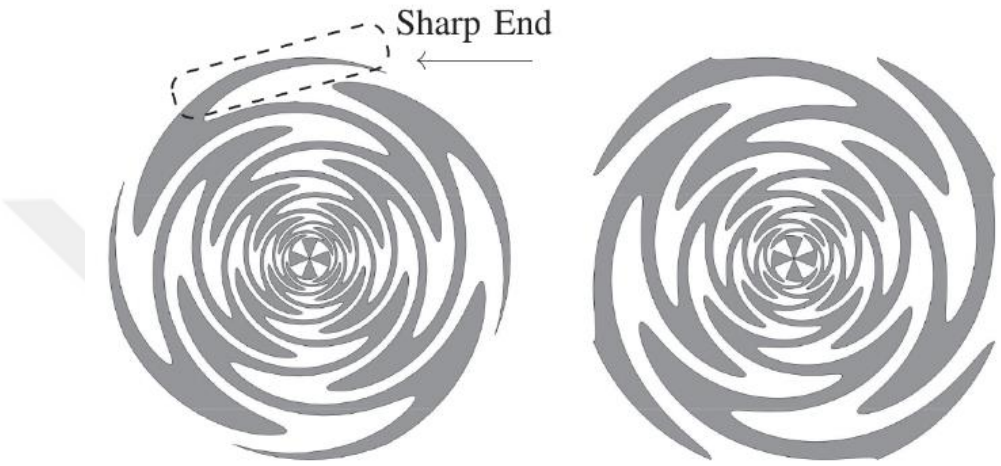

(a)

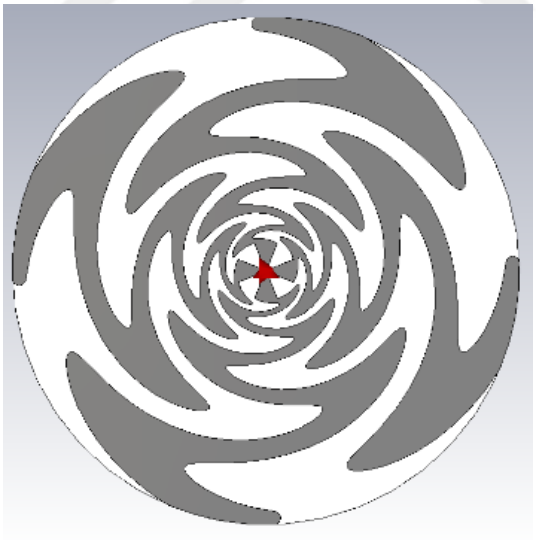

(b)

Figure 2.12 : Sharp end modification of the SFASA with substrate: (a) Modification in [12]. (b) New modification.

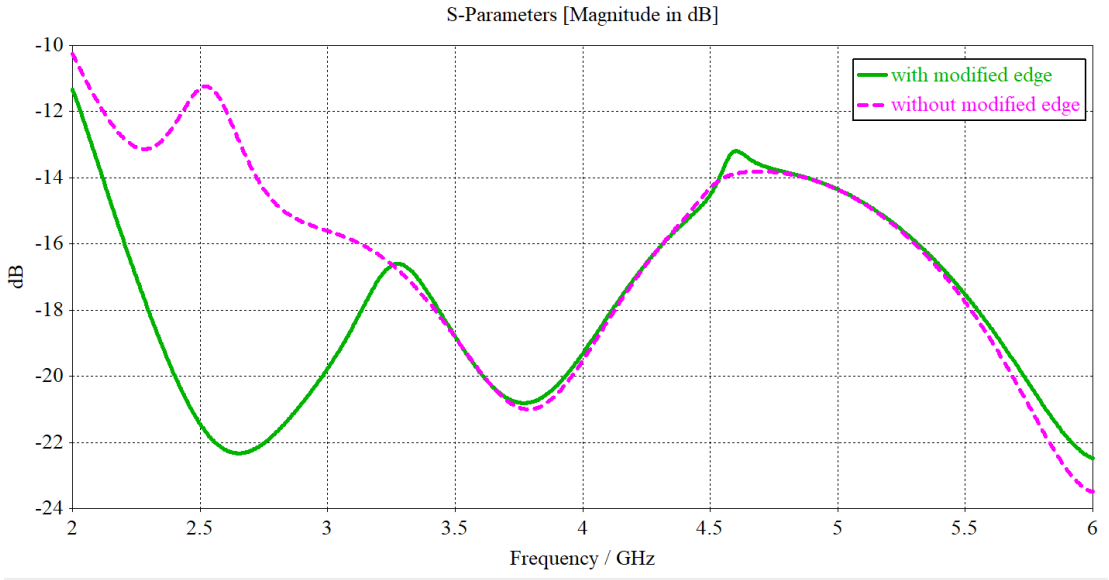

Figure 2.13 : Effect of Sharp end modification on the return loss of the antenna.

2.6 Feeding point Modification

Another important factor to be considered when designing a sinuous antenna is how to smoothly connect the feeding network to the antenna without causing much damage to the symmetry of the antenna. The type of feeding used in Figure 2.2(b) is not a practical type of connection to connect the two ports to a feeding network. Therefore, the four arms of the antenna must be modified in order to practically fit in a feeding network. It should be noted that the modification of the arms causes the neighboring arms to have an asymmetric geometry thus reducing the performance of the antenna especially at higher frequency since the modifications are done at the center on the geometry which is the high frequency area. Although, with an optimized modification, the antenna can still maintain its fundamental properties. There are several types of feed modifications suggested in literature. Figure 2.14 shows the different type of feeding modifications proposed in [18], [14] and [15] respectively.

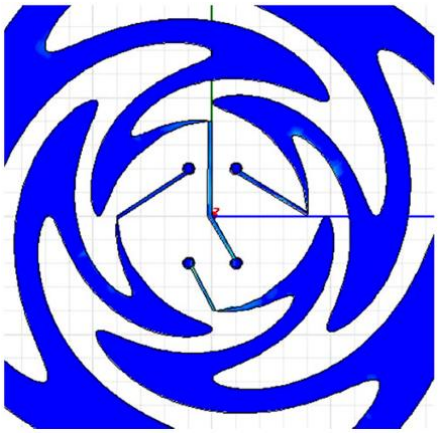

(a)

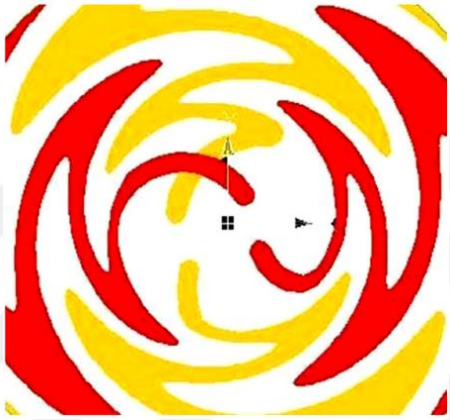

(b)

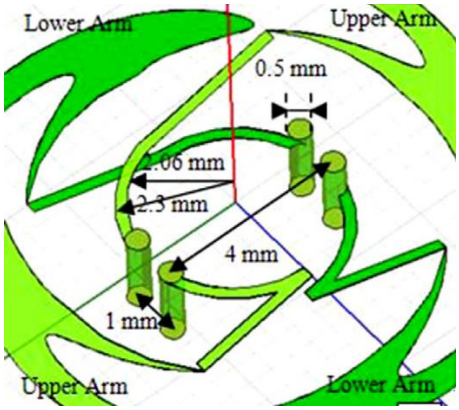

(c)

Figure 2.14 : Feeding modification of the FASA: (a) Modification in [18]. (b) Modification in [14]. (c) Modification in [15].

In this thesis two new type of modifications were introduced and for reference purposes they will be named as Feed1 and Feed2. In the Feed1 modification, all four arms are placed on top of the substrate as shown in Figure 2.15(a). Two opposite arms are used to create each port resulting in a two port configuration. The two positive

arms are design in such a way that they will be on same side in order to easily connect it to the feeding network and same as the two arms that will be connected to the ground. The four arms are connected to the bottom of the substrate via 0.5mm diameter pins. During the optimization of the modified parts, it was discovered that the best performance was obtained when the distance between the two opposite arms are kept as short as possible without having a bad coupling between the two ports. Figure 2.15(b) shows the minimum distances found which are practically suitable for combining the antenna with a feeding network.

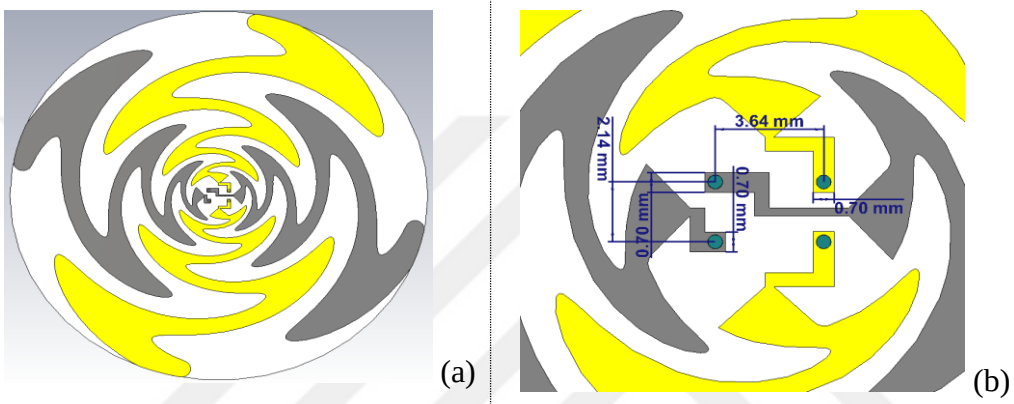

(a) (b)

Figure 2.15 : Feed1 modification of the FASA: (a) Feed1 geometry. (b) Feed1 dimensions.

In the case of the Feed2 modification, one pair of the arms is placed on one side of the substrate while the other pair is on the other side. In other words, arm-pairs are printed on both sides of the substrate. Figure 2.16(a) and Figure 2.16(b) shows the geometry and optimized dimensions of the modified upper and bottom sides of the substrate respectively.

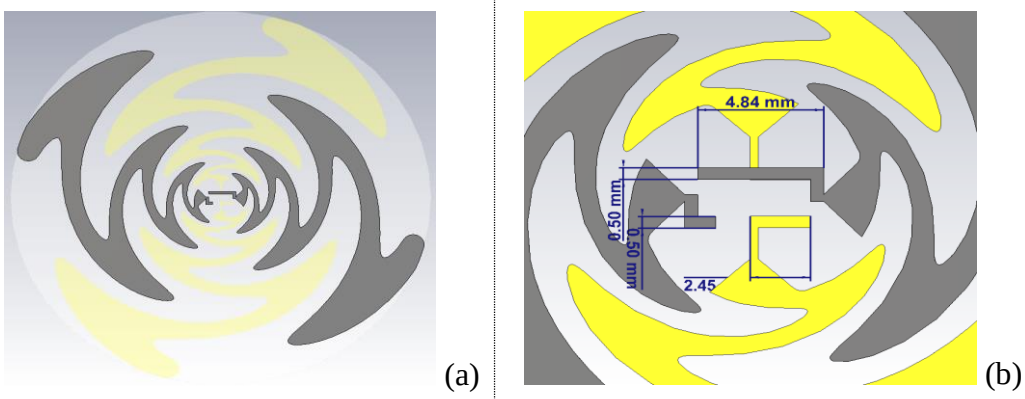

(a) (b)

Figure 2.16 : Feed2 modification of the FASA: (a) Feed2 geometry. (b) Feed2 Dimensions.

In order to investigate the new input impedance for the Feed1 and Feed2 feeding modifications, Rogers 0.81mm-R04003C substrate is used on both antennas and the input impedance of the two discreet ports are varied from 276Ω to lower input impedances to find the best match for both modifications. Several input impedances are reported as in [15] [19]. In this case, the average input impedance with the best match is found to be around 180Ω as shown in Figure 1.17(a) and Figure 1.17(b) for Feed1 and Feed2 modifications respectively.

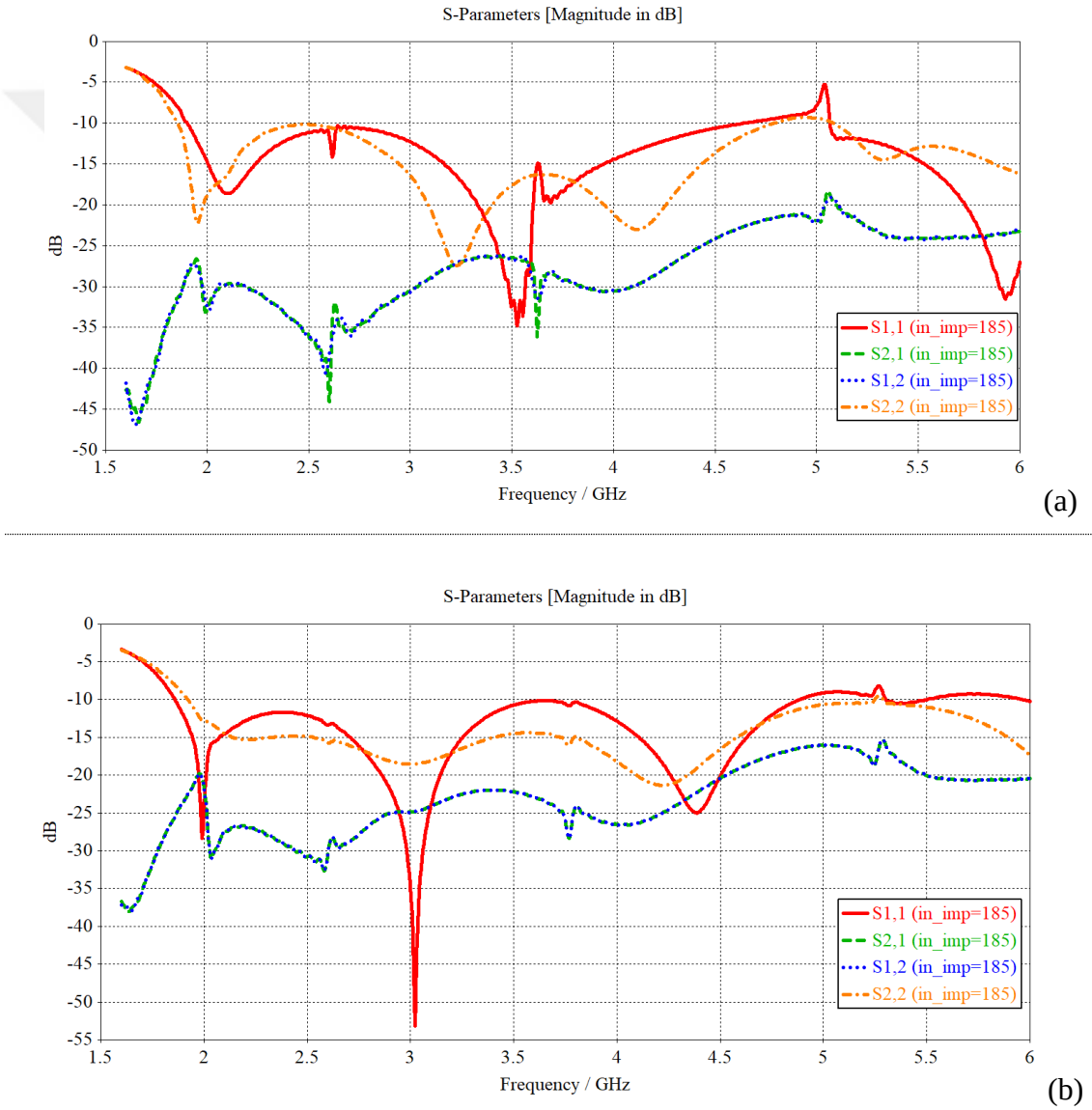

Figure 2.17 : S-parameters of the modified with average input impedance of 185Ω: (a) Feed1. (b) Feed2.

2.7 Radiation Patterns of the Modified Four-Arm Sinuous Antenna

As in the standard feed antenna, the principle cuts $\phi = 0^{\circ}$ and $\phi = 90°$ are used to analyzed the radiation pappterns of the two feed point modified antennas. With the new feeding point modifications made, there is small alteration in the symmetry of the antenna. Therefore, the radiation patterns for both ports will be analyzed. Figure 2.18 shows the radiation patterns of the Feed1, Feed2 and the standard feed combined for the selected frequency points. From the radiation patterns, both modified antennas still maintain their bidirectional behavior across the intended frequency band. The AR of the modified antennas is also analyzed and compared with the standard feed for the principle cut $\phi = 0^{\circ}$ as shown in Figure 2.20. The AR for both modified feeds is found below 2dB except for the feed2 at 5 GHz which found to be around 3 dB [15] compared the AR of the modified antennas shown in Figure 2.14 and the results found here show better AR especially the Feed1 modification in 2-5GHz frequency band. Additionally, Figure 2.19 shows the comparison of the maximum gain at broadside for Feed1, feed2 and the standard feed. The maximum gain of the modified antennas is consistent with the standard feed but the Feed2 modification is a bit below the standard feed.

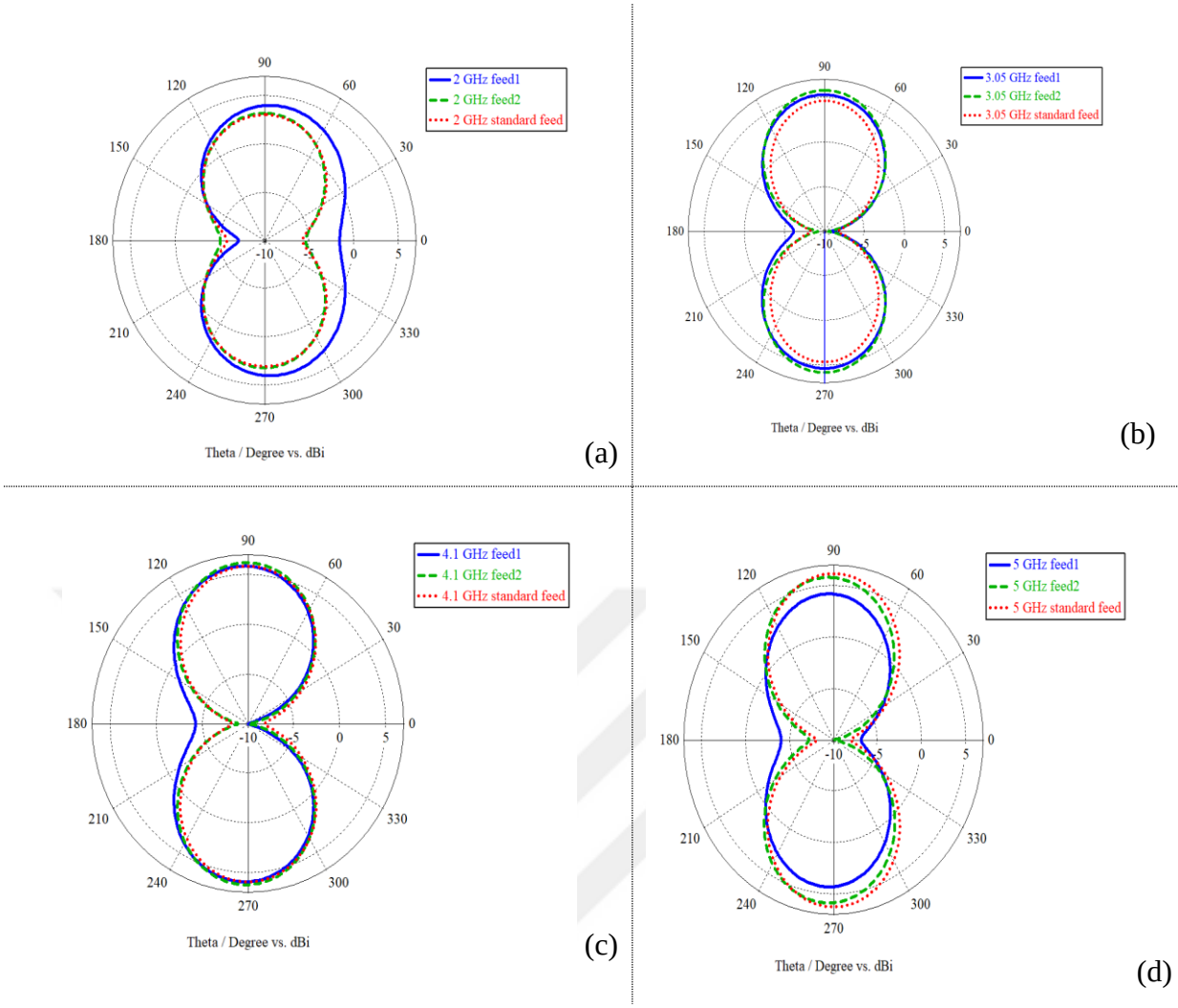

Figure 2.18 : Comparison of the radiation patterns of the modified feeds with the SFASA: (a) 2GHz, $\phi = 0^{\circ}$. (b) 3.05 GHz, $\phi = 0^{\circ}$. (c) 4.1GHz, $\phi = 0^{\circ}$. (d) 5GHz $\phi = 0^{\circ}$.

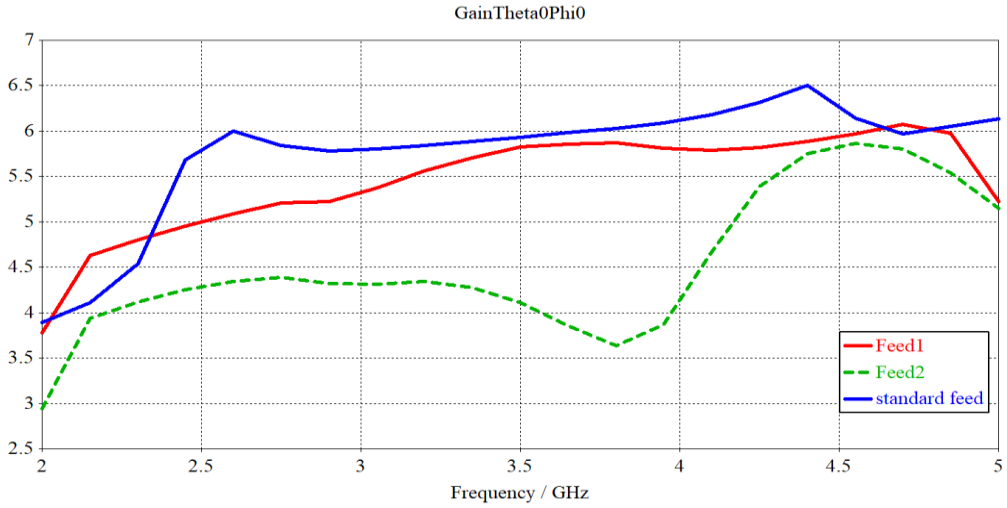

Figure 2.19 : Comparison of the maximum gain at broadside of the modified feeds with the SFASA.

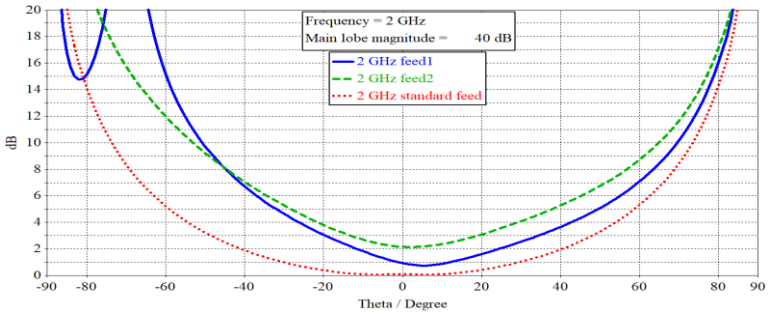

(a)

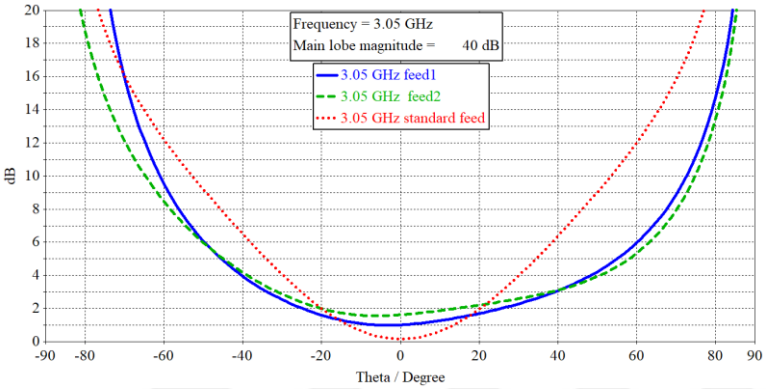

(b)

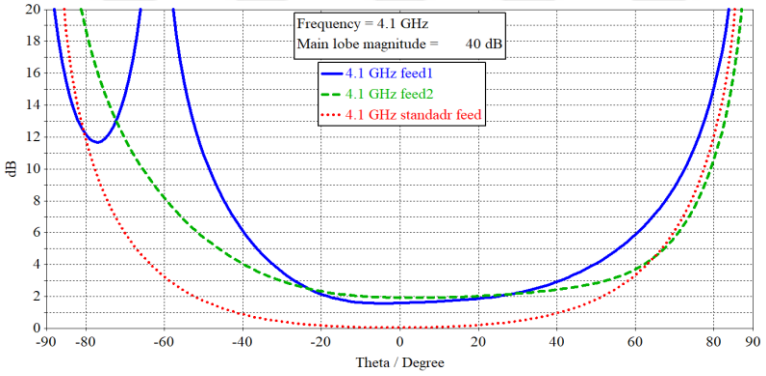

(c)

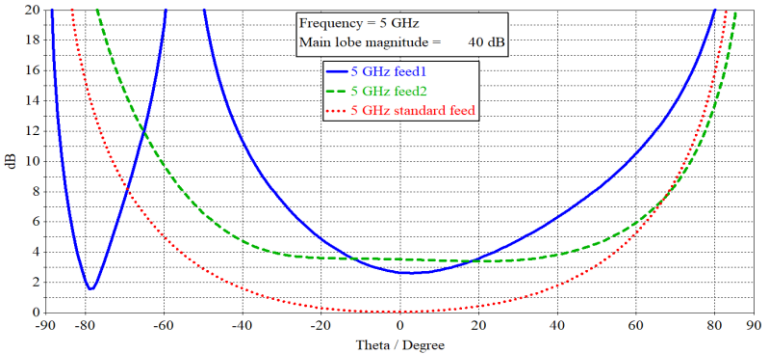

(d)

Figure 2.20 : Comparison of the axial ratios of the modified feeds with the SFASA: (a) 2GHz, $\phi = 0^{\circ}$. (b) 3.05 GHz, $\phi = 0^{\circ}$. (c) 4.1GHz, $\phi = 0^{\circ}$. (d) 5GHz $\phi = 0^{\circ}$.

3. FEEDING NETWORK DESIGN

In planar antenna design, feeding networks are required to practically excite the radiating elements. For the four arm sinuous antenna, the feeding network is designed based on the intended bandwidth and the type of polarization. To have a single linearly polarized antenna, a mere two sinuous arms is enough to achieve this. Nonetheless, to realize a dual linear polarization, it is essential to use the four arm geometry. Figure 3.1(a) shows a block diagram of the feed network containing two baluns attached to two ports which is necessary to attain dual linear polarization. Likewise, a 90° Hibrid and a balun is used in the feed netework for dual circular polarization as shown in the block diagram of Figure3.1(b)

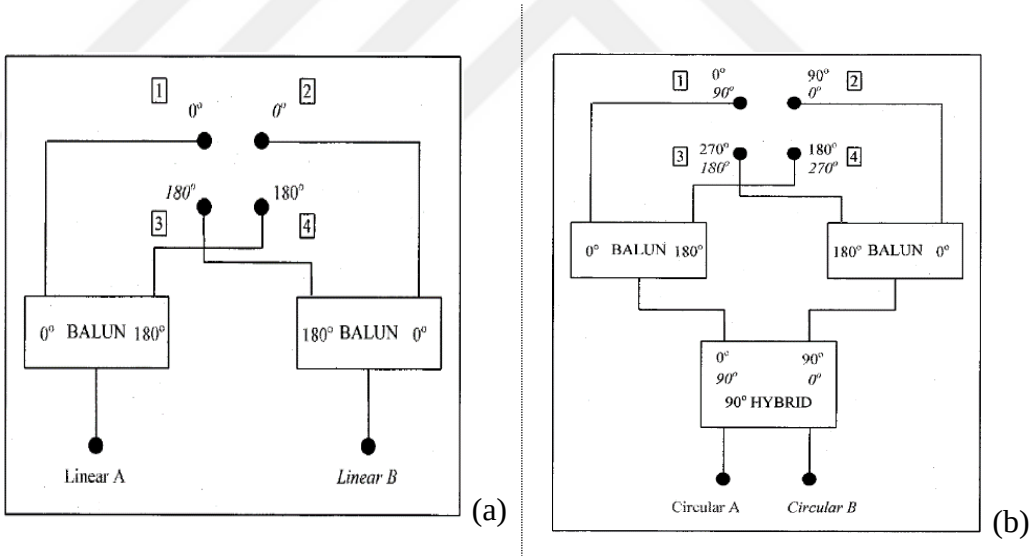

Figure 3.1 : FASA feed network: (a) linear polarization. (b) Circular polarization.

From Figure 3.1(a), it can be seen that at the input of the antenna, the balun's paired lines are intersecting each other. This intersection of the feed lines is the main contributor to the complexity of practically designing a feed network to achieve dual linear or dual circular polarization without altering the symmetry of the antenna by modification of the feeding point. Thus for such a wideband antenna, designing a

practical and an appropriate feeding network is necessary to maintain the wideband and frequency independent properties of the antenna.

3.1 Balun Design

Since the self-complimentary four-arm sinuous antenna is a wideband antenna with frequency independent input impedance, a wideband balun is necessary to feed the antenna in order to maintain the characteristics of the antenna. The term balun is used to describe a transformer developed to transform an unbalance mode into a balance mode. The four-arm sinuous antenna is considered as a balance configuration and in this case it is intended to be fed by an unbalance 50Ω coaxial cable. In the previous sections, the input impedance of the sinuous antenna without substrate was taken as 276Ω. Later on, the addition of the substrate decreased the input impedance to around 185Ω. Therefore, it is necessary to have a feeding network that can transform the unbalance 50Ω to a balance input impedance while satisfying both the wideband and frequency independent properties of the sinuous antenna.

The microstrip balun is the most commonly used broadband balun. Figure 3.2(a) and Figure 3.2(b) shows the two linearly and exponentially tapered microstrip baluns respectively. Both baluns are known to have a wideband characteristic but the exponentially tapered has a wider bandwidth than the linearly tapered [20]. In both cases, the conversion from a balance to unbalance line depends on a steady change of the cross-section of the line. Typically, for the unbalance line (the input), the cross-section of the line look like a microstrip while at the balance line (output), the width of the strips is equal to each other which in turn made up a balance strip double line.

Calculating the width of the microstrip line at the input of the balun can be done by simple calculations or with the help of available microstrip line calculators. The ground plane of the microstrip line is not infinite but should be kept significantly larger than the positive feed line depending on the best optimized results. On the balance port (output), there is no longer a microstrip but instead a paired strip. Both the upper and lower with of the paired strips are of equal length. The image and uniqueness theorem can be used to approximate the widths for a desired impedance. The image theorem is depicted in Figure 3.3 and according to the figure, the impedance of the double strip line is twice that of the microstrip line while both widths are equal. Therefore, with the

help of the microstrip line calculator, obtaining the desired width just requires the specification of the desired input impedance and half the distance between the two strips [21].

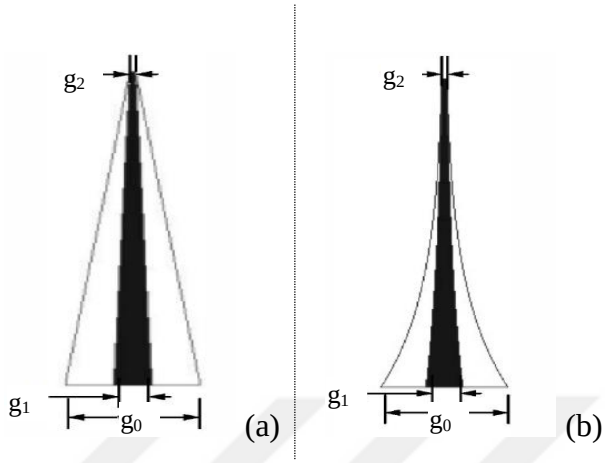

Figure 3.2 : Microstrip baluns: (a) linearly tapered. (b) Exponentially tapered.

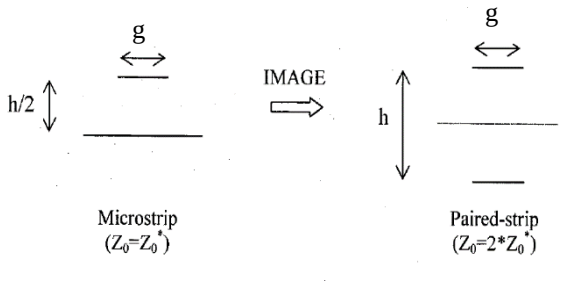

Figure 3.3 : The image theory: microstrip to paired strip.

In this thesis, the exponentially tapered microstrip is used to develop the feeding network as shown in figure3.2b. the curve of the exponentially taper can be described by the equation:

$$y = ue^{px} \tag{3.1}$$

Where *u* and *p* are determined by the dimension of the balun and for the positive line, a and b are defined by:

$$u = \frac{g_1}{2}\ ,\ \ p = ln\left(\frac{g_2}{g_1}\right)/L_f \tag{3.2}$$

For the ground part, the expression for *u* and *p* is

$$u = \frac{g_0}{2}\ ,\ \ p = ln\left(\frac{g_2}{g_0}\right)/L_f \tag{3.2}$$

where L_f is the length of the feed network

In this thesis, since the desired frequency bandwidth is from 2-5GHz, FR4 material with a dielectric constant $\varepsilon_r = 4.3$ and a thickness of 1.6mm is used to fabricate the feeding network. Although FR4 it's not a high frequency material but can have satisfactory performance for the bandwidth of interest in this thesis. In addition, material is chosen because of its availability for the fabrication of the antenna.

Figure 3.4 shows the final structure for the two port exponentially tapered microstrip balun. The balun is designed with respect to the modified feed points of the designed Feed A and Feed B four arm sinuous antenna. The baluns are kept symmetric to each other and the g_1, g_2, g_0 parameters are calculated based on the unbalance input impedance taken as 50Ω and the balance as 185Ω. The dimensions of the feed network are given in table 1.

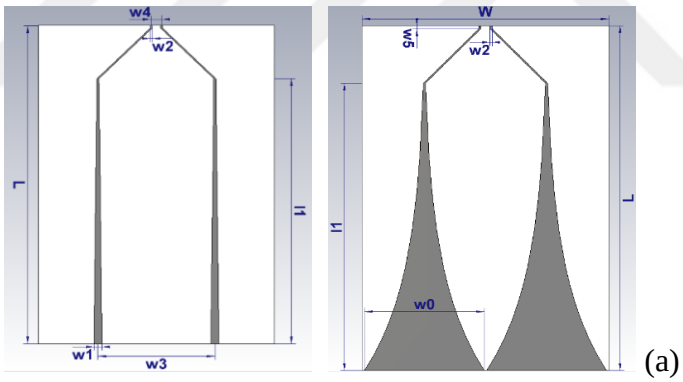

Figure 3.4 : The design exponentially tapered microstrip baluns: (a) Front and back view of the Feed1 balun. (b) Front and back view of the Feed2 balun.

Table 3.1 : Feed network dimensions.

Parameters	Feed1(mm)	Type2(mm)
L_F	120	120
l1	100	100
w	80	84
w0	38.87	35.05
w1	2.73	2.73
w2	0.7	0.5
w3	39.64	47.64
w4	3.64	3.84
w5	1.02	10.02
w6		10.85

3.2 Performance of the Baluns

The performance of the feeding network for the Feed1 and Feed2 were measured by terminating the balance ports(outputs) with a 185Ω lumped elements and measuring the return loss of the 50Ω unbalance(input) ports which was feed using SMA connectors as shown in Figure 3.5. The results show that the return loss and isolation of the two ports for both feed networks. For the Feed1, the return loss was at most -11dB for the entire desired band while its -13dB for the Feed2 feeding network. In [14] reported a return loss of -12dB for 200Ω output termination is reported.

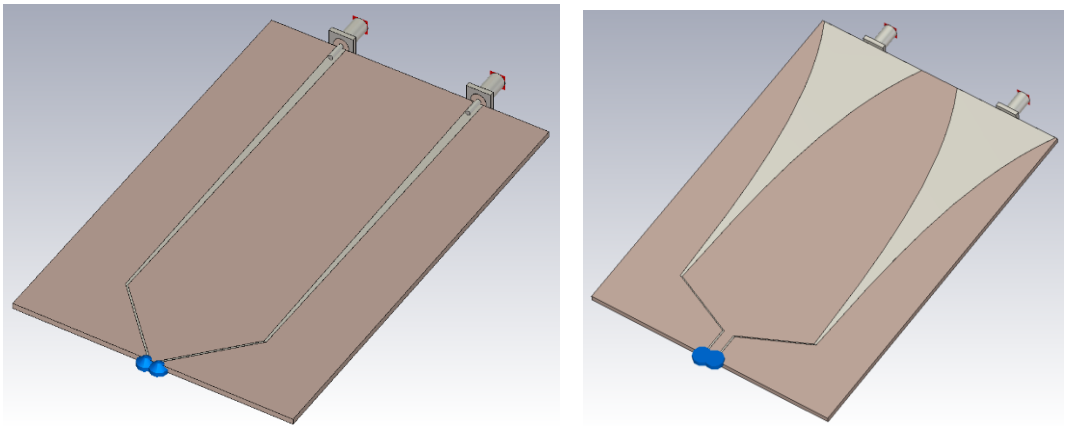

Figure 3.5 : Feed network impedance matching with 185Ω resistor.

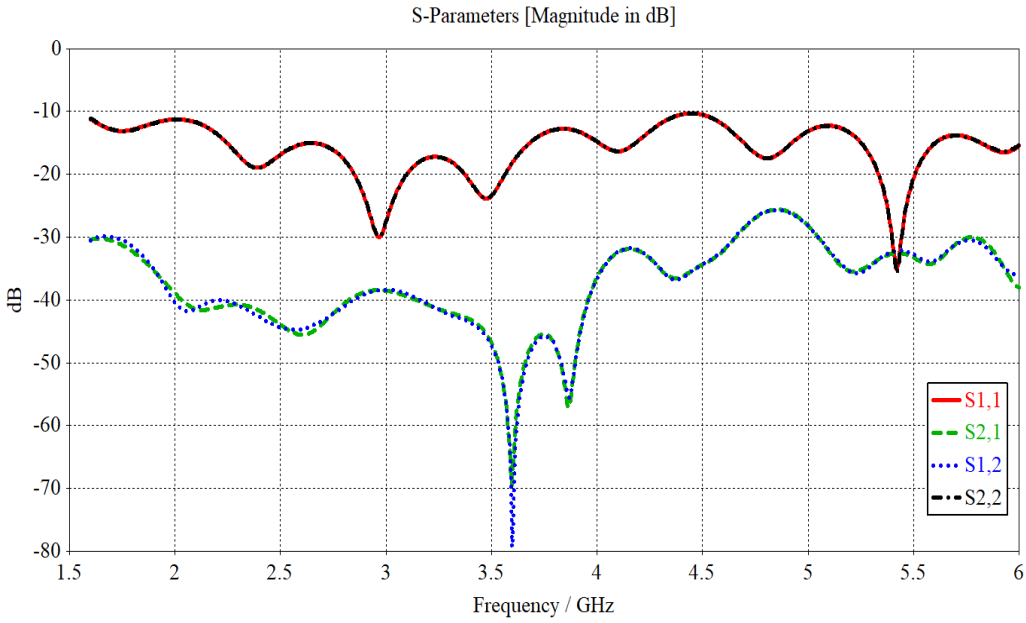

(a)

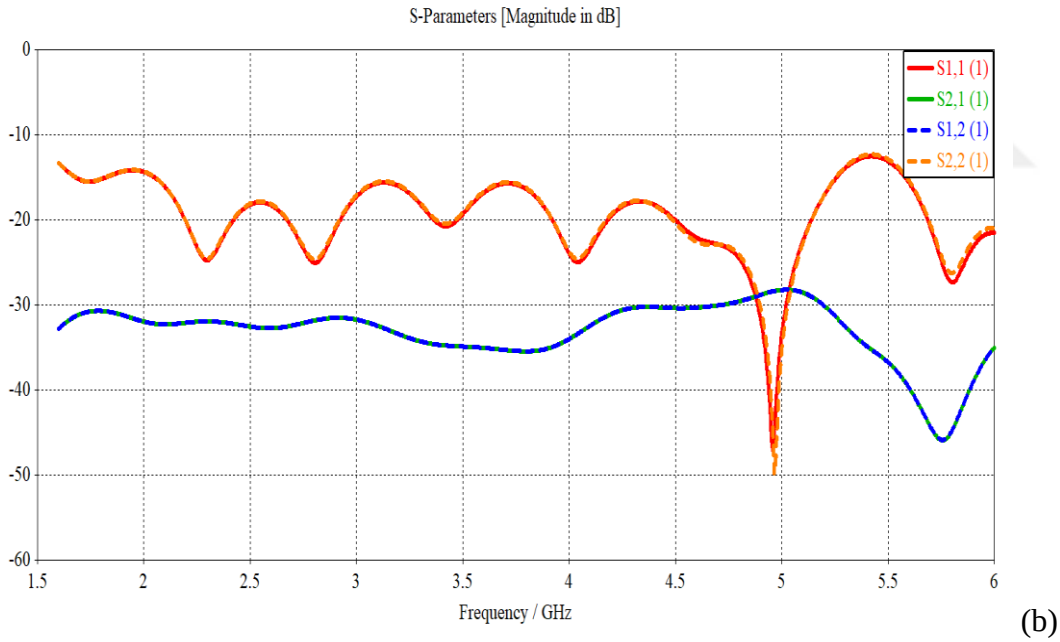

(b)

Figure 3.6 : The S-parameters of the matched feed network with 185Ω resistor: (a) Feed1 s-parameters. (b) Feed2 s-parameters.

4. INTEGRATION OF THE BALUNS WITH THE FOUR-ARM FEED POINT MODIFIED ANTENNAS

In this section, both the Feed1 and Feed2 modified antennas are integrated with their respective feeding baluns. Figure 4.1(a) shows the Feed1 antenna with the balun and how the pins connect the feed network with the radiating elements. Similarly, Figure 4.1(b) shows the configuration of the feed2 with the feed network and its connections. It should be noted that some parameters were modified and the final dimensions of both antennas is given in Table 4.1 It can be seen that in both cases the substrate of the antennas is increased. This was done to reduce the effect of the addition of the cavity backed reflector.

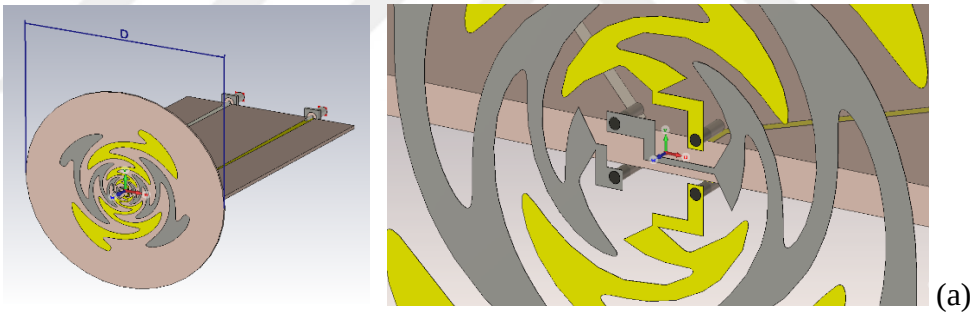

(a)

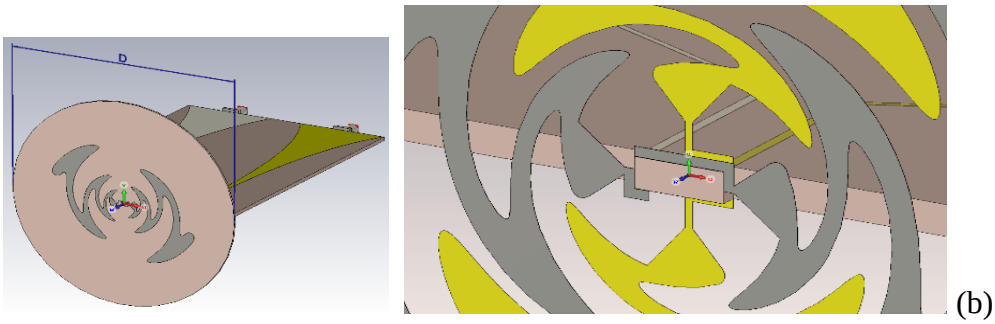

(b)

Figure 4.1 : The modified antennas integrated with the baluns: (a) Feed1 geometry and connections. (b) Feed2 geometry and connections.

4.1 Performance of The Integrated Antennas

Initially, the reflection coefficients of the antennas are analyzed. Figure 4.2(a) shows the s-parameters of the Feed1 antenna. It can be seen from the figure that the return loss of both ports is at most -12dB while keeping up an isolation at most -20dB across the interested frequency bandwidth. Similarly, Figure 4.2(b)shows identical return loss and isolation for the Feed2 antenna. Although intended frequency is from 2-5GHz, both figures show that the antennas have -10dB return loss beyond 2GHz. This is due the that the outer radius is reduced because the available substrate is limited for fabrication during the time of this thesis.

The radiation patterns of the integrated antennas is also analyzed for $\phi = 0^{\circ}$ and $\phi = 90^{\circ}$ principle cuts. Figure 4.3 shows the radiation patterns of the Feed1 and Feed2 antennas and both antennas are still maintaining bidirectional patterns. The axial ratio of both antennas is also analyzed and plotted in Figure 4.4(a) for feed1 and Figure 4.4(b) for feed2 at the $\phi = 90^{\circ}$ principle cut. Both antenna show axial ratio below 3dB. Furthermore, the maximum gain at broadside is also plotted in Figure 4.5

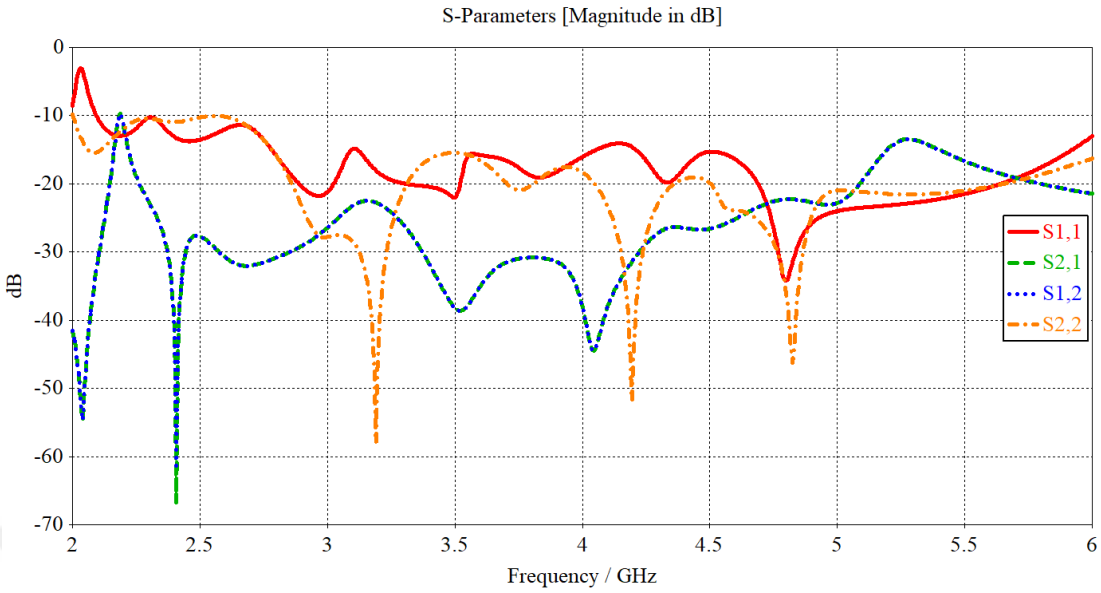

(a)

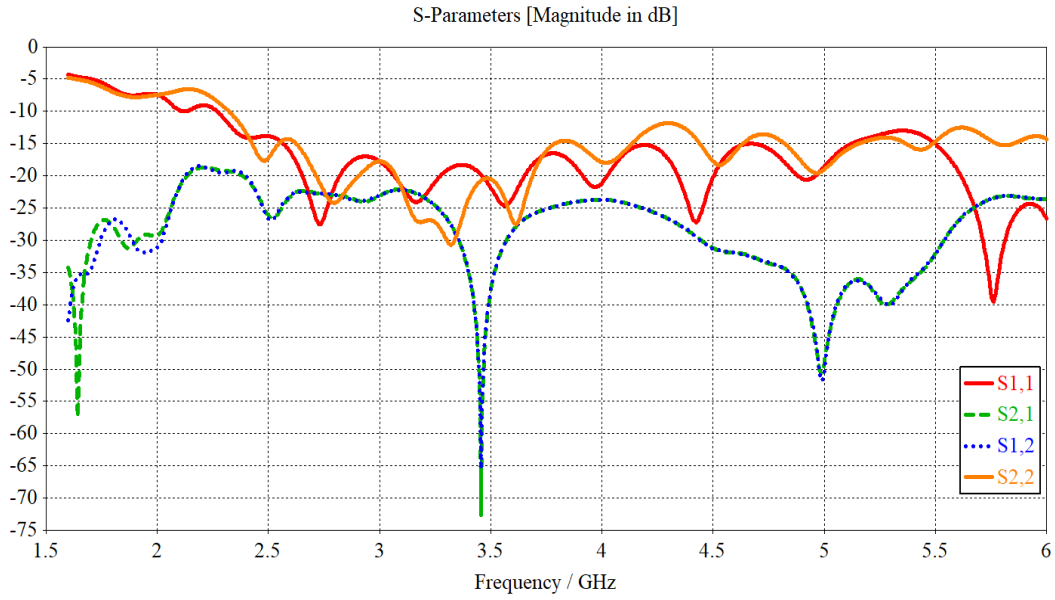

(b)

Figure 4.2 : The s-parameters of the integrated antennas: (a) Feed1. (b) Feed2.

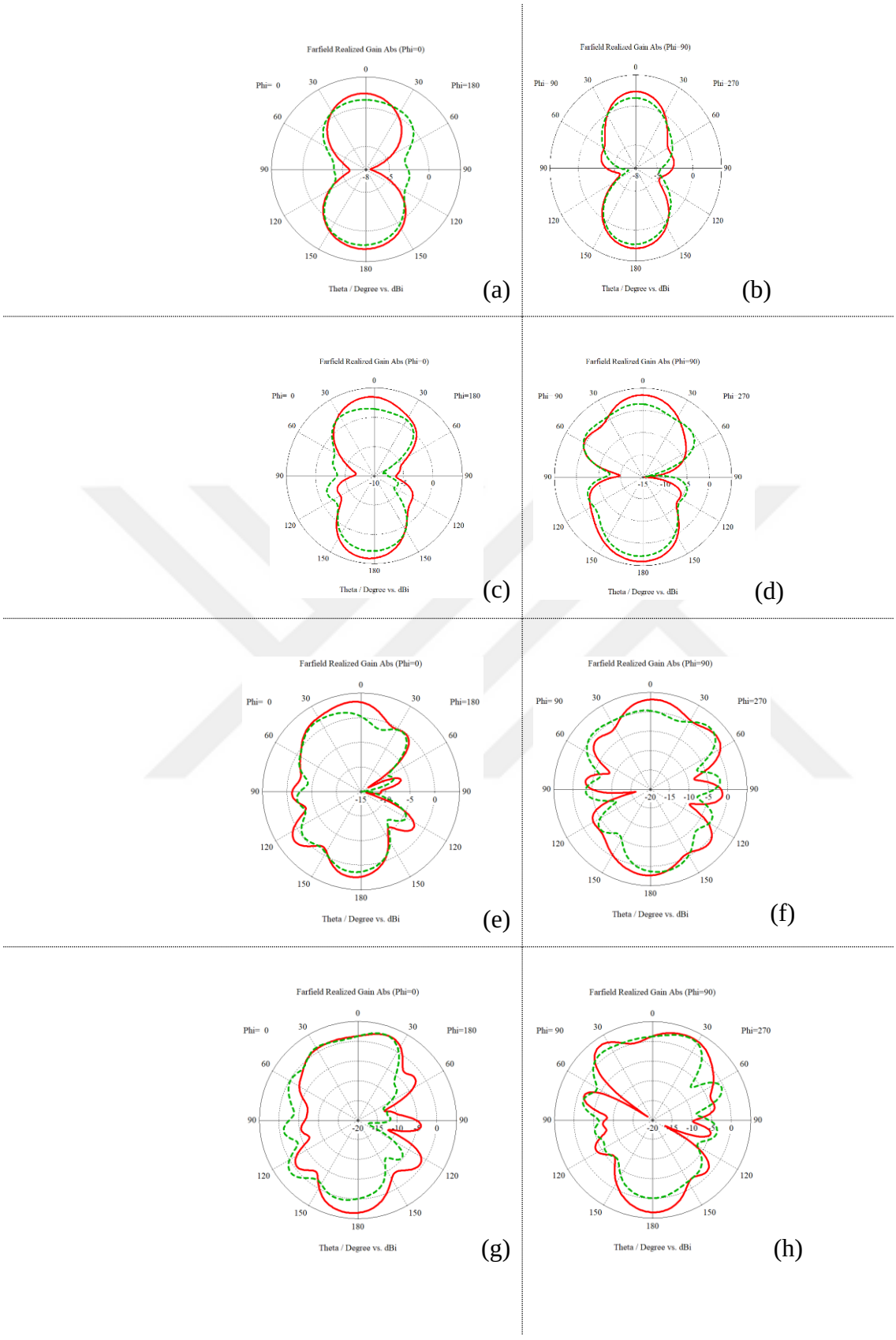

Figure 4.3 : Radiation patterns of the modified integrated four-arm sinuous antenna of Feed1 and Feed2: (a) f_0 = 2GHz, $\phi = 0^{\circ}$. (b) f_0 = 2GHz, $\phi = 90^{\circ}$. (c) f_0 = 3.05GHz, $\phi = 0^{\circ}$. (d) f_0 = 3.05GHz, $\phi = 90^{\circ}$. (e) f_0 = 4.1GHz, $\phi = 0^{\circ}$. (f) f_0 = 4.1GHz, $\phi = 90^{\circ}$. (g) f_0 = 5GHz, $\phi = 0^{\circ}$. (h) f_0 = 5GHz, $\phi = 90^{\circ}$.

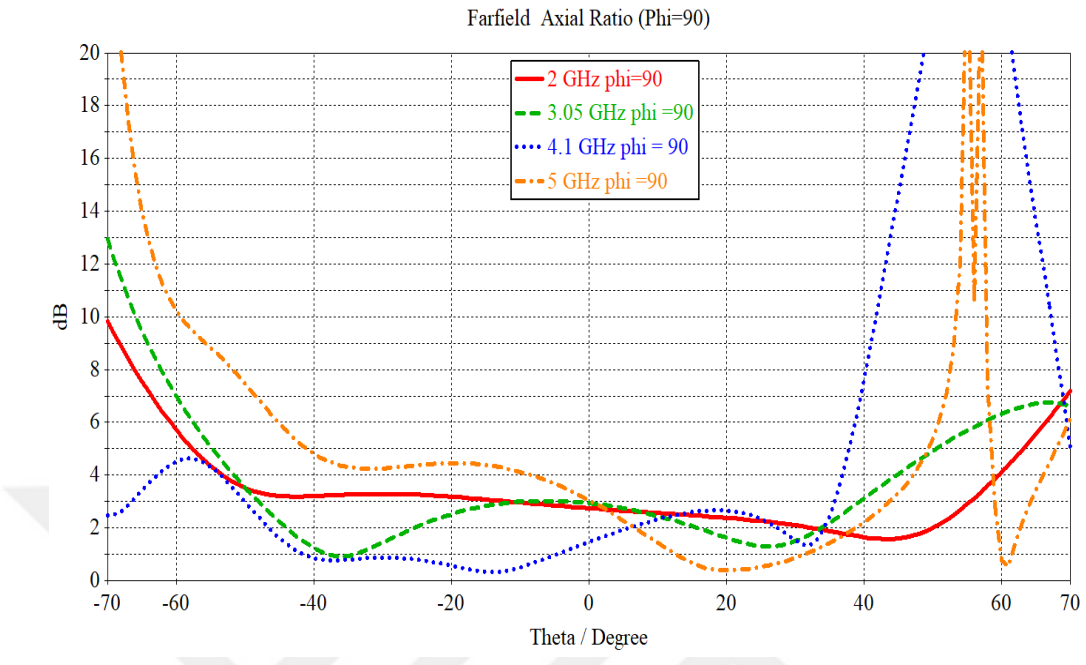

(a)

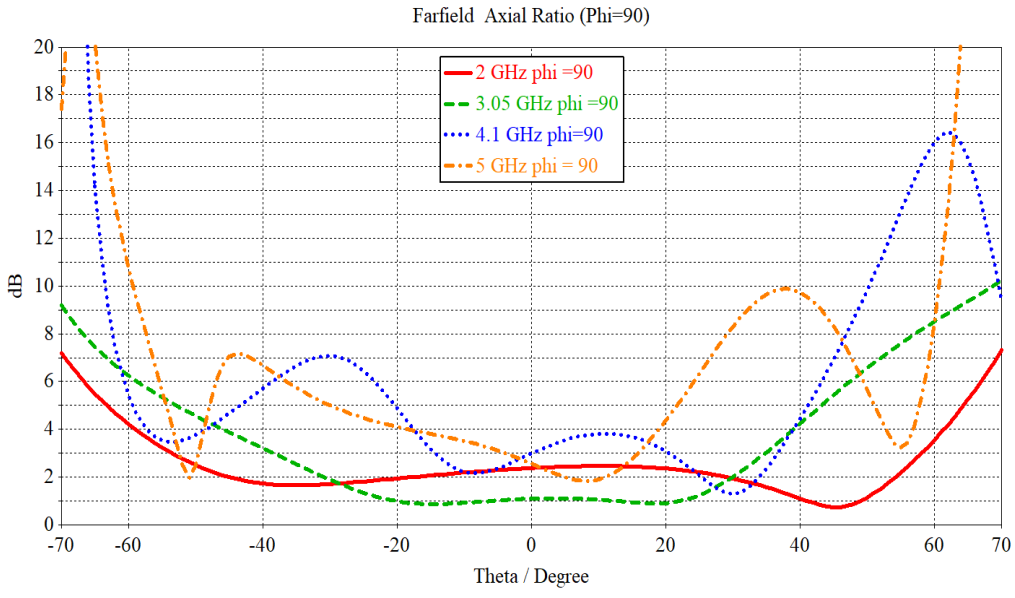

(b)

Figure 4.4 : AR of the modified integrated antennas at $\phi = 90^{\circ}$: (a) Feed1. (b) Feed2.

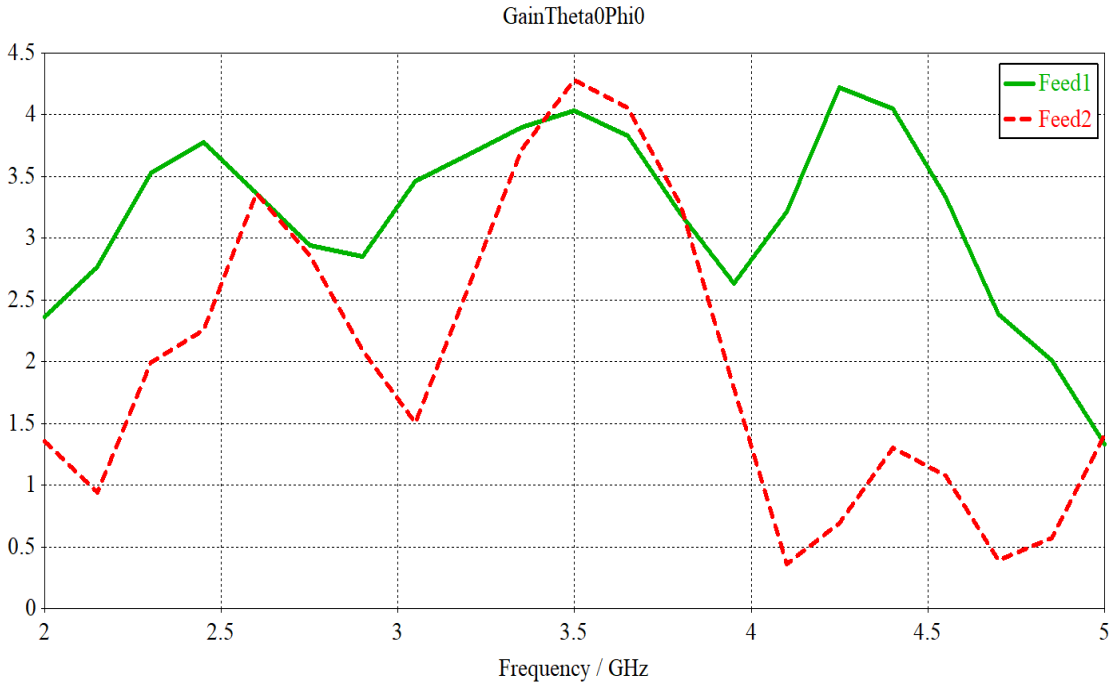

Figure 4.5 : Maximum Gain of the modified integrated antennas at broadside.

4.2 The Modified Feed Four-Arm Sinuous Antenna with Cavity-backed Configuration

In many applications, a unidirectional sinuous antenna is preferred and this can be accomplished by placing a cavity on the rear side of the substrate. In general, the cavity is filled with an absorbing material in order to absorb all the backside radiation. Although using an absorbing material reduces the maximum gain of the antenna almost 50% [13]. In this thesis, the designed cavity-backed four arm sinuous antenna is simulated with and without an absorbing material. Both the Feed1 and Feed2 cavity-backed antennas are simulated and the final configurations are given in figure 4.6(a) and Figure 4.6(b). Figure 4.6(c) shows how the absorbing material is placed inside the cavity and the placement is identical in both antennas. The preloaded ECOSORB LS-24 absorber is used during the simulations. The final dimensions of both antennas is given in Table 4.1. Increasing the depth of the cavity C affects the resonance of the antenna. Therefore, the height of the cavity was optimized to have a better performance.

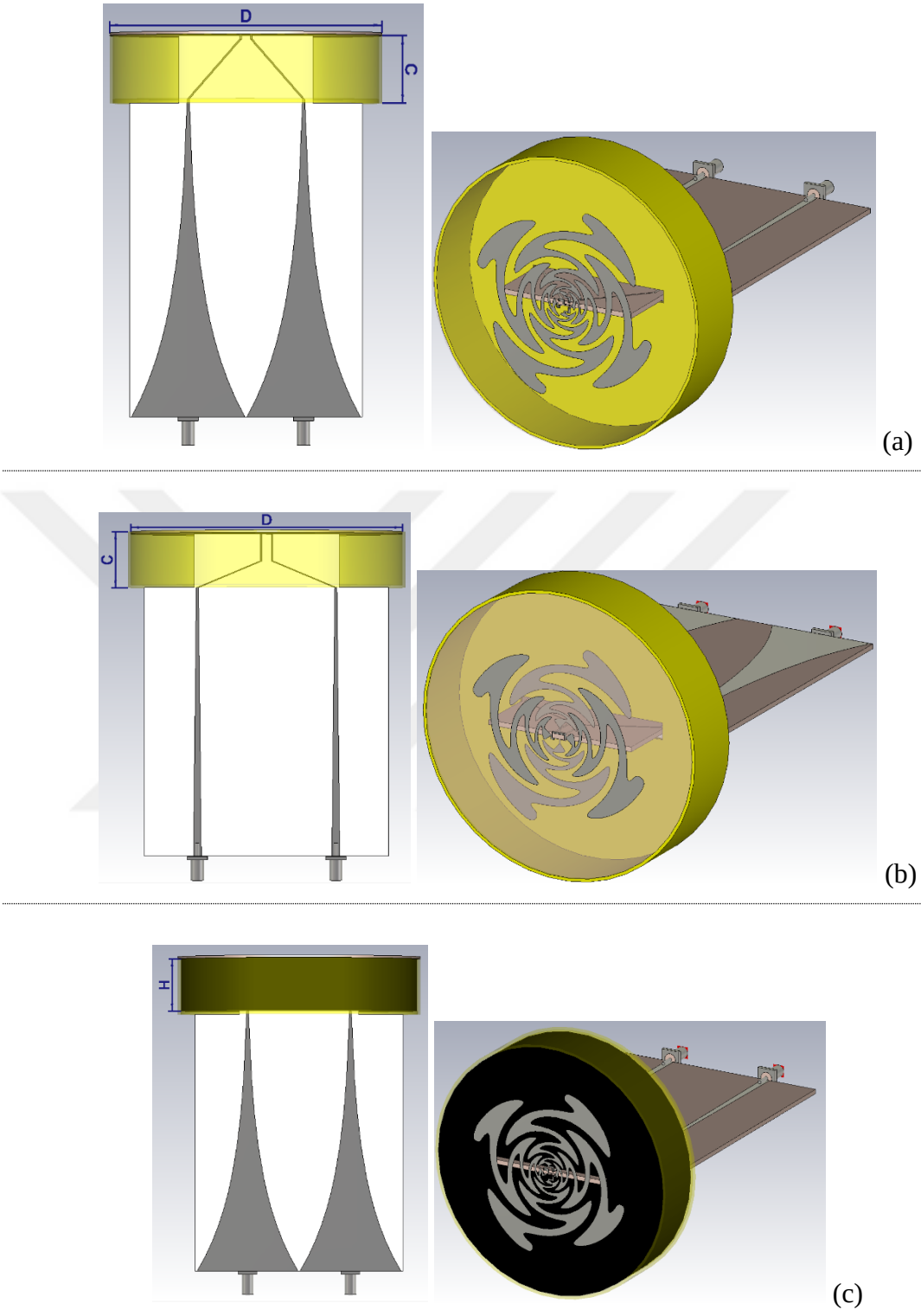

Figure 4.6 : Configurations of the antennas with cavity-backed: (a) Feed1 configuration. (b) Feed2 configuration. (c) Feed1 with absorber.

Table 4.1 : Final dimensions of the modified Feed1 and Feed2 antennas.

Parameters	Feed1(mm)	Feed2(mm)
α	45°	45°
τ	0.7	0.7
δ	22.5°	22.5°
Di	12.72	12.72
Do	63.5	63.5
D	93.5	93.5
C	21	21
H	20	20

4.3 Performance of The Modified Feed Cavity-Backed Four-Arm Sinuous Antenna

The reflection coefficients of Feed1 and Feed2 antennas are analyzed with and without absorbing material. Figure 4.7 shows the s-parameters comparison of the Feed1 antenna with and without an absorbing material. Even without the absorbing material, the antenna has good return loss within the interested frequency band although there is some variation especially in the lower frequency band. The antenna with an absorbing material shows a better return loss and isolation in the 2-5GHz frequency band but using absorbing material can be costly in gain performance. Similarly, Figure 4.8 shows the s-parameters comparison of the Feed2 antenna with and without an absorbing material. In both cases, the return loss and isolation of the antennas is improved with the addition of an absorber.

The radiation patterns of both antennas are plotted in Figure 4.8 for the $\phi = 0^{\circ}$ and $\phi = 90^{\circ}$ principle cuts. The radiation patterns show a unidirectional pattern since the back radiations are no longer present and the 3D radiation patterns of the Fee1 antenna is shown in Figure 4.9. The axial ratios of both antennas is given in Figure 4.9(a) and (b) respectively. Both antenna still maintains a low axial ratio below 3dB.

The maximum gain at broadside is given in Figure 4.11(a) and (b) for the Feed1 and Feed2 antennas with and without an absorbing material. It can be seen that both antennas have a high gains without the absorbing material from 2-4.5 GHz but then fluctuates to a much lower gain when the absorbing material is used.

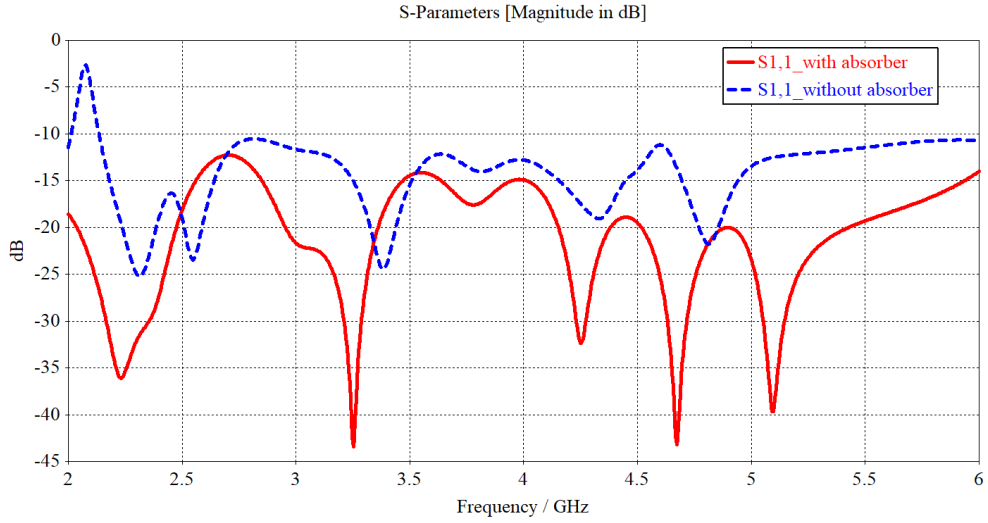

(a)

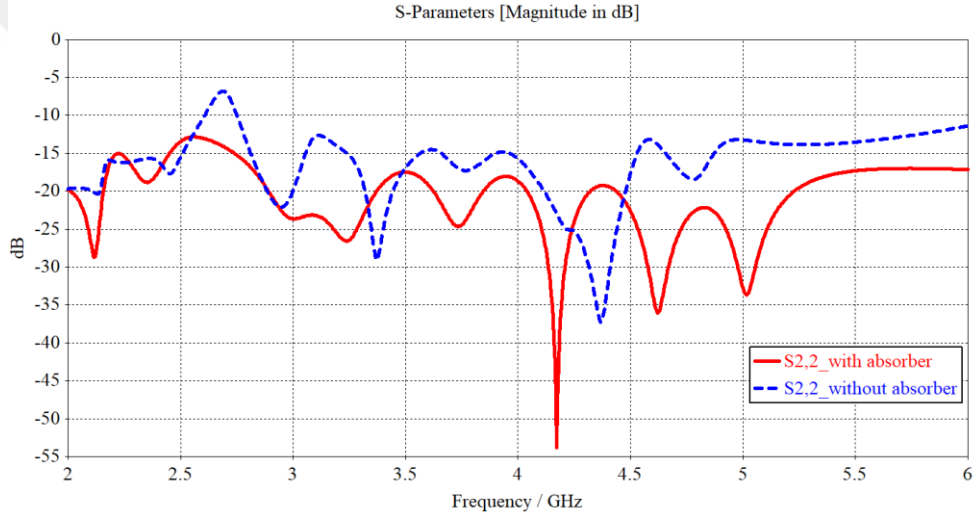

(b)

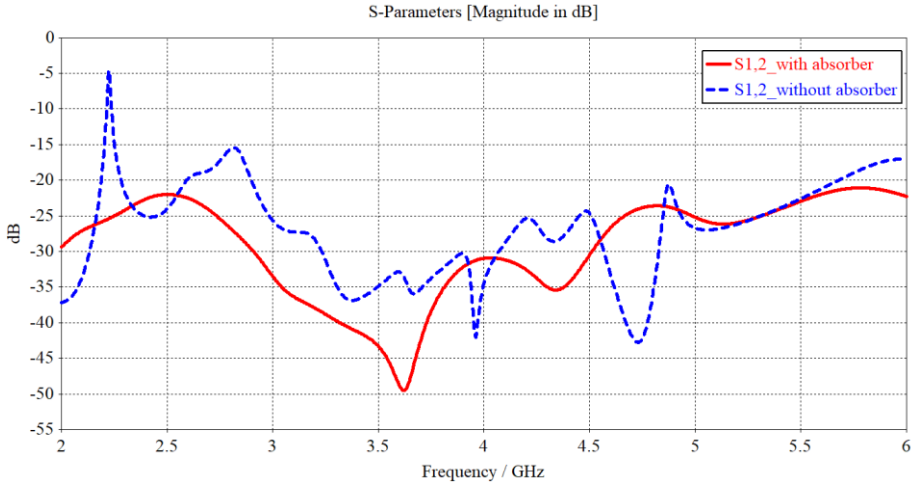

(c)

Figure 4.7 : S-parameters comparıson of the cavity-backed Feed1 antenna with and without absorber: (a) Port1 return loss. (b) Port2 return loss. (c) Isolation.

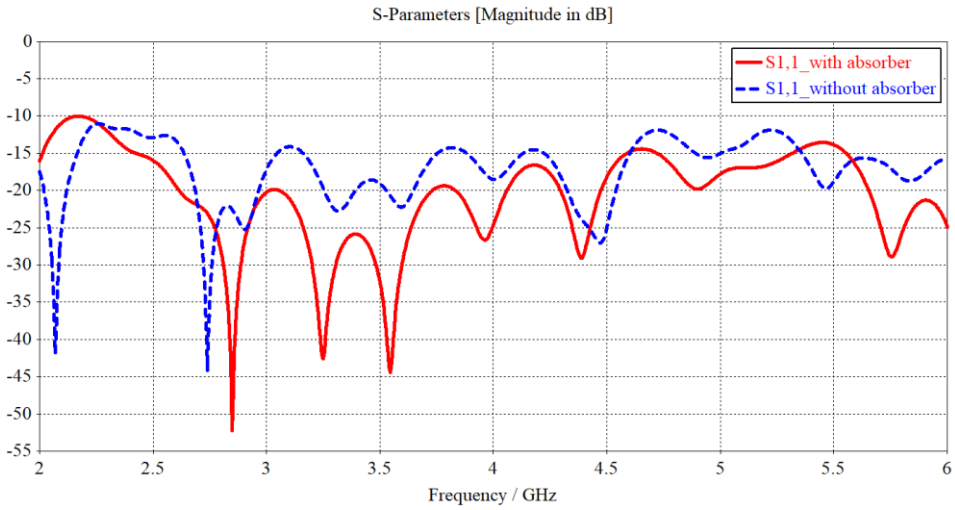

(a)

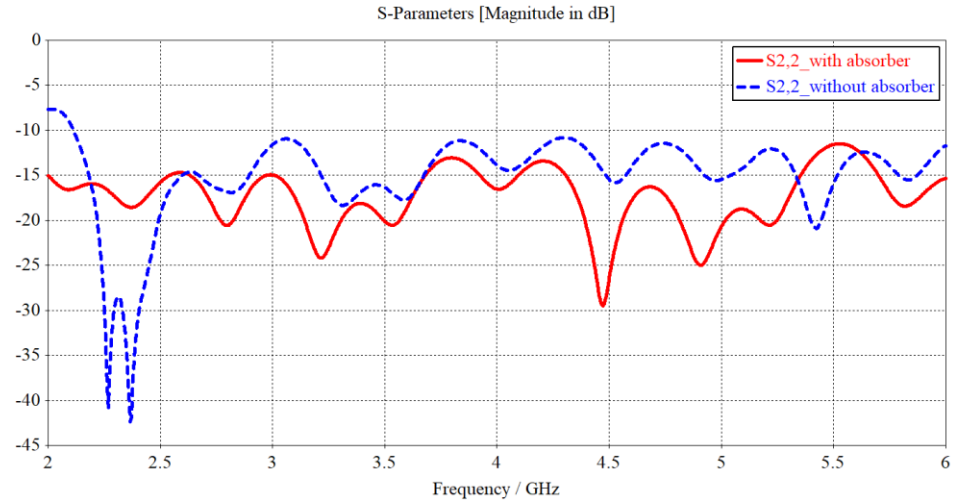

(b)

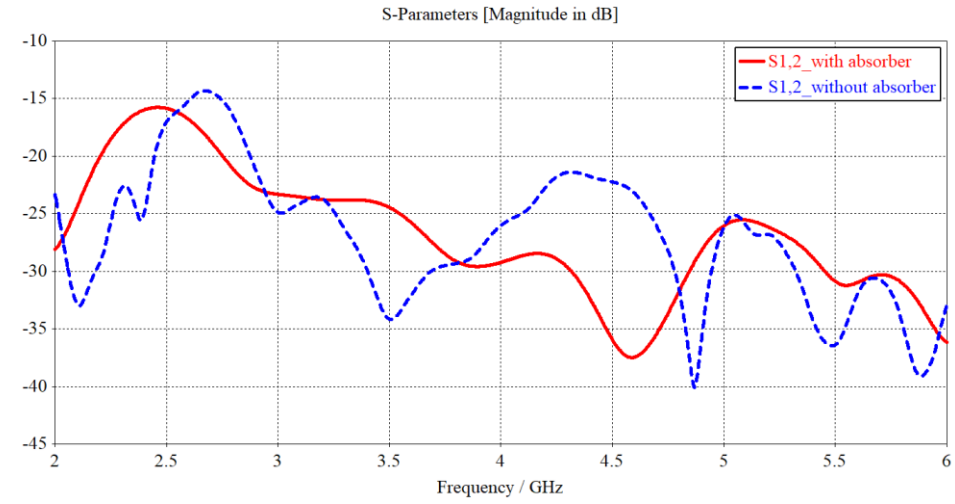

(c)

Figure 4.8 : S-parameters comparıson of the cavity-backed Feed2 antenna with and without absorber: (a) Port1 return loss. (b) Port2 return loss. (c) Isolation.

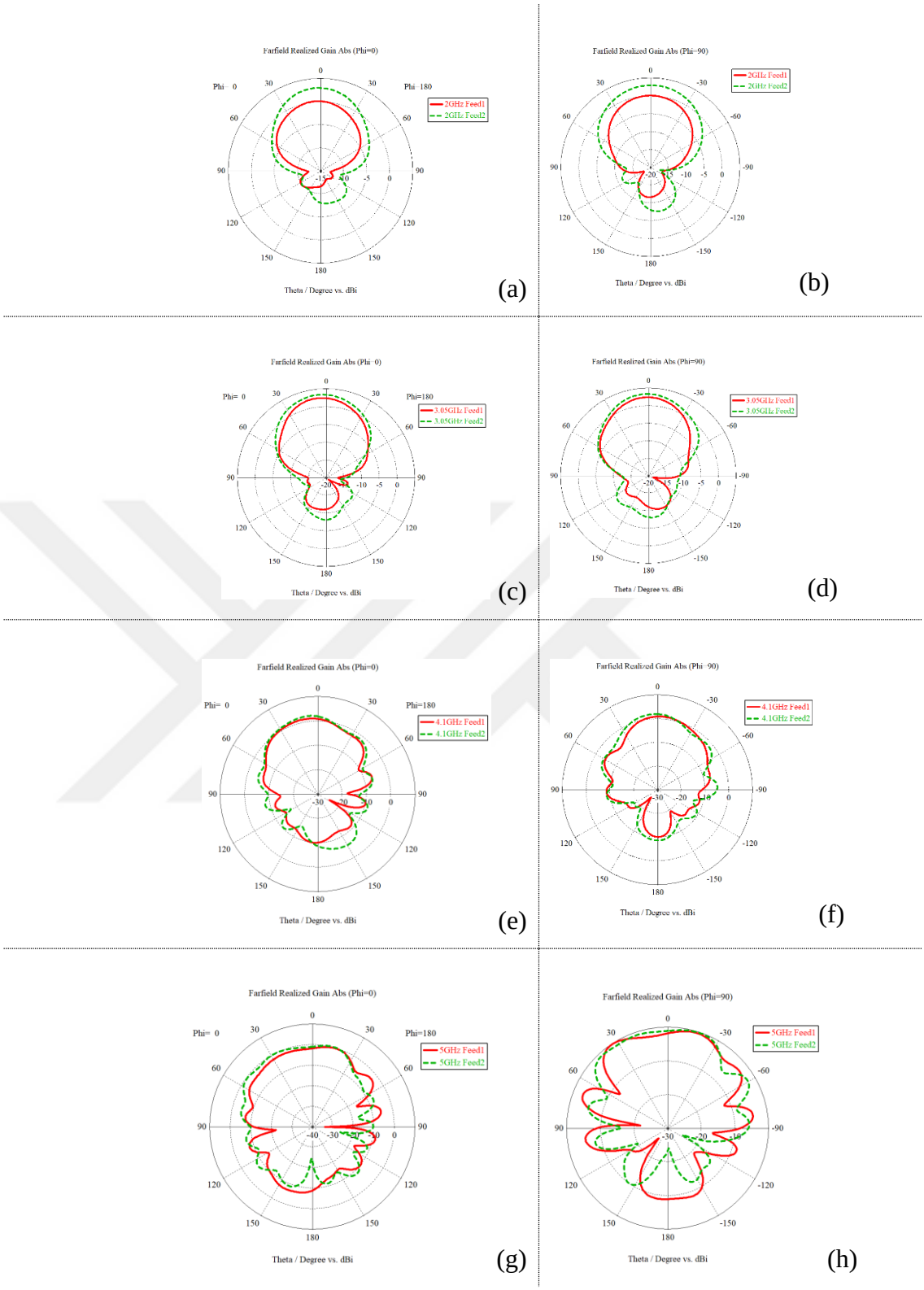

Figure 4.9 : Radiation patterns of the modified cavity-backed four-arm sinuous antenna of Feed1 and Feed2 with absorbing material: (a) 2GHz, $\phi = 0^{\circ}$. (b) 2GHz, $\phi = 90^{\circ}$. (c) 3.05GHz, $\phi = 0^{\circ}$. (d) 3.05GHz, $\phi = 90^{\circ}$. (e) 4.1GHz, $\phi = 0^{\circ}$. (f) 4.1GHz, $\phi = 90^{\circ}$. (g) 5GHz, $\phi = 0^{\circ}$. (h) 5GHz, $\phi = 90^{\circ}$.

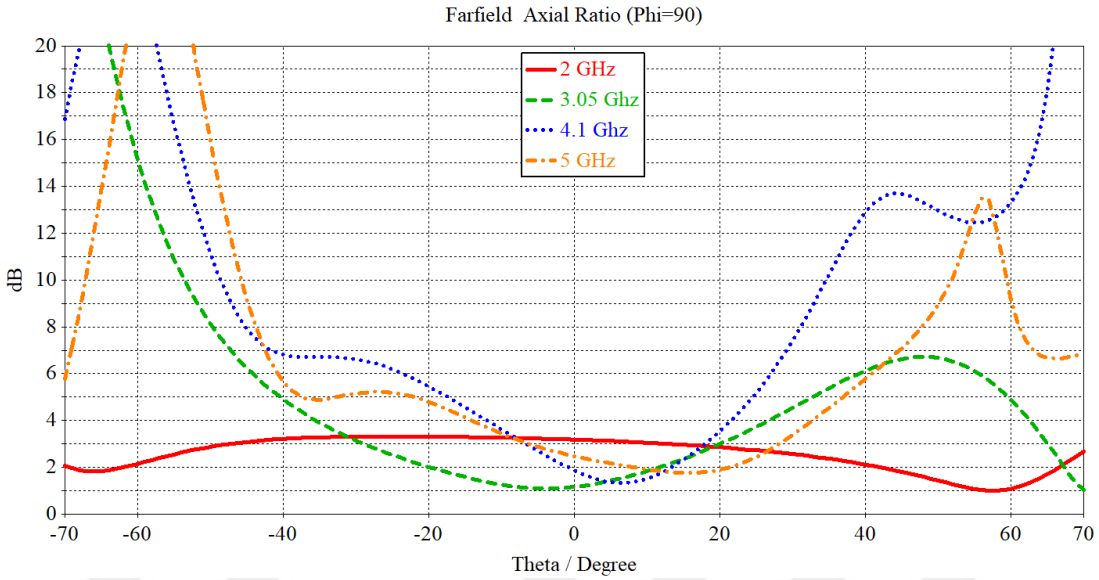

(a)

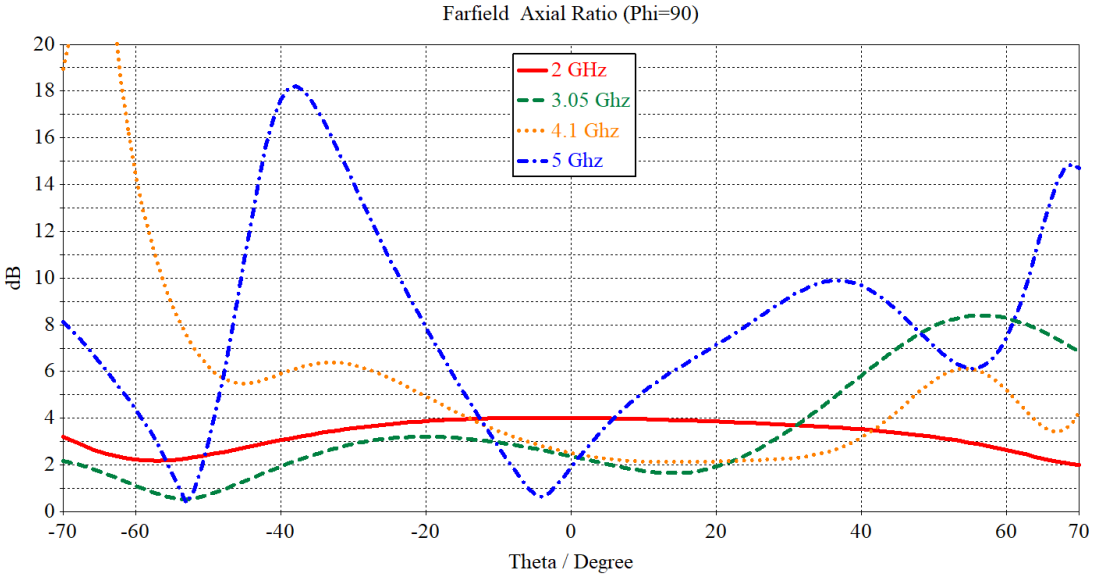

(b)

Figure 4.10 : AR of the modified cavity-backed antennas at $\phi = 90^{\circ}$: (a) Feed1. (b) Feed2.

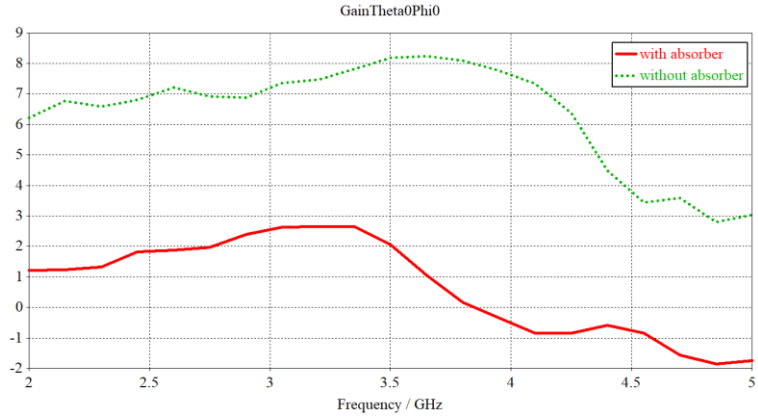

(a)

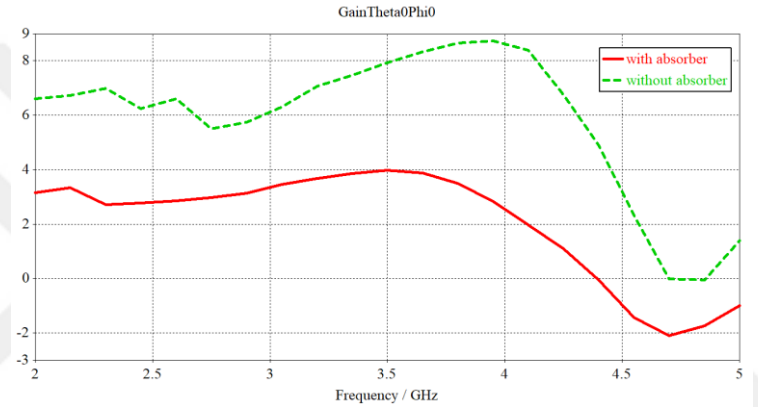

(b)

Figure 4.11 : Comparıson of the maximum Gain of the modified cavity-backed antennas at broadside with and without absorbing material: (a) Feed1. (b) Feed2.

4.4 Fabrication and Measurement of the Cavity-Backed Modified Feed1 Four-Arm Sinuous Antenna

To validate the simulation results, the modified Feed1 antenna is fabricated and the S-Parameters of the antenna is measured using the N5230A PNA Series network analyzer. The Feed1 antenna is opted because it was easier to fabricate. Figure 4.12 shows the fabricated antenna before adding the metallic cavity. At first, the antenna is measured before cavity integration and the simulated and measured s-parameters of port1 and port2 are given in Figure 4.13(a) and Figure 4.13(b) respectively. The measured results plotted in Figure 4.13 shows good agreement with the simulation results. Both ports have a measured return loss at most -11dB and good isolation of around -20dB between 2-5GHz.

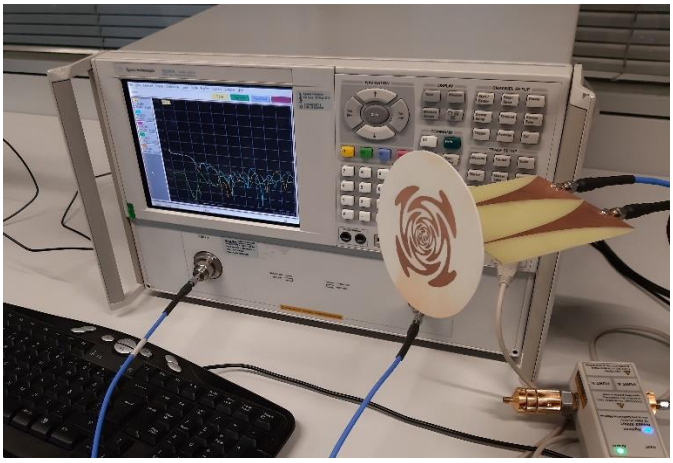

Figure 4.12 : Fabricated Feed1 FASA without cavity-backed measurement set-up.

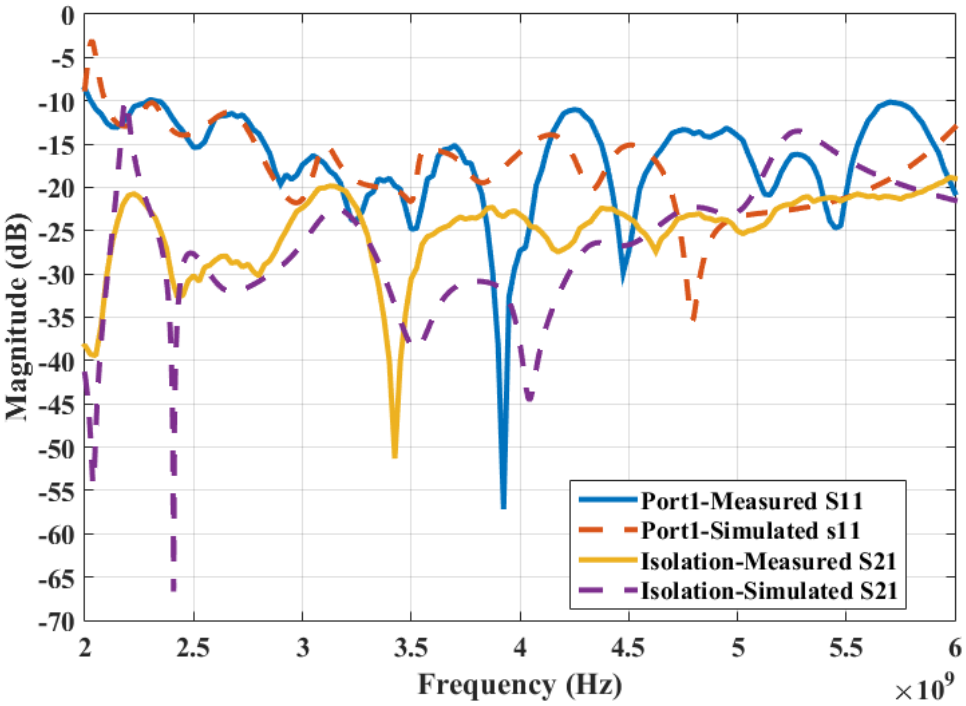

(a)

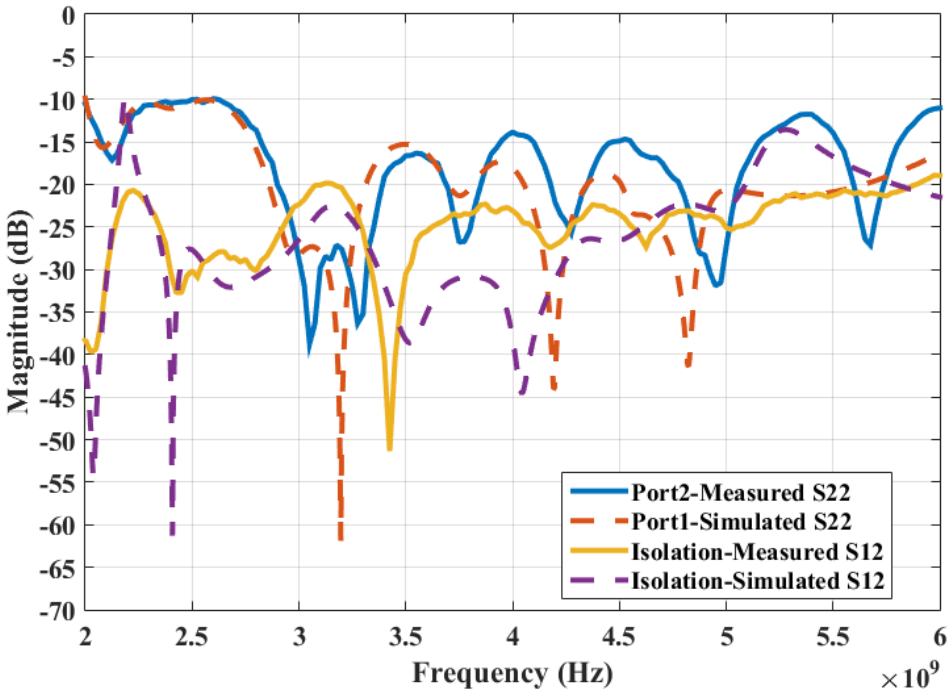

(b)

Figure 4.13 : S-parameters of fabricated Feed1 FASA without cavity-backed: (a) Port1 return loss and isolation. (b) Port2 return loss and isolation.

Furthermore, the antenna is integrated with the absorber filled cavity-backed as shown in Figure 4.14. The simulated and measured s-parameters of the antenna are plotted in Figure 4.15. The measured results observed are in good agreement with the simulated results. Both ports of the antenna have a return loss better than -12dB for the entire 2-GHz frequency bandwidth while keeping good isolation of -20dB.

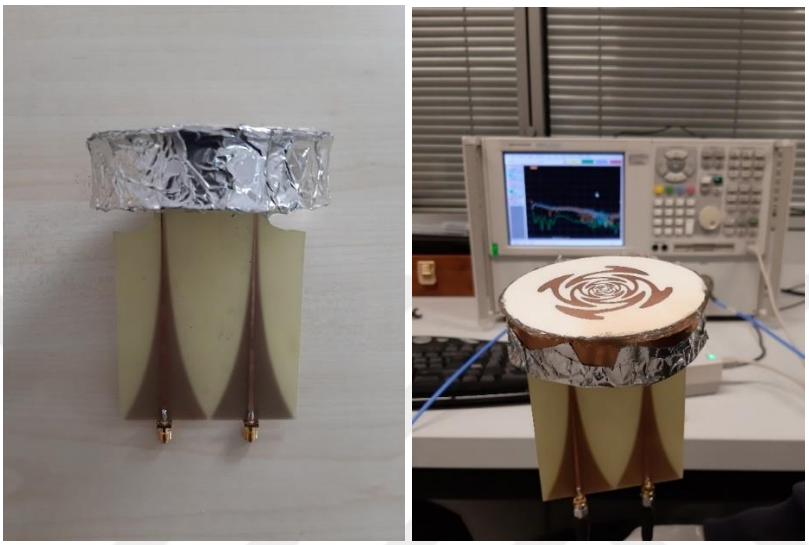

Figure 4.14 : Fabricated Feed1 FASA with absorber filled cavity-backed measurement set-up.

To measure the dual linear polarization property of the antenna, a measurement setup is arranged in an anechoic chamber as shown in Figure 4.16. The setup consists of the fabricated sinuous antenna and a standard linear polarized double ridged broadband horn antenna (BBHA 9120 A 0.8-5 GHz). The horn antenna is placed at the far-field of the sinuous around 2 meters. During the measurement, the orientation of the sinuous antenna is placed such that port1 is the vertically oriented arms (along the y-axis) and port2 is the horizontally oriented arms (along the x-axis). Note that the radiation direction of both the vertically and horizontally oriented arms is in the z direction which is the direction pointing to the horn antenna. Since the electric field is perpendicular to the radiation direction, the co-polarized electric field of the vertically oriented arms is in the x-direction (E_θ) while the co-polarized electric field is in the y-direction(E_ϕ) for the horizontally oriented arms. Similarly, the horn is oriented horizontally and vertically with respect to port1 and port2 of the sinuous antenna. Both antennas were calibrated and port1 of the network analyzer is connected to port1 of sinuous antenna while port2 of the network analyzer is connected to the horn antenna.

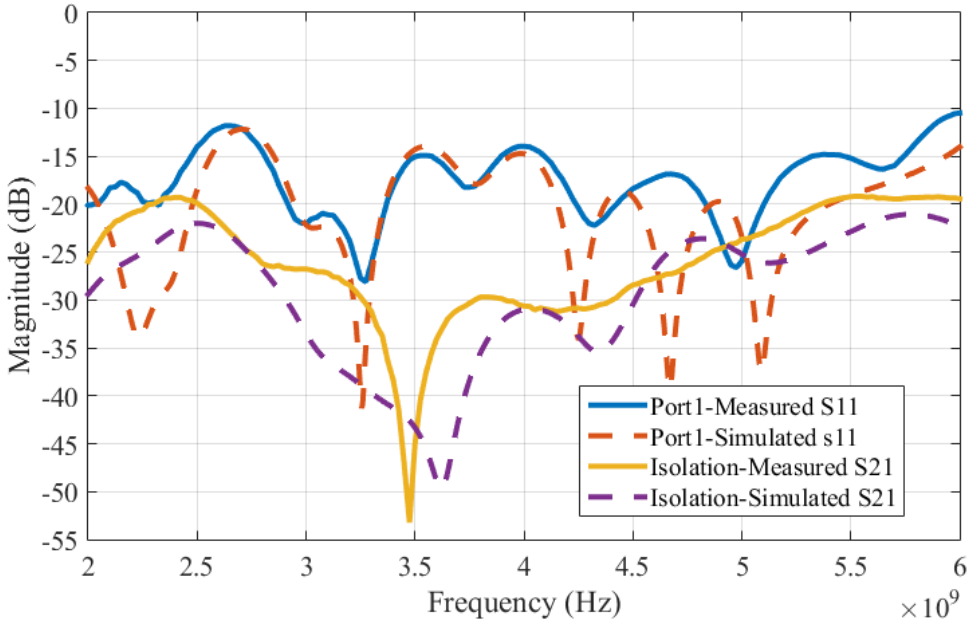

(a)

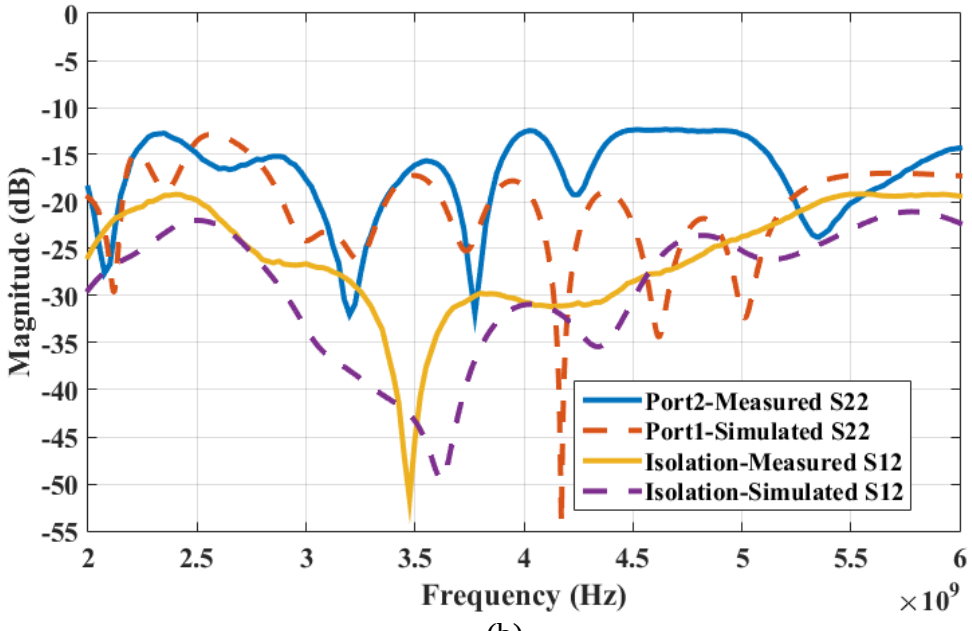

(b)

Figure 4.15 : S-parameters of fabricated Feed1 FASA with absorber filled cavity-Backed: (a) Port1 return loss and isolation. (b) Port2 return loss and isolation.

The horn antenna is first vertically oriented and then horizontally oriented. the S-parameters were measured in both cases. After the measurements were taken for the port1 of the sinuous antenna, port2 is then connected and similar orientation of the

horn and measurements were repeated. The S_{21} parameters are ploted in Figure 4.17(a) and Figure 4.17(b) for port1 and port2 of the sinuous antenna respectively. The measured results show that port1 (vertically oriented sinuous arms) is co-polarized with the horn antenna when the horn is vertically oriented and cross-polarized when the horn is horizontally oriented. Conversely, port2 (horizontally oriented sinuous arms) is co-polarized with the horizontally oriented arms and cross-polarized with the vertically oriented horn. This is what is expected since the electrical field of the horn antenna.

To measure the maximum gain of the sinuous antenna at broadside, the same measurement setup is maintained. The Friss transmission equation is then utilized to calculate the maximum broadside gain of the sinuous antenna using the standard horn antenna as a reference. The simulated and measured gains are plotted in Figure 4.18(a) and (b) for port1 and port2 of the sinuous antenna respectively. The results indicate almost similar measured gain results are obtained compared with the simulated gain across the bandwidth. Although there is a difference between the simulated and measured results but this can be due the fact that the anechoic chamber contained some other equipment that can interfere with the measurements.

Figure 4.16 : Polarization measurement setup.

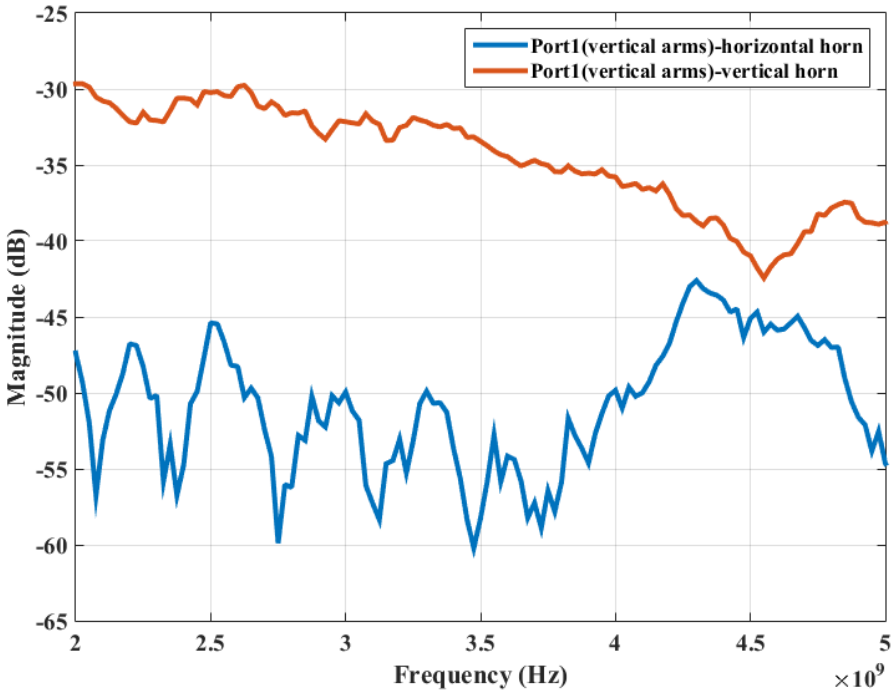

(a)

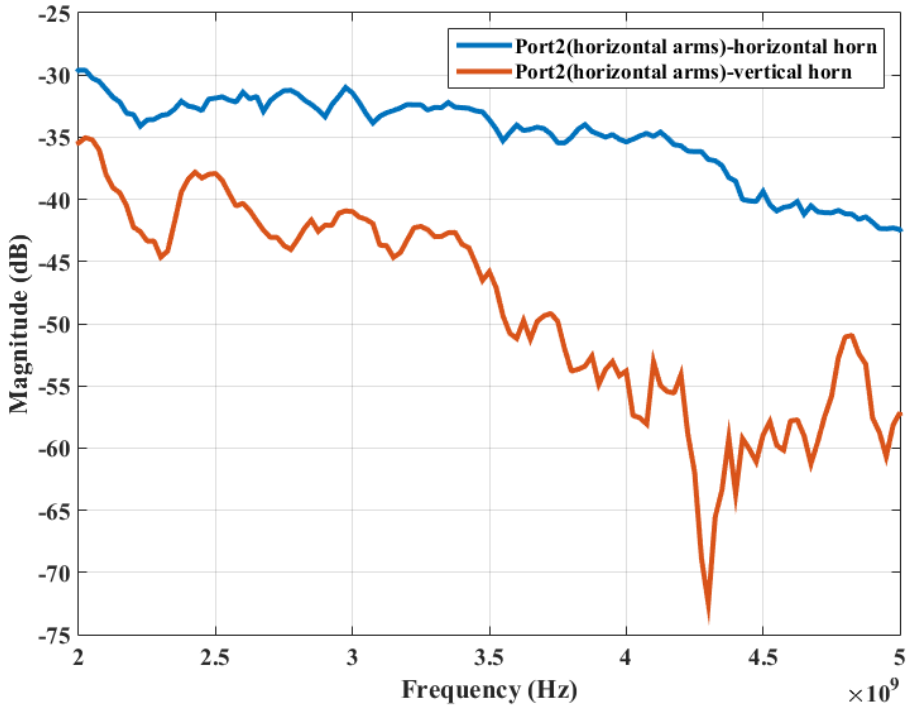

(b)

Figure 4.17 : S_{21} plots: (a) Port1 sinuous antenna co and x-polarized. (b) Port1 sinuous antenna co and x-polarized.

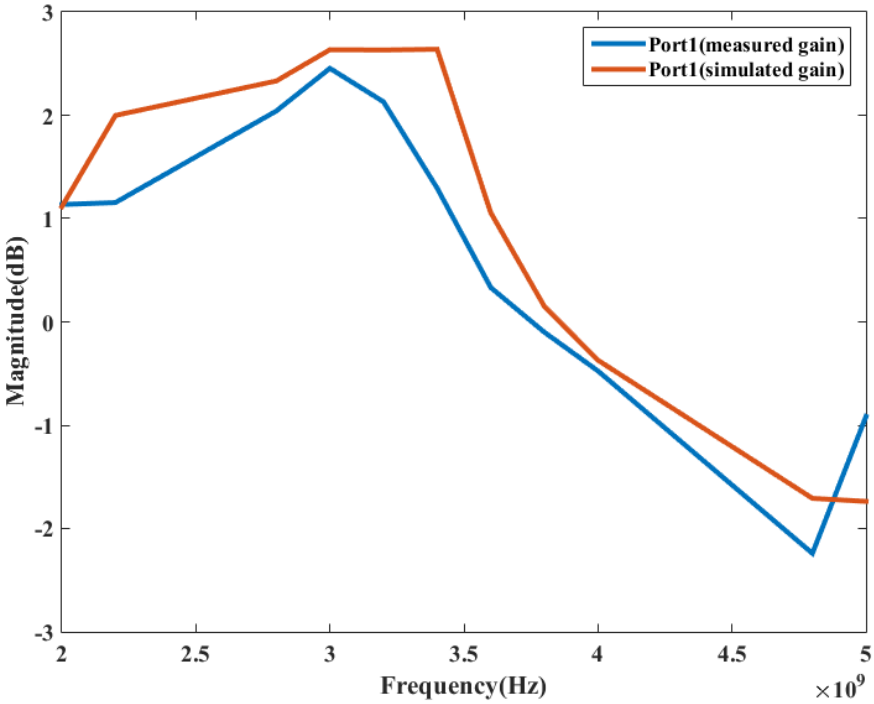

(a)

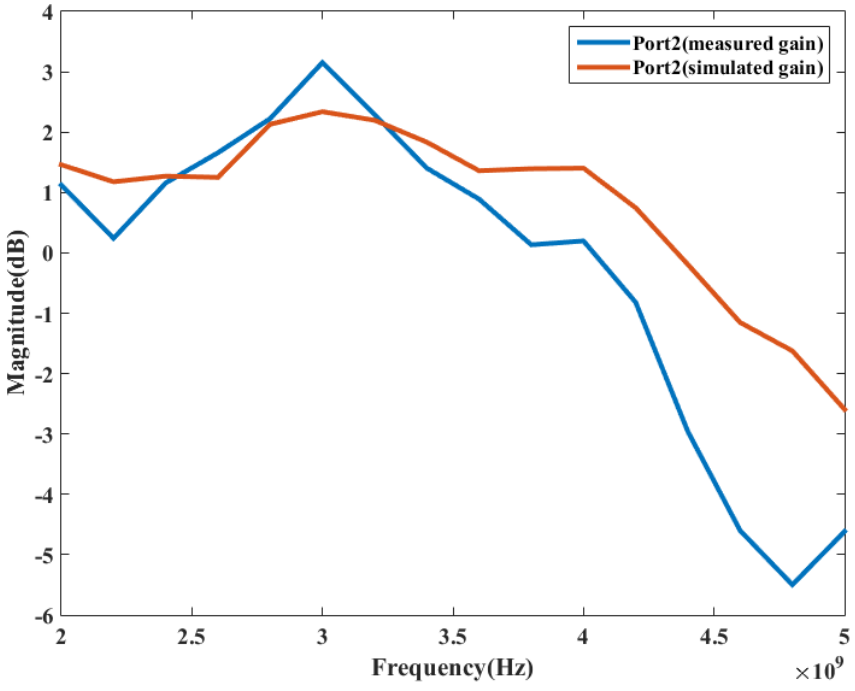

(b)

Figure 4.18 : Maximum gain at broadside: (a) Port1 simulated and measured gain. (b) Port2 simulated and measured.

5. CONCLUSION

In this thesis, two different feed point modification approaches are implemented to design a four-arm dual polarized sinuous antenna working in the 2-5GHz frequency band. It is worth mentioning that realizing accurate phase progression between the arms of a sinuous antenna demands a complex and expensive feed network. There are several approaches proposed for feeding wideband antennas such as the sinuous antenna in literature. Feeding a four-arm sinuous antenna using a microstrip balun has its limitations due to the geometry of the standard sinuous antenna. Therefore, the feeding point of the standard feed sinuous antenna is modified to incorporate a microstrip feeding network. Even though the modification proposed is not a symmetric type of modification, but it is optimized to still maintain the desired characteristics of the dual polarized sinuous antenna such as nonsymmetrical radiation patterns and low AR.

The performance of the standard feed sinuous antenna is first analyzed with and without a substrate and the change in the input impedance was obtained. Obtaining the input impedance with the addition of a substrate is vital since the output of the feeding network or the balance port is designed according to that. The average input impedance which gave a good matching for both the standard and the modified feed antennas is found to be 185Ω for the interested frequency bandwidth. An additional modification which helps to lower the return loss of the antennas at low frequencies was also made. This modification is done by chamfering the sharp ends of the antenna and the effects was seen on the low frequencies of the antenna. An exponentially tapered microstrip balun with an input of 50Ω at the unbalance port and an output of 185Ω at the balance port is design. The balun is simulated by terminating the output with a 150Ω resistor and feeding the input with a 50Ω port and the return loss obtained show that the balun can transform a 50Ω unbalance port to a 185Ω balance port. With the baluns the designed, the integrated antennas with the baluns show a good return loss, a low AR

and bidirectional radiation pattern across the 2-GHz frequency bandwidth and the comparison with the standard feed also show a good agreement.

To obtain a bidirectional radiation pattern, the modified four-arm sinuous antennas are integrated with a cavity backed. The cavity backed antennas are simulated with and without an absorber. Putting an absorber in the cavity helps to absorb the backside radiation and it was also seen that a good matching was achieved at low frequencies with the addition of an absorber. Finally, one of the modified antennas is fabricated and measured using the N5230A PNA Series network analyzer. The fabricated antenna was first measured without the cavity-backed and the measured results show similar s-parameters with the simulated results over the interested frequency bandwidth. Then the antenna was integrated with the cavity filled with ECOSORB LS-22absorber and measured. Similarly, the measured return loss and isolation of the two ports show good agreement with the simulated results. To test for the dual linear polarity of the antenna, a measurement setup consisting of the sinuous antenna and a standard linear polarized horn antenna was made in an anechoic chamber and measurements were performed to test the co and cross- polarization of the two ports of the sinuous antenna. Additionally, the maximum gain at broadside of the sinuous antenna was also measure using the Friss transmission formula. In the future, the radiation patterns of the antenna will be measured. In addition, the antenna will be tested for microwave imaging applications.

REFERENCES

[1] **DuHamel, R. H.** (1987). Dual polarized sinuous antenna. US Patent 4658262.

[2] **Rumsey, V. H.** (1957). Frequency Independent Antennas. IRE National Convention Record. 1, 114–118

[3] **DuHamel, R. H., and Isbell, D. E.** (1957). Broadband Logarithmically Periodic Antenna Structures, *IRE National Convention Record*. 1, 119–128.

[4] **Suh, S. Y. (**2002). A comprehensive investigation of new planar wideband antennas. *PHD Thesis in Electrical and Computer Engineering*, Blacksburg, Virginia.

[5] **Hershey, J. E. (**2000). Wideband antennas – A short survey. *General Electric Company*.

[6] **Johnson, R. C. (**1993). Antenna Engineering handbook. *McGraw-Hill, Inc.*, Chapter 14

[7] **Kraus, W. L. (**1988). Antenna. *2nd edition*, McGraw-Hill, Inc., Chapter 15.

[8] **Balanis, C. A.** (2005). Antenna theory analysis and design**,** 3rd edition**.** USA: *A John Wiley & Sons, Inc*.

[9] **Dyson, J. D.** (1959): The Equiangular Spiral Antenna, *IRE Trans. Antennas Propagat.* 7, 181–187 April.

[10] **Filipovic, D. S., and Volakis, J. L.** (2003). Novel Slot Spiral Antenna Designs for Dual-Band/Multiband Operation**.** *IEEE Trans. Antennas Propagat.* 51, 3, 430–440 March.

[11] **DuHamel, R. H., and Ore, F. R.** (1958)**.** Logarithmically Periodic Antenna Designs. *IRE National Convention Record*, 1, 139–152.

[12] **Dylan, A. C., and Scott, J. W. R. (**2019): On the Design of Sinuous Antennas for UWB Radar Applications. *IEEE Antennas and Wireless Propagation Letters*. 18, 7, July.

[13] **Salem, P.** (2006). Dual polarized sinuous antenna and ultra-wideband feed design and integration**.** Diploma Thesis. USA: University of Ottawa.

[14] **Pour, A. K. M., Faraji, D. R., and Rashed, M. J.** (2005). The sinuous antenna—a dual polarized feed for reflector-based searching systems. *International Journal of Electronics and Communications (AEÜ)*. 59, 392–400.

[15] **Amir, J., and Manouchehr, K.** (*2011).* A new approach for feeding sinuous antenna. *International Journal of Electronics and Communications (AEÜ)*. 65, 4, 312-319 April.

[16] **Kang, Y., and Kim, K.** (2015). Investigation of the effects of sharp-ends removal in the sinuous antenna arms on the radiation patterns. *IEEE Int. Symp. Antennas Propag. USNC/URSI Nat. Radio Sci. Meeting*. 1989–1990 July.

[17] **Kang, Y., Kim, K., and Scott, W. R.** (2015)**.** Modification of sinuous antenna arms for UWB radar applications. *IEEE Trans. Antennas Propag.* 63, 11, 5229–5234 Nov.

[18] **Gonnet, P., Sharaiha, A., Terret, C., and Skrivervik, A.** (1999)**.** Feeding networks for sinuous antennas. *Microwave Opt TechnolmLett.* 20, 195–200.

[19] **Xiaolu, Z., Guang, F., and Zhiya, Z.** (2013). A Planer Sinuous Antenna and the Relevant balun. 2013 International Workshop on Microwave and Millimeter Wave Circuits and System Technology.

[20] **Masanori, K., and Narutoshi, S.** (1992) Analysis and Synthesis of Tapered Microstrip Transmission Lines. *IEEE Transactions on Microwave Theory and Techniques.* 40, 8, August.

[21] **Vinayagamoorthy, K., Coetzee, J., and Jayalath, D.** (2012)**.** Microstrip to Parallel Strip Balunas Spiral Antenna Feed**.** *IEEE Vehicular Technology Conference (VTC Spring).* Yokoham. 1-5.

CURRICULUM VITAE

Name Surname: **Sulayman Joof**

Place and Date of Birth: **Manjai Kunda 18-01-1989**

E-Mail: **joo@itu.edu.tr**

B.Sc.: 2017, Istanbul Technical University, Electronics and Telecommunication Engineering

List of Publications:

- **T. Yilmaz, B. Saçlı, G. Cansız, S. Joof, C. Aydınalp, M. Çayören, I. Akduman and B. Önal**. (2019). Microwave Dielectric Spectroscopy of Renal Calculi: A Large Scale Study on Dielectric Properties from 500 MHz to 18 GHz, IEEE Trans. on Dielectrics and Electrical Insulation,
- **B. Saçlı, C. Aydınalp, G. Cansız, S. Joof, T. Yilmaz, M. Çayören, B. Önal, and I. Akduman**, (2019). Microwave Dielectric Property Based Classification of Renal Calculi: Application of kNN Algorithm, Computers in Biology and Medicine.
- **C. Aydinalp, S. Joof, T. Yilmaz, and I. Akduman**., "Sensitivity and Sensing Depth Analysis of Open-ended Contact Probes for Cancer Diagnosis", 2019 PhotonIcs & Electromagnetics Research Symposium - Spring (PIERS-Spring), 17-20 June 2019, Rome, Italy.
- **C. Aydinalp, S. Joof, T. Yilmaz, N. P. Özsobaci, F. Ateş**., "In Vitro Dielectric Properties of Rat Skin Tissue for Microwave Skin Cancer Detection", 2019 International Applied Computational Electromagnetics Society Symposium (ACES), Miami, FL, USA, 2019.
- **Aydinalp, C., Joof, S., Yilmaz, T**. (2019). Sensing Depth Analysis of Open-Ended Coaxial Probe for Skin Cancer Detection. 23rd International Conference on Applied Electromagnetics and Communications (ICECOM), Dubrovnik, 2019.

- **S. Joof, G. Cansız, S. Özgür, T. Yılmaz, M. Çayören, and I. Akduman**, "Tissue Mimicking Phantoms for Microwave Brain Stroke Imaging", 18th Mediterranean Microwave Symposium (MMS2018), Istanbul, Turkey, 2018.
- **E. G. Önal, A. Keleşoğlu, B. Saçli, G. Cansiz, S. Joof, C. Aydinalp, and M. Çayören**, "Kidney Stone Classification with Electromagnetic Properties: Preliminary Results", 25th Telecommunications Forum TELFOR, Belgrade, Serbia, 2017.
- **T. Yilmaz, T. Ozturk, S. Joof**. "A Comparative Study for Development of Microwave Glucose Sensors". 32nd International Union of Radio Science General Assembly & scientific Symposium, 19-26 August 2017, Montreal, Canada. (Award winner).